A Finite Element Analysis of the Pullout Capacity of Suction Caissons in Clay

By

Christina G. Sgardeli

MEng Civil Engineering (2006)
Imperial College London

Submitted to the Department of Civil and Environmental Engineering in Partial Fulfillment of the Requirements for the Degree of

Master of Engineering in Civil and Environmental Engineering
at the
Massachusetts Institute of Technology

February 2009

Signature of Author _____

Department of Civil and Environmental Engineering
January 29, 2009

Certified by _____

Andrew J. Whittle
Professor of Civil and Environmental Engineering
Thesis Supervisor

Accepted by _____

Daniele Veneziano
Chairman, Departmental Committee for Graduate Students

A Finite Element Analysis of the Uplift Capacity of Suction Caissons in Clay

By

Christina G. Sgardeli

Submitted to the Department of Civil and Environmental Engineering on January 29, 2009 in partial fulfillment of the requirements for the degree of Master of Engineering in Civil and Environmental Engineering

Abstract

Suction caissons are increasingly becoming the foundation of choice for offshore structures in deep water. They are used extensively in Tension Leg Platforms and provide the most efficient foundations for many offshore wind turbine structures. One of their major advantages is the ability to withstand large uplift forces by mobilizing shear on their external and internal surface and by the suction forces induced in the enclosed soil plug. These suction forces can be relied upon for short-term loading, while the behaviour of the soil remains undrained, but are more questionable for the sustained loading induced by storms and loop currents. This study uses finite element analysis to investigate the uplift capacity of suction caissons under three loading conditions: a) short-term undrained loading, b) long-term drained loading and c) sustained loading for short and long periods of time. The study compares the capacity from 5 different geometries with length to diameter ratios, L/d = 0.5,0.65,1,2 and 3 under these three loading conditions. For the sustained loading case, a minimum time under which the load can be sustained is established for different load levels. The commercial finite element program Plaxis is used and a Mohr-Coulomb model is assumed for the soil. Comparisons are presented between the results of this study, the theoretical Mohr-Coulomb model predictions and other finite element analysis found in the research for undrained and drained loading.

Thesis Supervisor: Andrew J. Whittle
Title: Professor of Civil and Environmental Engineering

Acknowledgements

I would like to express my gratitude to my advisor, Professor Andrew Whittle, for his continuous support, patience and invaluable guidance throughout the development of this thesis and throughout my time at MIT. I would like to thank Dr. Eric Adams for giving me the opportunity to pursue one of the most challenging and enriching experiences at MIT. Special thanks to Kris Kipp and Jeanette Marchocki for being always approachable and supportive throughout these years.

I would like to thank all of my friends from the third floor and the MEng class, Giuseppe, Sherif, Maria, Ray, Naeem, Bruno, Nikos, Ali, Kenneth, Tricie and Siddharth for making my life there so interesting and enjoyable every day.

I would like to express my deepest gratitude to my family which has always supported me in every easy or hard choice I have made. Especially, I would like to thank my father, Antony, for being my inspiration and role model and my mother, Kaiti for all the strength and courage her unconditional love has given me. I would like to express my deepest gratitude to Giannis Fostiropoulos whose unconditional support has made all of this possible.

Despina, Shoshanna, Kosta, Stavro, Ruben, Giorgo, Yianni, Antoni, Nikola it has been an honor to be your friend and I cannot thank you enough for being there throughout the best and worst of times and for making these years a time I will treasure forever.

Table of Contents

Abstract 2

Acknowledgements 3

Table of Contents 4

List of Figures 6

1. Introduction 8

2. Background, soil model and limit calculation analysis 20

2.1 Problem description 20

2.2 Limit equilibrium solutions 23

2.2.1 Undrained response 23

2.2.2 Drained response 26

2.3 Drained capacity; sustained tensile loading 29

2.4 Literature review 30

3. Numerical Analysis of Caisson Response under Undrained Conditions 35

3.1 The finite element model 35

3.2 Results of base case geometry analysis 37

3.2.1 Load-deformation response 37

3.2.2 Breakdown of reaction forces 38

3.2.3 Failure mechanism 40

3.3 Effect of caisson geometry in undrained response 45

3.4 Comparison of results with existing research 48

4. Numerical Analysis of Suction Caisson Model under Drained Conditions 50

4.1 The finite element model 50

4.2 Results of Base Case geometry analysis 51

4.2.1 Load-deformation response 52

4.2.2 Breakdown of reaction forces 53

4.2.3 Failure mechanism 59

4.3 Effect of wall length 63

4.4 Comparisons of results with existing research 67

5. Numerical Analysis of Suction Caisson under Sustained Loading 69

5.1 The finite element model 69
5.2 Base case analysis 69
5.2.1 Load deformation response 70
5.2.2 Capacity under sustained loading 71
5.2.3 Failure mechanism 75
5.3 Sustained loading capacity for L/d ratios = 0.5,1,2 and 3 80
6. Results and Recommendations 89
References 91
Appendix A 94
Appendix B: Breakdown of undrained loading forces for L/d=0.5,1,2,3 95
Appendix C: Breakdown of drained loading forces for L/d=0.5,1,2,3 99

List of Figures

Figure 1-1 Snorre platform foundations 11
Figure 1-2 Europipe 13
Figure 1-3 Na Kika FDS mooring elevation and suction pile configuration (Source: Newlin 2003) 12
Figure 1-4 . Examples of typical diameter and skirt depths reported in the literature 13
Figure 1-5 Common suction caisson designs 14
Figure 1-6 Forces acting on a suction caisson during installation 15
Figure 1-7 Typical elements of suction caissons 16
Figure 1-8 Nkossa suction foundation prior to installation 18
Figure 2-1 Undrained shear strength (s_u) and initial effective stress (σ'_{v0}) profiles, γ'=11.2kN/m^3 21
Figure 2-2 Forces acting on the caisson under undrained loading 23
Figure 2-3 Forces acting on the caisson under drained loading 26
Figure 3-1 Axisymmetric model in Plaxis for a cylindrical element (Source: Plaxis v.8 reference manual) 35
Figure 3-2 Base case geometry and finite element mesh 36
Figure 3-3 Load deformation response for base case geometry 38
Figure 3-4 Built-up of friction and base resistance forces as applied uplift force increases 40
Figure 3-5 Shear stresses on external caisson wall at the beginning of uplift loading, (stage A Figure 3.4) 41
Figure 3-6 Shear stresses on external caisson wall corresponding at stage G in Figure 3.4 41
Figure 3-7 Development of plastic points during undrained loading for base case geometry 43
Figure 3-8 Incremental total displacements and deformed mesh at failure 44
Figure 3-9 Effect of caisson geometry on undrained load-deformation response 45
Figure 3-10 Mobilization of external side friction. 47
Figure 3-11 Mobilization of internal side friction 47
Figure 3-12 Comparison of results from current studies with existing literature for undrained loading 49
Figure 4-1 Distribution of nodes and stress points in interface elements and their connection to soil elements 51
Figure 4-2 Load-deformation response for L/d=0.65 52
Figure 4-3 The effect of interfaces on the load-displacement response 53
Figure 4-4 Horizontal effective stress distribution on the external caisson wall 55
Figure 4-5 Horizontal effective stress distribution on the internal caisson wall 55
Figure 4-6 Horizontal displacements at failure 56
Figure 4-7 Shear stress on external caisson wall 57
Figure 4-8 Shear stress on external caisson wall 57
Figure 4-9 Build-up of friction resistance as applied uplift force increases 58
Figure 4-10 Development of plastic points during drained loading. 60
Figure 4-11 Deformed mesh at failure-drained loading case 61
Figure 4-12 Vertical displacements at failure-drained loading case 62
Figure 4-13 Incremental vertical displacements at failure-drained analysis for base case geometry 62
Figure 4-14 Effect of caisson geometry on drained load-deformation response 63
Figure 4-15 Normalized external wall horizontal stress 65
Figure 4-16 Mobilization of external side friction 66
Figure 4-17 Mobilization of internal side friction 67
Figure 4-18 Comparison of results from current studies with existing literature for drained loading 68
Figure 5-1 Sustained loading displacements for different load levels 70

Figure 5-2 Time displacement curve for P/Pult,undrained=69% 71
Figure 5-3 Lid displacement and excess pore water pressure with time for base case geometry. 74
Figure 5-4 Development of excess pore pressures with time for $P/P_{ult,undrained}$=69% 77
Figure 5-5 Development of plastic points with time for $P/P_{ult,undrained}$=69% 78
Figure 5-6 Deformed Mesh at t = 45 days....79
Figure 5-7 Vertical displacement of caisson at t=45.... 81
Figure 5-8 Vertical Displacement at t=45days 79
Figure 5-9 Sustained loading displacements for different load levels.....80
Figure 5-10 Lid displacement and Excess Pore Water Pressure with time for L/d=0.5 geometry.....81
Figure 5-11 Sustained loading displacements for different load levels.....82
Figure 5-12 Lid displacement and excess eore water pressure with time for L/d=1 geometry. 83
Figure 5-13 Sustained loading displacements for different load levels.....84
Figure 5-14 Lid displacement and excess pore water pressure with time for L/d=2 geometry. 85
Figure 5-15 Sustained loading displacements for different load levels, L/d=3. 86
Figure 5-16 Lid displacement and excess pore water pressure with time for L/d=3 geometry. 87
Figure 5-17 Effect of caisson geometry on minimum period over which loads can be sustained....88

1. Introduction

1.1 Suction piles

Over the last decades, oil and natural gas exploration and production have been moving into deeper waters (depths from 1,000 to 2,500m). This transition became technologically and economically viable through the development of innovative structures and foundations, including suction caissons and anchors. At the same time, there is large growth in wind turbine projects which are being planned further offshore where the winds are stronger and more reliable. Here the use of anchors can provide a technical and cost effective solution to make these projects financially viable.

Suction caissons are hollow cylindrical foundations with a closed top. They are installed by the action of their buoyant self weight and by applying differential pressure between the caisson chamber and the surrounding ocean. The terms suction anchors, skirted and bucket foundations refer to the same general configuration as suction caissons. Details about their differences are provided in Section 1.2.

Suction caissons and anchors have proven to be competitive alternatives to more traditional foundation solutions such as piles and drag anchors in various types of soils and for a wide range of fixed and floating offshore structures. Firstly, there are significant cost savings compared to traditional piles and anchors. The fabrication costs are usually lower and due to their small weight, the installation equipment needed is less expensive, while the installation times become significantly shorter compared to piles. Simplified installation procedures lessen the risk from storms hence increase installation safety.

At the same time, suction piles have a number of operational advantages over traditional foundations. In short term loading they can provide a significant uplift resistance due to the development of suction pressures which can be sustained over significant time periods.

Another advantage of suction foundations is that they can be positioned very accurately and do not require drag-in operation or proof loading and thus when they are used to anchor floating structures they help reduce interference issues between the moorings of adjacent structures. This is particularly important for wind farms, where there is a large density of mooring cables. Furthermore, suction foundations have environmental and economic benefits as they can be retracted and potentially redeployed at different sites (Andersen and Jostad, 1999).

1.2 History and types

Shallow water oil production structures historically comprised jacket foundations with steel frame superstructures which were fixed to the sea floor through driven cylindrical open-ended steel piles. The discovery of oil in the North Sea, where the soil is generally stiffer than in other areas such as the Gulf of Mexico, allowed the use of shallow foundations in the design of massive gravity structures that rely on deadweight for stability. The design of the gravity platforms introduced the use of vertical walls-called skirt piles- which extended into the foundation soils in order to increase the lateral stability. A pump was used to remove the water trapped between the sea floor and the base of the gravity foundation. At the same time, in Norway, smaller steel tubes with closed tops and open bottoms-termed bucket foundations- were placed under the legs of the traditional jacket foundations and installed with the aid of suction (Tjelta, 1994). These first bucket foundations, had depth to diameter ratios that ranged between 0.5 and 1.5 and were designed to act in compression while tensile loading was resisted by surcharge applied at their top.

At deeper water sites, the use of jacket foundations became uneconomical and led to the design of tension leg platforms (TLPs) which are floating structures supported by buoyancy and tethered to the sea bed. Initially, driven pile foundations were used to anchor TLP structures, but the evolution from bucket foundations has also led to the deployment of suction caissons as permanent foundations for TLPs.

The Snorre platform in the North Sea was the first TLP to implement the suction caisson concept (Fines et *al.*, 1991). The Snorre platform is located in soft clay at a water depth of 310m. The foundations consist of four legs, each one having three bucket foundations as shown in Figure 1.1. During the design of the platform, two large scale offshore installation trials were conducted using instrumental steel cylinders that penetrated 22m into the ground. Dead weights were placed on top of the suction foundations in order to ensure that the loading remained purely compressive thus leaving the tensile capacity un-utilized (Iskander et *al.*, 2002). Since then, many studies have examined the potential of suction piles to provide significant tensile capacity.

In 1995, the piles at the end of the Europipe jacket structure were replaced with bucket foundations Tjelta (1994). The significance of this project lies in the fact that it was the first time that bucket foundations were used as the only permanent foundation with suction providing the primary foundation installation system in dense sand. Similar structures had only been installed in soft to firm clays (for example Snorre).

The Europipe site in the North Sea consists or a 25m layer of dense to very dense sand overlying stiff to hard clay at a water depth of 70m. Four suction piles were used at the legs of the jacket as shown in Figure 1.2. Their diameters were 12m and the skirt length 6m. The largest tensile load was 13.9MN and the largest compressive load 56.7MN (Bye et *al.,* 1995). Tjelta (1994, 1995) performed a series of field tests, FE analysis and used previous field experience to prove the feasibility of using suction caissons to provide tensile resistance in dense to very dense sands.

The Na Kika Floating Development System (FDS) is located in the Gulf of Mexico and was built to handle oil and gas production from five independent fields located at water depths between 1,400 and 2,300m (Newlin, 2003). As shown in Figure 1.3 it is supported by a semi-taunt mooring system with suction piles at the bottom which are being loaded predominantly in the lateral direction. Suction is only used as an installation technique and the underpressure is not

used to provide resistance to tensile loads during service. The platform was designed based on safety criteria for the whole system (Newlin, 2003). Probability distributions for maximum mooring line tension was based on results of long term mooring analyses which account for the global response of the platform when subjected to a Gulf of Mexico environmental database. For the anchor resistance, a probability distribution function was generated based on limited existing data on skirted foundations and on random variations in overburden pressure and undrained shear strength.

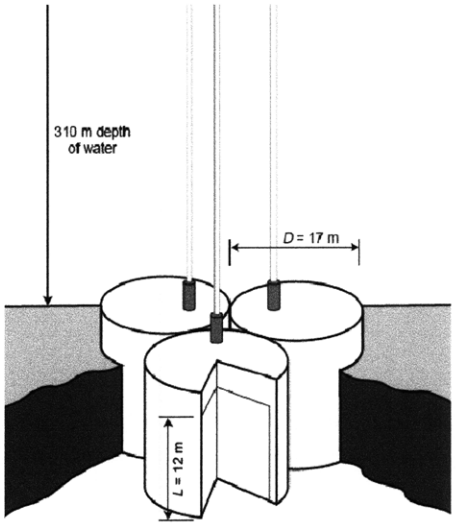

Figure 1-1 Snorre platform foundations (Source: Zdravkovic et *al.* 2001)

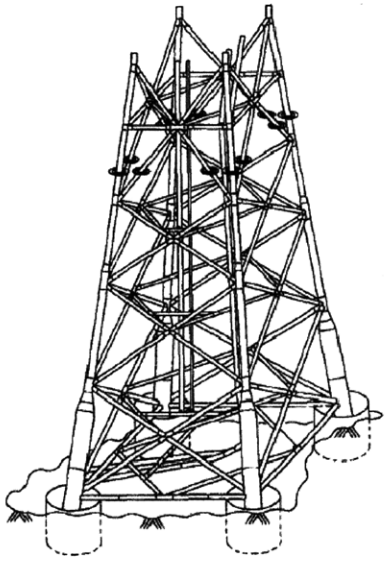

Figure 1-2 Europipe (Source: Bye et *al.* 1995)

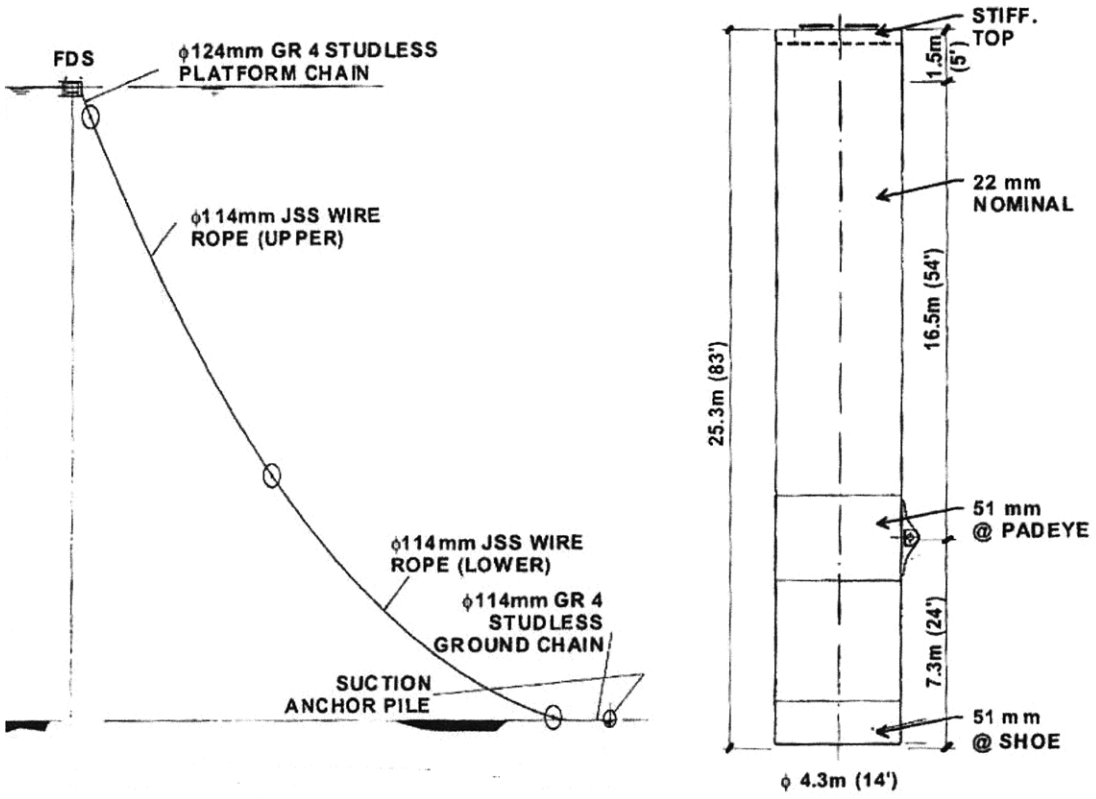

Figure 1-3 Na Kika FDS mooring elevation and suction pile configuration (Source: Newlin, 2003)

The term suction caisson refers to the cylindrical open bottom foundation installed with the use of suction at its top part. Other terms which usually refer to the same structure are skirted foundations or skirted anchors. Usually the terms skirted or suction foundation is used when the concept is applied to fixed platforms and the term skirted or suction anchors when the concept is applied to floaters (Andersen and Jostad, 2004).

Suction caissons are typically used in sands as shallow foundations and have length to diameter ratios, $L/d \leq 1$. In clays, suction caissons are typically used as anchors and the L/d ratio can be as large as 6. Randolph and Chen (2007) report that the majority of modern suction caissons have ratios between 3 and 6. Houlsby and Byrne (2004) present typical diameter and skirt depths reported in the literature. Suction caissons have smaller wall thickness than the tubular driven

piles they replaced. Chen and Randolph (2007) report that for suction caissons the ratio of diameter to thickness, d/t is in the range 60-200 while for piles the equivalent range is 30-50.

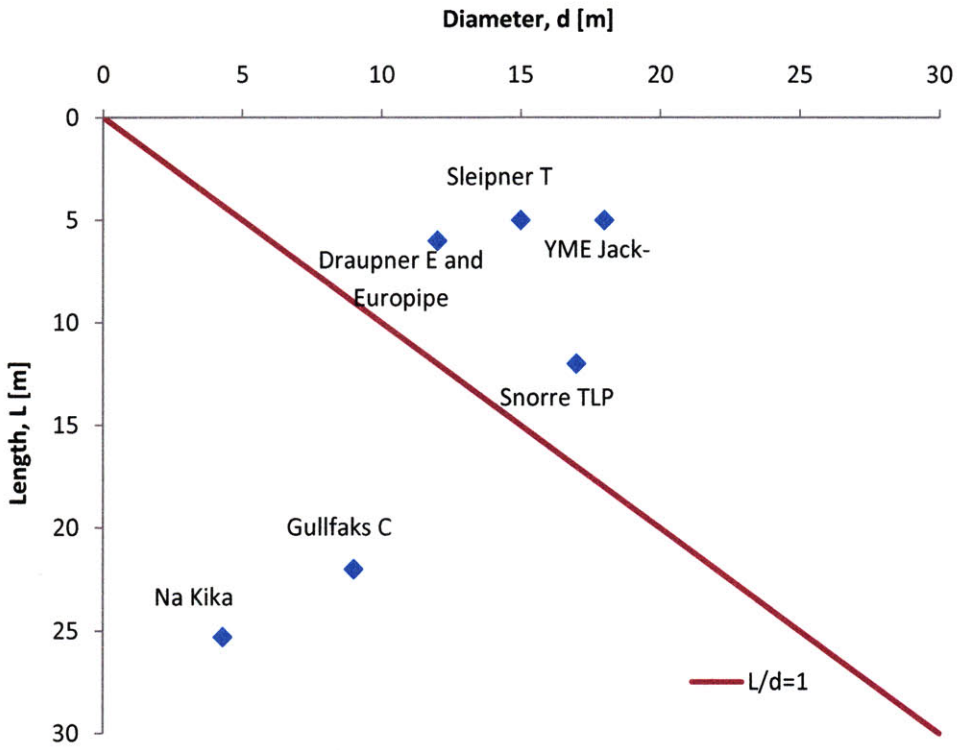

Figure 1-4 . Examples of typical diameter and skirt depths reported in the literature. Source: Houlsby and Byrne (2004)

Suction anchors can be used separately or clustered and have a number of structural features that improve their performance. Figure 1.5 shows some of the most common designs (Delft University of Technology). One variation to the original caisson design are flat back anchors which can be either triangular or square in order to provide horizontal stability during transportation and prevent deck skidding. As shown in Figure 1.5 internal stiffeners or external flaps can be used to increase the caisson soil interface area and hence increase the frictional resistance.

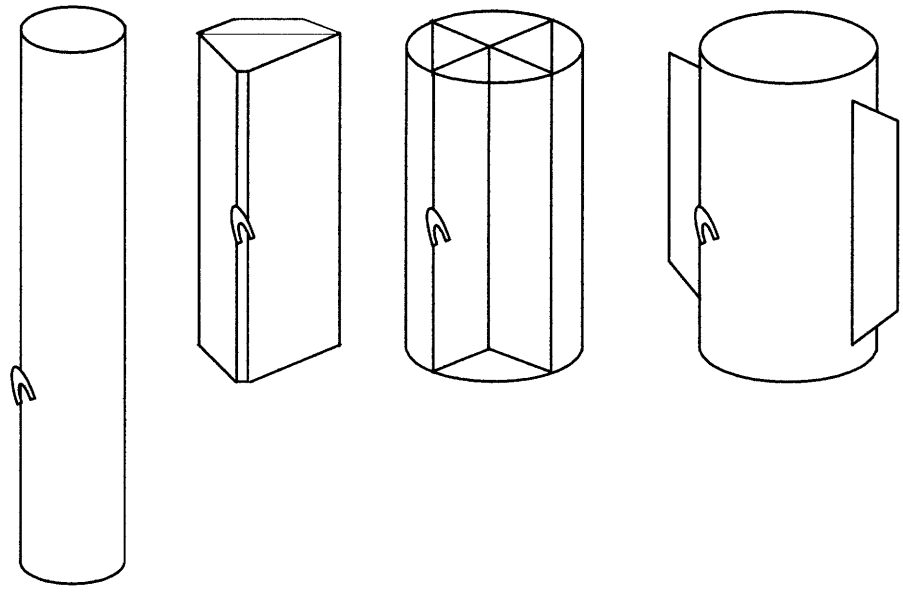

Figure 1-5 Common suction caisson designs (Source: Delft University of Technology)

1.3 Detailed description, installation and loading conditions

During the first stage of the installation, suction caissons penetrate into the soil under their self weight. Further penetration is achieved by pumping water out of the top part of the caisson thus creating an underpressure inside the caisson. The difference between the hydrostatic water pressure outside the caisson and the pressure below its lid induces a penetration force that pushes the caisson into the required depth. The forces that act on the caisson during installation are shown in Figure 1.6.

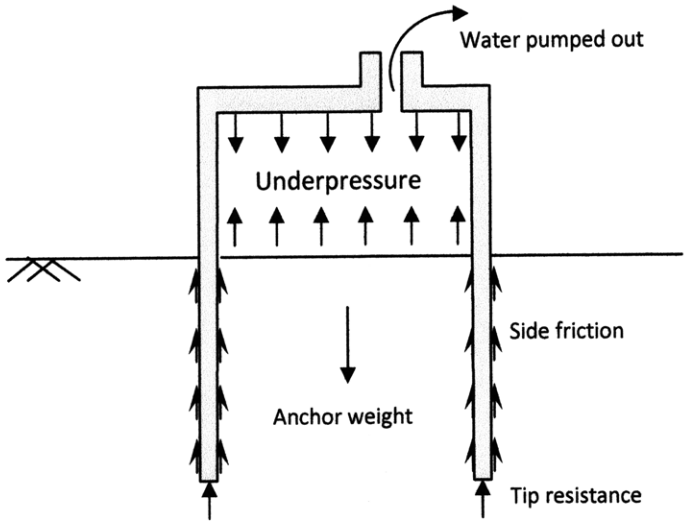

Figure 1-6 Forces acting on a suction caisson during installation

Upon installation the shear strength along the outside wall will be reduced to the remoulded shear strength. After installation, there is a setup in stresses acting on the pile due to redistribution and dissipation of installation pore pressures and thixotropy (Andersen and Jostad, 2004). Andersen and Jostad (2004) propose a method to calculate the strength after installation by assuming that caisson penetration is accommodated by purely inward soil movement. In this case the radial stress does not change and only shear is applied on the soil adjacent to the external caisson wall. This method suggests a shear strength between 58-65% of the intact shear strength after 90% consolidation for normally consolidated clays. Subsequent field measurements by Andersen et *al.* (2004) indicate that only 30-50% of the soil displaced by the caisson tip flows inward during the combined self-weight and suction installation. For the purposes of this study, it is going to be assumed that the caisson is wished in place and so the results of the finite element analysis should be viewed in light of this fact.

Figures 1.7 and 1.8 show a suction caisson used in the Nkossa platform (Colliat, 1995) and a schematic representation of a suction anchor. The main components of a typical suction pile are shown in Figure 1.7. In some cases, where the loading is mainly horizontal and the vertical

load can be supported by caisson self weight and friction, the caisson lid is retrievable (Andersen and Jostad, 1999). Since the underpressure is not necessary for the operation of the foundations, the lid can be retrieved to reduce fabrication costs.

In many cases tethers are attached on the external surface of the caisson which is inside the soil. A pad-eye is used for that purpose. In addition, caissons can have pad eyes near the lid that are used during the installation process as shown in Figure 1.7.

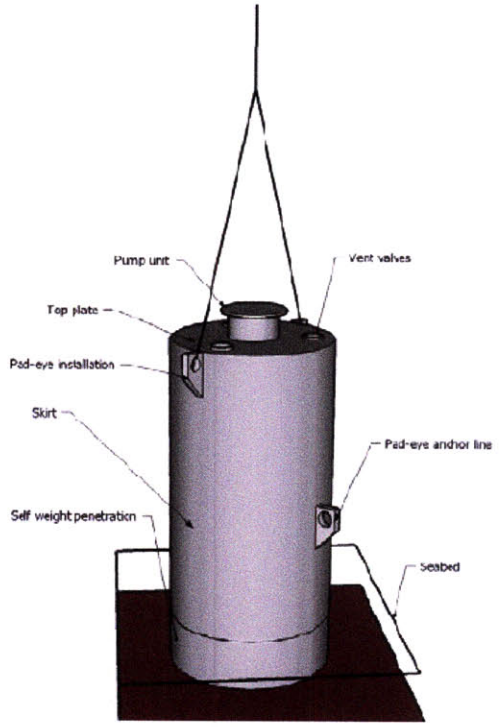

Figure 1-7 Typical elements of suction caissons (Source: Delft University of Technology)

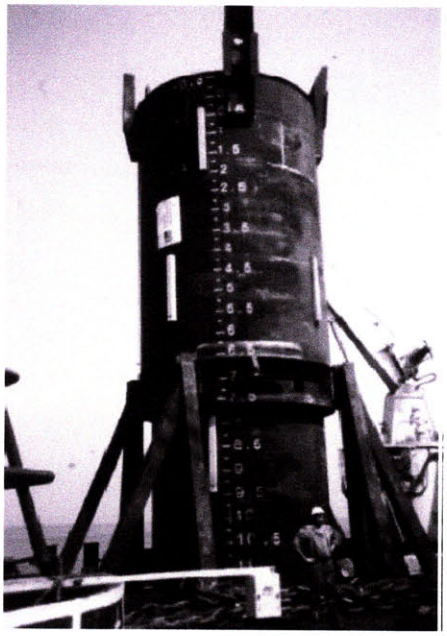

Figure 1-8 Nkossa suction foundation prior to installation (Source: Colliat, et *al.* 1995)

Suction foundations may be subjected to permanent loads and high and low frequency cyclic loads. Loads include vertical, horizontal and moment components. Permanent loads usually consist of the weight of the caisson structure and the weight or pretension loads from the platform. High frequency cyclic loads are caused by waves that occur during the design storm. The design storm is composed of a number of cyclic loads with varying magnitudes (See Section 2.3 for more discussion).

Low frequency cyclic loads can be caused by wind, current, tide, storm surge and waves. Resonance oscillations may also cause low frequency cyclic loads. The period of these loads is higher than the wave period and may be several hours or more. Loop current loads may also be classified as a low frequency load. Due to rate effects, the shear strength of clays may be lower for long duration loads and low frequency cyclic loads than for high frequency cyclic loads (Andersen and Jostad, 1999).

1.4 Literature review

Understanding about the behaviour of suction caissons has been obtained by field measurements, model caisson experiments and finite element analysis. Field tests on small and full scale caissons have been used to determine the effects of caisson installation and the subsequent caisson performance. Field tests can provide reliable data given the specific site characteristics, but have high costs. Examples of field tests include Hogervorst (1980), Tjelta et *al.* (1986) and Tjelta (1995) for the purposes of Europipe.

A large number of laboratory tests on suction caissons can be found in the literature. One category are centrifuge tests which simulate the stress conditions and soil response at the field scale. Examples of centrifuge caisson tests include Clukey et *al.* (1995) and Randolph et *al.* (1998).

Another category, are tests on model suction caissons under 1-g and controlled laboratory conditions. (Wang et *al.* 1977, Steensen-Bach 1992, Rao et *al.* 1997, El-Gharbawy and Olson 1999, El-Gharbawy et *al.* 1999, Whittle et *al.* 1998, Byrne and Houlsby 2002). The caissons studied were of L/d ratio in the range of 2-12 and were tested under various loading conditions. Some of the early laboratory tests on model suction caissons conducted (for example Finn and Byrne, 1972 and Wang et *al.* 1977) were focused on studying caisson feasibility and identifying important parameters governing their performance. More recent laboratory tests (Rao et *al.* 1997, El-Gharbawy and Olson 1999) focus on optimizing their design.

One of the first publications on suction caisson was an experimental and theoretical and finite element study by Finn and Byrne (1972) which is further discussed in Chapter 2. Recent finite element studies of caisson behaviour involve axisymmetric and three-dimensional numerical simulations. Some examples include Sukumaran et *al.* (1999), Erbrich and Tjelta (1999), El-Gharbawy and Olson (2000), Zdravkovic et *al.* (2001) and Deng and Carter (2002). Most of these studies attempt to determine the caisson capacity under different loading and drainage conditions. Sukumaran et *al.* (1999) and Erbrich and Tjelta (1999) used the commercial finite element code ABAQUS, El-Gharbawy and Olson (2000) used the commercial finite element code PLAXIS developed for geotechnical computations, Zdravkovic et *al.* (2001) used the three dimensional Fourier series aided finite element method (FSAFEM) and Deng and Carter (2002) used the finite element software AFENA.

In all cases the suction caisson was wished in place, with no attempt to simulate the installation process. In addition, a perfectly rigid interface was assumed between the caisson and the surrounding soil skeleton. The initial state of stress in the soil skeleton was typically estimated in terms of the submerged unit weight and the lateral earth pressure coefficient at rest, K_0.

Chen and Randolph (2007) note that currently there are no established design guidelines for the uplift capacity of suction caissons in marine clays. Calculations are usually based on conventional design methods for open-ended driven piles (e.g. API, 1993) and also on the results of an industry sponsored study (Andersen et *al*,. 2005).

1.5 Scope of this study

The purpose of this study is to conduct finite element analysis of the response of suction caisson subjected to tensile vertical loading under three loading conditions:

(a) undrained loading representing the short term performance of suction caissons in clay

(b) drained loading representing the long term performance of suction caissons

(c) constant sustained loading; in this case excess pore pressures are let to dissipate with time and this loading condition represents the caisson behaviour in the medium term

Theoretical limit equilibrium models for loading conditions (a) and (b) are presented in Chapter 2. These solutions are used as a reference when assessing the results of the finite element analysis. In addition, a number of significant theoretical and finite element studies on these 3 loading cases are discussed in Chapter 2.

Chapters 3, 4 and 5 present the results of the finite element analysis for each of the three loading cases. The finite element code Plaxis v.8.5 is used for all the analyses.

Chapter 6 discusses the findings and presents the conclusions of this study.

2. Background, soil model and limit calculation analysis

2.1 Problem description

This research uses finite element analysis to model the response of suction caisson subjected to tensile vertical loading under three loading conditions:

(a) continuous monotonic tensile loading applied within a relatively short time, such that there is no migration of pore fluid within the surrounding soil (undrained shear)

(b) continuous monotonic tensile loading, such that the response is fully drained and excess pore pressure never develop or dissipate instantaneously (drained conditions)

(c) sustained tensile loading such that excess pore water pressures develop instantaneously after the full load is applied and are allowed to dissipate over time

The caisson is modelled as wished-in-place so that the surrounding soil remains undisturbed (i.e. no deformations or change of in-situ stresses, pore pressures or soil properties). Furthermore it is assumed that the shear resistance at all soil-caisson interfaces is controlled by the shear strength of the soil adjacent to the caisson. A perfectly rough interface is assumed such that $\tan\delta' = \tan\phi'$, where δ' is the interface friction angle and ϕ' the internal friction angle.

The finite element analyses assume that the soil is isotropic and can be characterized by the Mohr-Coulomb, elastic-perfectly plastic soil model. The Mohr-Coulomb model is generally considered a rather crude approximation of the behaviour of typical marine clays and the use of Modified Cam Clay (MCC) or MIT-E3 models has been preferred in similar analysis found recently in the literature (Deng and Carter, 2002 (MCC) and Zdravkovic et *al.*, 1998 (MIT-E3)). One of the purposes of this research is to assess the effectiveness of using a simple Mohr-

Coulomb model to predict the ultimate caisson capacity by comparing the results with previous studies that use more complex models.

An undrained shear strength ratio s_u / σ'_{v0} =0.33 is used. This ratio is typical of low plasticity K_0 -normally consolidated clays (such as Boston Blue Clay) in triaxial compression (Zdravkovic et *al.* 2001, Hight et *al.* 1987). It should be noted that anisotropic models would use a much smaller undrained shear strength ratio in triaxial extension or direct simple shear modes. Ladd (1992) shows that medium to high plasticity K_0 -normally consolidated clays have on average undrained strength ratio s_u / σ'_{v0} =0.2. The effective stress and shear strength profiles for the current numerical experiments are shown in Figure 2.1.

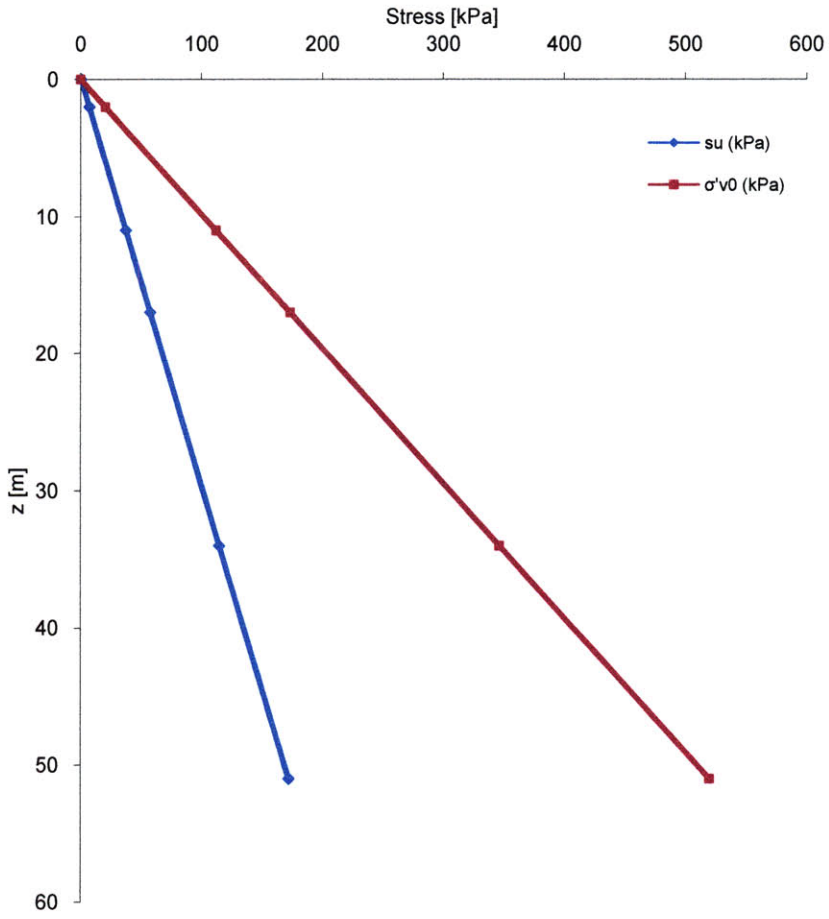

Figure 2-1 Undrained shear strength (s_u) and initial effective stress (σ'_{v0}) profiles, γ'=11.2kN/m^3

The soil strength can also be expressed in terms of the Mohr-Coulomb effective stress parameters (c', ϕ'). For undrained shearing with dilation angle ψ=0^0 and cohesion c'=0 in plane strain conditions, the following relationship can be used to represent undrained strength using effective stress parameters:

$$\frac{s_u}{\sigma'_{v0}} = \frac{(1+K_0)\sin\phi'}{2} \tag{2.1}$$

The derivation of this relationship is shown in Appendix A.

The soil is assumed to have a friction angle ϕ'=28^0. The friction angle chosen is typical of high to medium plasticity normally consolidated clays found in the marine environment (Poulos, 1988). The coefficient of lateral earth pressure K_0 is obtained by solving Equation 2.1 for the specified friction angle and undrained strength ratio. This yields K_0=0.49. The assumed submerged unit weight of the soil, γ'=11.2 kN/m^3. It was assumed that the soil is saturated and that Darcy's law governs flow of pore fluids through the voids of the soil skeleton. In offshore problems, the pore pressures at the mudline ($u_{mudline}$) are very large. Therefore, for the calculations we define a pore pressure $\bar{u} = u - u_{mudline}$. Thus initial pore pressure is hydrostatic with the groundwater table located at the top of the soil surface.

The following section describes each of the three loading conditions and provides a limit equilibrium analysis which is used to assess the results of the finite element analysis in Chapters 3-5. We expect the limit equilibrium solutions presented here to give the same capacity as the finite element analysis in Chapters 3-5 apart from the K_0 issue and the neglect of the tip resistance.

2.2 Limit equilibrium solutions

2.2.1 Undrained response

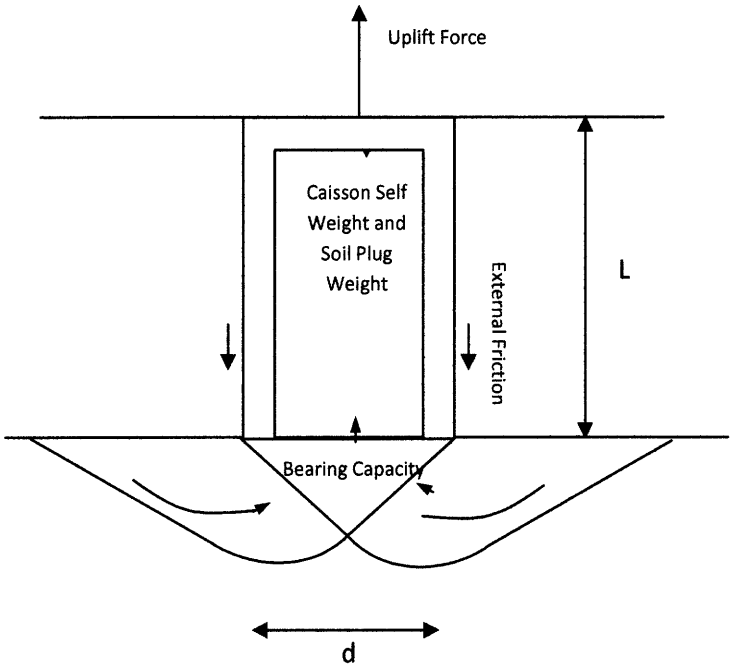

Figure 2-2 Forces acting on the caisson under undrained loading

At the end of the caisson installation, the caisson is forced to remain at the soil surface because of the pressure differential induced during suction installation. In clays, as soon as there is an uplift force, the suction caisson mobilises significant pullout capacity through the development of negative changes of pore water pressure inside the soil plug and at the bottom of the caisson. The length of time these suction changes can be maintained depends on the loading conditions and the drainage properties of the soil. When the caisson is loaded at a sufficiently high rate so that fully undrained conditions apply the suction will in theory not break down.

Most previous studies suggest that the undrained response provides the upper limit to the pullout capacity of suction caissons (ex. Finn and Byrne, 1972 and Deng and Carter, 2002). It is generally accepted that the ultimate capacity under undrained conditions can be calculated by assuming a reverse bearing capacity failure mechanism as shown in Figure 2.2. Finn and Byrne (1972) were the first to suggest this mechanism and argued that the response should be

equivalent in tension or compression, the same way it is for a flat punch welded on an identical material. Subsequent experimental and finite element studies widely confirmed the reverse bearing capacity theory for suction caissons (for example Wang et *al.* 1977, Andersen et *al.* 1993 and others).

The caisson self weight (P_c) also contributes to resisting the uplift forces. Under undrained conditions there is no drainage or change of volume and the soil inside the caisson remains attached to the lid and the skirt. As the caisson fails forming a reverse bearing capacity mechanism, the soil plug, which has a weight P_s remains attached to the caisson and contributes to the caisson resistance. At the same time frictional resistance develops at the external caisson-soil interface ($P_{f,ext}$).

Then the ultimate capacity of the caisson ($P_{ult,undrained}$) is expressed as:

$$P_{ult,undrained} = P_b + P_{f,ext} + P_c + P_s \tag{2.2}$$

The bearing capacity (P_b) of the caisson is obtained from the classical bearing capacity theory (Skempton, 1951).

$$P_b = A\zeta_s\zeta_e N_c s_{u(tip)} \tag{2.3}$$

Where: A : caisson base area

ζ_s : shape factor

ζ_e : embedment factor

N_c : bearing capacity factor

$$\zeta_s = 1 + 0.2 * D / D = 1.2$$

$$\zeta_e = 1 + \sqrt{0.053(L / d)} = 1.18$$

The external friction is obtained from:

$$P_{f,ext=} \int_{As,ext} f_s dA_{s,ext}$$

Where f_s is the skin friction per unit area along the caisson wall, and $A_{s,ext}$ the area of the external caisson surface. Assuming the soil caisson interface is rough: $f_s = s_u$ at failure. Thus the external friction at failure is expressed as:

$$P_{f,ext} = \frac{1}{2}\pi dLs_{u(tip)} \tag{2.4}$$

In order to compare the results with existing research, it is useful to define the net pullout capacity:

$$P_{ult(net),undrained} = P_{ult,undrained} - P_{ult} - P_c = \frac{1}{2}\pi dLs_{u(tip)} \tag{2.5}$$

Finite element analysis was used for five different geometries. The base case geometry is a cylindrical caisson (γ_c=24kN/m^3) with length L = 11m, diameter d = 17m and thickness t = 1m. The caisson axial capacity is calculated using limit equilibrium:

$$F_b = A\zeta_s\zeta_e N_c s_{u(tip)} = 62{,}210\text{kN}$$

$$P_{f,ext} = \frac{1}{2}\pi dLs_{u(tip)} = 10{,}870\text{kN}$$

$$P_c = \gamma_c\pi[R^2L - (R-t)^2(L-t)] = 17{,}510\text{kN}$$

$$P_s = \gamma'\pi(R-t)^2(L-t) = 18{,}010\text{kN}$$

$$P_{ult(net)} = P_b + P_{f,ext} = 73{,}080\text{kN}$$

2.2.2 Drained response

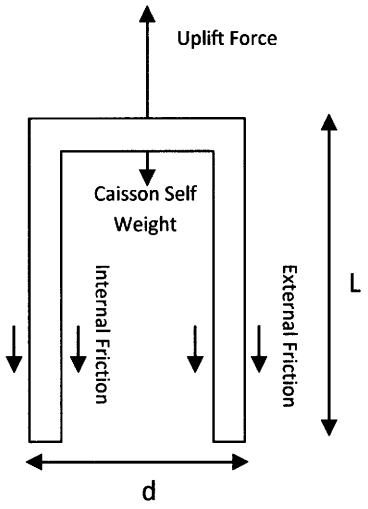

Figure 2-3 Forces acting on the caisson under drained loading

When the caisson is pulled at a sufficiently slow rate or when long term conditions are considered then excess pore water pressures dissipate fully and the response is drained. In order to simulate the drained capacity of the caisson, the first scenario in the analysis assumes that no passive suction develops at the bottom of the caisson after installation and the application of the full anchor load. Thus, when the drained capacity is reached, the soil plug inside the caisson remains in its initial position and the caisson slides upwards. In this case the pull out force is resisted by friction on the internal and external walls of the caisson as well as by a small force at the tip. Experimental studies in the literature (ex. Luke et *al.*, 2005) find that the tip resistance is very small in practice. Then the ultimate capacity of the caisson ($P_{ult,drained}$) is expressed as:

$$P_{ult,drained} = P_{f,ext} + P_{f,\text{int}} + P_c \tag{2.6}$$

Where $P_{f,ext}$ and $P_{f,\text{int}}$ are the skin friction on the external and internal walls and P_c is the submerged weight of the caisson.

Then the net pullout capacity is:

$$P_{ult(net),drained} = P_{f,ext} + P_{f,\text{int}} \tag{2.7}$$

The external and internal skin frictions are obtained from:

$$P_{f,ext=} \int_{As,ext} f_s dA_{s,ext} \tag{2.8a}$$

$$P_{f,\text{int}=} \int_{As,\text{int}} f_s dA_{s,\text{int}} \tag{2.8b}$$

Where f_s is the skin friction per unit area along the caisson walls and $A_{s,ext}$ and $A_{s,\text{int}}$ the areas of the external and internal caisson surface. At any depth z, f_s can be expressed as:

$$f_s = \sigma'_h \tan\delta' \tag{2.9}$$

Where σ'_h is the effective horizontal stress acting on the soil caisson interface friction angle.

At failure: $$\sigma'_h = K\sigma'_v \tag{2.10}$$

It is difficult to estimate the exact value of K considering that the soil has been disturbed and then reconsolidated. Even when the caisson is assumed to be wished in place, there is some initial settlement as a result of the caisson self weight. Here it will be assumed K_0 conditions continue to apply during failure and that the vertical effective stress σ'_v remains constant:

$$\sigma'_h = K_0\sigma'_{v0} \tag{2.11}$$

After solving Equations 2.8-2.9, the external and the internal frictions are:

$$P_{f,ext}=\frac{1}{2}\pi dLK_0 \tan\phi'\sigma'_v\big|_{z=L} \tag{2.12a}$$

$$P_{f,int}=\frac{1}{2}\pi(d-2t)K_0 \tan\phi'(L\sigma'_v\big|_{z=L}-t\sigma'_v\big|_{z=t}) \tag{2.12b}$$

Thus the net pullout capacity is:

$$P_{ult(net),drained}=P_{f,ext}+P_{f,int}=\frac{1}{2}\pi K_0 \tan\phi'\gamma'\left[dL^2+(d-2t)(L^2-t^2)\right] \tag{2.13}$$

Finite element analysis was used for five different geometries. The base case geometry is a cylindrical caisson (γ_c = 24kN/m^3) with length L = 11m, diameter d = 17m and thickness t = 1m. The caisson axial capacity is calculated using limit equilibrium:

$$P_{f,ext}=\frac{1}{2}\pi dLK_0 \tan\phi'\sigma'_v\big|_{z=L} = 8{,}650\text{kN}$$

$$P_{f,int}=\frac{1}{2}\pi(d-2t)K_0 \tan\phi'(L\sigma'_v\big|_{z=L}-t\sigma'_v\big|_{z=t}) = 7{,}570\text{kN}$$

$$P_c=\gamma_c\pi[R^2L-(R-t)^2(L-t)] = 17{,}510\text{kN}$$

$$P_{ult(net),drained}=P_{f,ext}+P_{f,int} = 33{,}730\text{kN}$$

2.3 Drained capacity; sustained tensile loading

The maximum tensile load applied to the suction caisson is associated with the maximum wave in the most extreme storm. These loads will typically occur in just a few seconds (Clukey et *al.*, 2004) and the response in clays will remain undrained. A further consideration is the cyclic nature of the storm load and in some cases (e.g. the Gulf of Mexico) loop current loading which can be sustained for several days or even weeks (Clukey et *al.*, 2004). Cyclic loading can be dealt with by considering the effects of a characteristic storm to the shear strength of the soil. Det Norske Veritas (2005) recommendations for the design of suction piles in clays uses a characteristic storm with a constant wave height that produces the 100-year reduction in shear strength, and duration of 3 to 6 hours.

For loop current loading the period over which the load is sustained is even longer and the capacity of the caisson is expected to be between the undrained and the drained capacities depends on the drainage properties of the soil.

The third loading scenario examined in this study is that of the sustained constant tensile loading. Immediately after the application of the load, the resisting forces are the ones described in the undrained loading scenario. During the sustained loading, significant pore pressure dissipation can occur. This reduction in pore pressures can enhance the external skin friction (Clukey et *al.*, 2004), but may decrease the influence of the pore pressure reductions that mobilize the full reverse bearing capacity. Since in many cases the contribution of the reverse bearing to the overall capacity can be as high as 50%, the dissipation of excess pore water pressures can have a critical impact on the caisson performance. The finite element analysis in Chapter 5 examined this reduction in the caisson capacity for a number of different geometries and predicts the maximum time that a certain load can be sustained before caisson pull-out occurs.

2.4 Literature review

As discussed in Chapter 2, a significant number of field tests, experimental, finite element and theoretical research have been reported in the last three decades. Here we introduce the assumptions and the results of five finite element studies which attempt to establish the capacity of suction caissons in clays while providing different approaches and looking at different aspects of caisson behaviour under tensile loading.

Finn and Byrne (1972) were among the first to investigate the performance of suction piles and set the framework for much of the future research. They conducted laboratory model studies in order to establish the factors that affect the pullout capacity of the suction caisson and the mechanisms that develop under different conditions. They suggested two possible failure mechanisms: a general shear failure and a local shear failure depending on whether drainage was allowed or not. The general shear failure was a reverse bearing failure which occurred under undrained conditions. When the sealing against drainage was not perfect or when the rate of load application was small partial drainage occurred and eventually the caisson slid upwards. Finn and Byrne observe that the mechanism of general shear failure cannot usually occur in complete form because the elastic deformations necessary are quite large and eventually lead to a breakdown in the suction during shallow depth tests.

A large proportion of the research on the axial tensile capacity of suction caissons examines the axial capacity with the horizontal capacity and investigates the effects of combined horizontal and vertical loading. One of the first studies to attempt this was by Zdravkovic et *al.*, 2001 followed by a number of papers by Deng and Carter.

Zdravkovic et *al.* (2001) present a parametric short term pullout capacity analysis and examine the effects of load inclination, skirt length, caisson diameter, soil adhesion and anisotropy. They plot combinations of vertical and horizontal loading at failure and examine how horizontal loading reduces the vertical capacity and vice versa. They find that the vertical and horizontal

capacity curves for different lengths and identical diameters are self similar, and that controlling for the L/d ratio forces all curves to collapse to a single vertical against horizontal capacity curve. One of the findings of their finite element analysis is that for tether inclination smaller than 10 degrees to the horizontal, the vertical capacity can reduce by 20%. Furthermore, Zdravkovic et *al.* (2001) is one of the first studies to look at the effects of anisotropy. They compare results from the anisotropic MIT-E3 and the Modified Cam Clay models and find that anisotropy reduces the capacity by approximately 22%.

Deng and Carter (2002) present a theoretical investigation of suction caissons under axial tensile loading for three different soil conditions; undrained, drained and partially drained. Theoretical limit equilibrium solutions are derived, based on the results of a finite element study and then validated by previous field experiments and model test results.

Deng and Carter (2002) express the undrained capacity as a function of the caisson L/d ratio and the characteristics of the soil. Starting from the theoretical limit equilibrium model shown in section 2.2.1 they transform the equations as follows:

Equation 2.4 can be expressed as $P_{f,ext} = \frac{1}{2}\pi dLs_{u(tip)}$ or $P_{f,ext} = \alpha A\zeta_s\zeta_e s_{u(tip)}$ where α is a constant of proportionality. Then the net caisson capacity can be written as:

$$P_{ult(net),undrained} = P_b + P_{f,ext} + A\zeta_s\zeta_e N_c s_{u(tip)} + \alpha A\zeta_s\zeta_e s_{u(tip)} = N_p\zeta_s\zeta_e s_{u(tip)} \quad (2.14a)$$

From finite element predictions the value of N_p was expressed as:

$$N_p = 7.9\left(\frac{L}{d}\right)^{-0.18} \quad (2.14b)$$

This result is used to compare the results of the finite element analysis under undrained conditions presented in Chapter 3.

For the drained case, Deng and Carter (2002) transform Equation 2.9 by introducing a drained uplift factor (η) to take account of the relationship between the interface angle (δ') and the soil friction angle (ϕ'), and the difference between K_0 and $\frac{\sigma'_h}{\sigma'_v}$.

The dimensionless factor η is introduced to take account of the relationship between the interface friction angle δ' and the soil friction angle ϕ', as well as the correlation between the horizontal effective stress in the soil σ'_h to the original in situ vertical effective stress σ'_{v0}. For normally consolidated soil Mayne et.*al.* (1982) approximation is used: $K_0 = 1 - \sin\phi'$. Then Equation 2.9 may be written as:

$$f_s = \sigma'_h \tan\delta' = \eta K_0 \tan\phi' = \eta\gamma' z(1-\sin\phi')\tan\phi' \tag{2.15}$$

By combining Equations 2.8 and 2.15, the net capacity per unit area is expressed as:

$$p_{u(net),drained} = 4\eta\left(\frac{L}{d}\right)(1-\sin\phi')\tan\phi'\sigma'_v\big|_{z=L} \tag{2.16a}$$

It is assumed that η depends only on the L/d ratio and the results of a finite element analysis are used to obtain an expression for η:

$$\eta = 0.91\left(\frac{L}{d}\right)^{-0.46} \tag{2.16b}$$

In Chapters 3 and 4 we use Equations 2.14 and 2.16 and compare the net pullout capacity with the results from our finite element analysis.

One of the more recent and advanced finite element studies is presented by Maniar et *al.* (2005). The authors developed a computational procedure which attempts to accurately simulate the behaviour of suction caisson, including the effects of self-weight and suction

installation into clayey soils. The soil is treated as a two-phase medium consisting of a porous solid and water. The nonlinear behaviour of the soil skeleton is described by means of a bounding surface plasticity model. A frictional contact algorithm is used to describe the caisson-soil interaction and this is based on a slide-line formulation that allows large relative displacement between the caisson and the soil. Among other results, Maniar et *al.* (2005) predict the axial capacity of suction caisson under all three loading conditions described in this thesis and comparisons with laboratory measurements are provided. In most cases finite element predictions underestimated experimental results by about 15%. The differences were generally higher for the undrained loading conditions compared to the drained cases. Their finite element results for undrained loading indicate that 42-44% of the caisson capacity is due to forces at the base. In addition the interior friction was assessed to be significantly lower than the exterior friction and more specifically 3 to 6 times lower.

Clukey et *al.* (2004) perform centrifuge tests and finite element analysis on typical Gulf of Mexico clayey soils. Their purpose is to examine the caisson capacity under a sustained tensile load which is some percentage of the vertical uplift undrained capacity. Their centrifuge tests find that caissons with smaller L/d ratios under the same $P/P_{ult,undrained}$ experience the same normalized displacements after shorter holding periods.

The centrifuge results suggest that for an L/d ratio of approximately 4, the displacements are less than 5% of the diameter for a time period of about 2 months with a sustained load of 81% of the ultimate undrained capacity. This time increases to about 9 months for displacements equal to 10% of the diameter. Furthermore, for L/d ratios of about 5, the displacements were below 5% of the diameter for a time period of about 2 months and a sustained load of 87% of the ultimate undrained capacity. However, for a displacement of 7%d the holding times for these tests increased to nearly 2 years.

The results of the finite element study are consistent with the centrifuge tests. The simulations were performed in ABAQUS using the Modified Cam Clay soil model and a coupled pore

pressure and effective stress solution. The caisson capacity was recorded as the pullout load when the uplift displacement reached 10% of the caisson diameter. For L/d ratios of approximately 5 and a loads of 81-87% of the undrained capacity, the holding times are between 1 and 2 years. Overall the results of this study suggest that for caissons with L/d of 5 the effect of pore pressures dissipation on the foundation holding capacity appear negligible for holding periods relevant to the loop currents and the cyclic storm loading.

3. Numerical Analysis of Caisson Response under Undrained Conditions

This chapter describes the axial uplift load response of wished-in-place suction caissons under undrained conditions, using finite element analysis. The soil response remains fully undrained until failure occurs.

3.1 The finite element model

All of the finite element analyses were performed using the commercial finite element code Plaxis v.8.5. An axisymmetric model was used in the analysis. This assumes a uniform radial cross section and loading around the central axis. An example of the axisymmetric representation of a cylindrical element is shown in Figure 3.1 below.

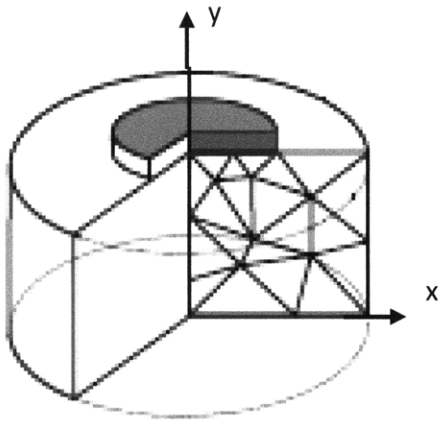

Figure 3-1 Axisymmetric model in Plaxis for a cylindrical element (Source: Plaxis v.8 reference manual)

A slightly different mesh was used for each of the 5 geometries considered. The finite element mesh for a reference geometry of d = 17m and L = 11m is shown in Figure 3.2. The soil is represented by 690 15-noded triangular elements. The caisson is modelled using dimensionless

5-noded plate elements. The interfaces are represented by 5-noded lines. Boundary conditions include full fixities at the bottom and vertical rollers at the vertical sides.

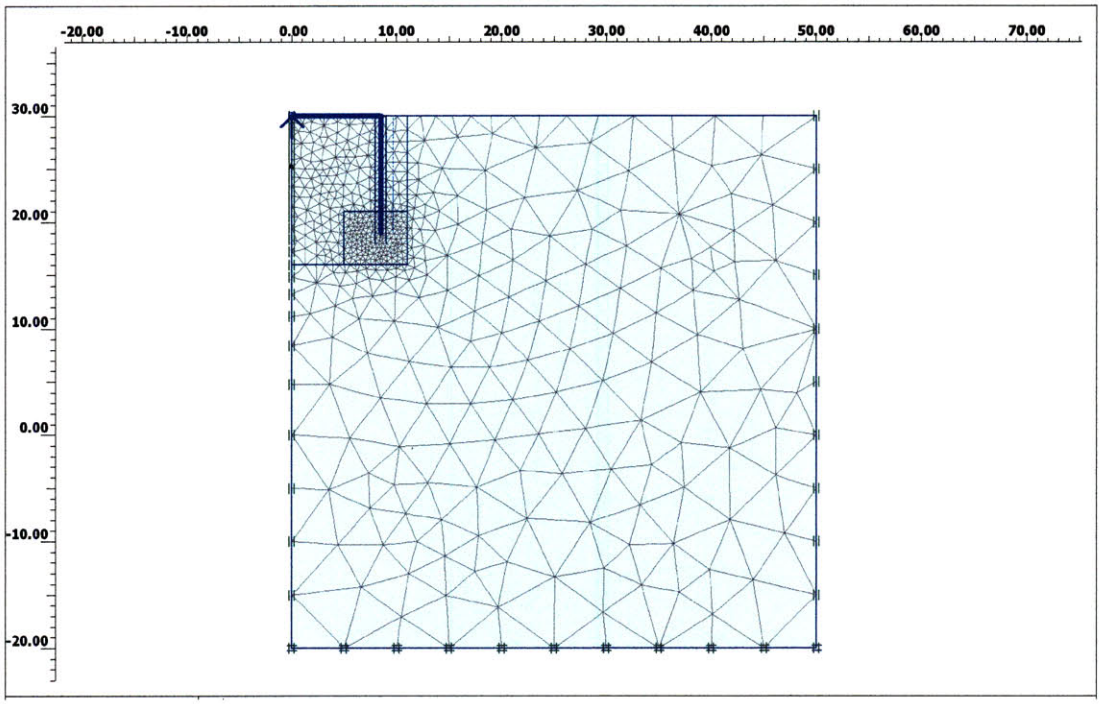

Figure 3-2 Base case geometry and finite element mesh

The caisson is modelled as an elastic material. The unit weight is assumed to be γ_c=24kN/m^3 and Poisson's ratio v=0.15[1]. The caisson is represented by 2D plate elements and a uniform caisson thickness of t=1m is assumed for both the walls and the lid of the caisson. The caisson is loaded in tension by applying a single force at the caisson centreline. A condition of no separation is imposed between the soil and the caisson lid. An interface is assumed between the soil and the external wall of the caisson. The adhesion coefficient is set to unity so that all of the shear stresses in the soil are transferred to the caisson wall.

The analyses were performed using 5 different caissons geometries. In order to investigate the effect of different length (L) to diameter (d) ratios, L/d=0.5, 0.65, 1, 2 and 3. These L/d ratios are

[1] The Young's modulus was set to 35*10^3 GPa[1] in order to ensure that the lid remains rigid during loading such that all points on the lid undergo equal increments of vertical displacement.

are representative of the suction caisson L/d ratios used in the offshore industry. The diameter was held constant at d = 17m and the skirt length was varied between L = 8.5m and L = 51m. The Snorre TLP (see Chapter 1) used suction caissons with similar dimensions (d = 17m and L = 12m) and the intention is to make further comparisons of the predictions of these studies, with studies on the predicted Snorre platform performance.

The first part of this chapter presents the full results for a base case geometry. The following sections describe the effects of the different geometries and finally, comparisons are made with existing literature.

3.2 Results of base case geometry analysis

A base case geometry (d = 17m, L = 11m) was chosen to illustrate the full results of the numerical analysis.

3.2.1 Load-deformation response

The load-displacement curve is shown in Figure 3.3. At the first stage of the calculations, the caisson was wished-in-place. The caisson self weight caused an initial settlement of δ_v = 0.15m. After the uplift force was applied, this initial displacement is reversed. This initial stage is omitted in Figure 3.3 and the load deformation curve is plotted from the point at which the initial installation displacements are reversed. Yielding occurs for loads larger than 70 MN and the lid displacement at that point is approximately δ_v = 0.14m. This corresponds to deformation to diameter ratio of δ_v/d = 0.8%. The ultimate capacity of the caisson is estimated as $P_{ult,undrained}$ = 110 MN. The net pullout capacity, $P_{ult(net),undrained}$ is defined as the pullout capacity less the caisson self weight and the weight of the soil inside the caisson. Here $P_{ult(net),undrained}$ = 74.4 MN.

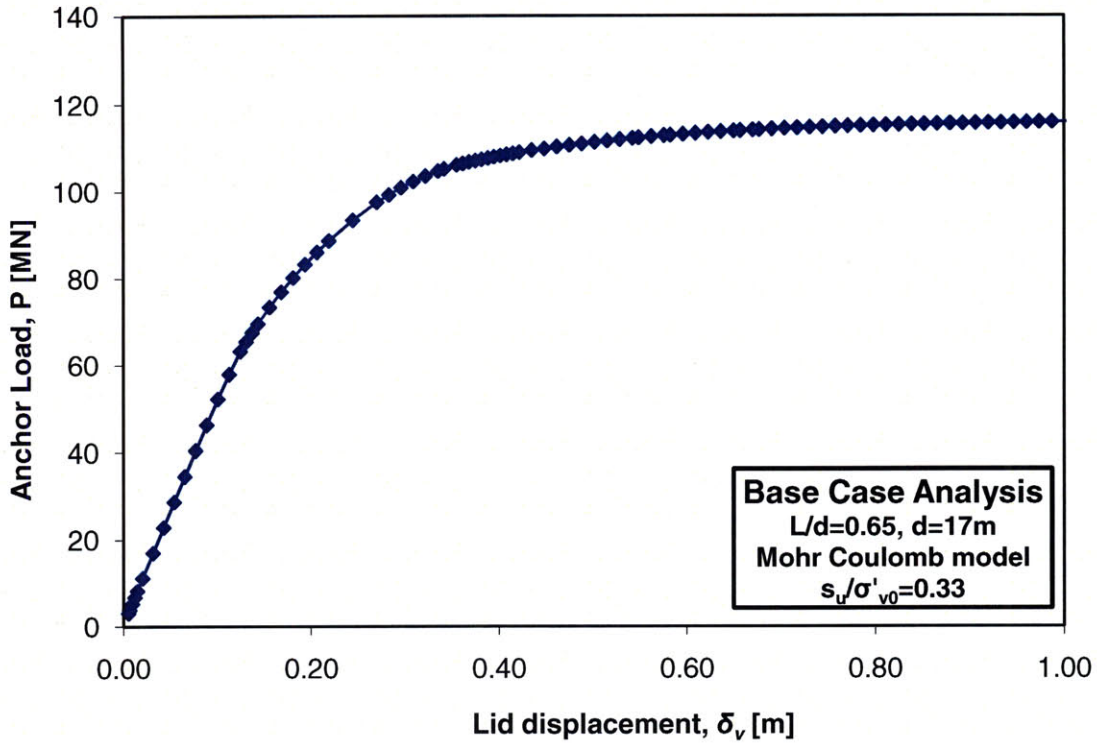

Figure 3-3 Load deformation response for base case geometry

3.2.2 Breakdown of reaction forces

As discussed in Chapter 2, we expect the following forces to be acting on the caisson at failure:

- Caisson self weight P_c = 17,510 kN
- Weight of the soil plug inside the caisson P_s = 18,010 kN
- External wall friction $P_{f,ext}$ = 10,870 kN
- Base resistance due to the development of the reverse bearing mechanism P_b = 62,210kN

Figure 3.4 shows the relative magnitude of the side friction ($P_{f,ext}$) compared to the total resistance of the caisson (P_{total}), and the sum of the caisson self weight (P_c) and the weight of

the soil plug inside the caisson (P_s). The friction force magnitude was obtained at various stages during the loading of the caisson, by integrating the shear stress along the external soil-caisson wall interface. At failure, the external wall friction force is $P_{f,ext}$ = 11,060kN, within 2% of the predicted pullout capacity. As shown in Chapter 2, we expect the magnitude of the side friction to reach 10,870kN. This small deviation could be attributed to resistance along the internal wall of the caisson and resistance at the caisson tip, both of which are neglected in the theoretical limit analysis calculations.

In the analysis of the finite element results, it was assumed that at all points during loading the full caisson weight and the full weight of the soil plug are acting on the caisson. Thus the base resistance (P_b) was calculated by subtracting the friction force ($P_{f,ext}$) and the plug and caisson weights ($P_s + P_c$) from the applied uplift force (P_{total}).

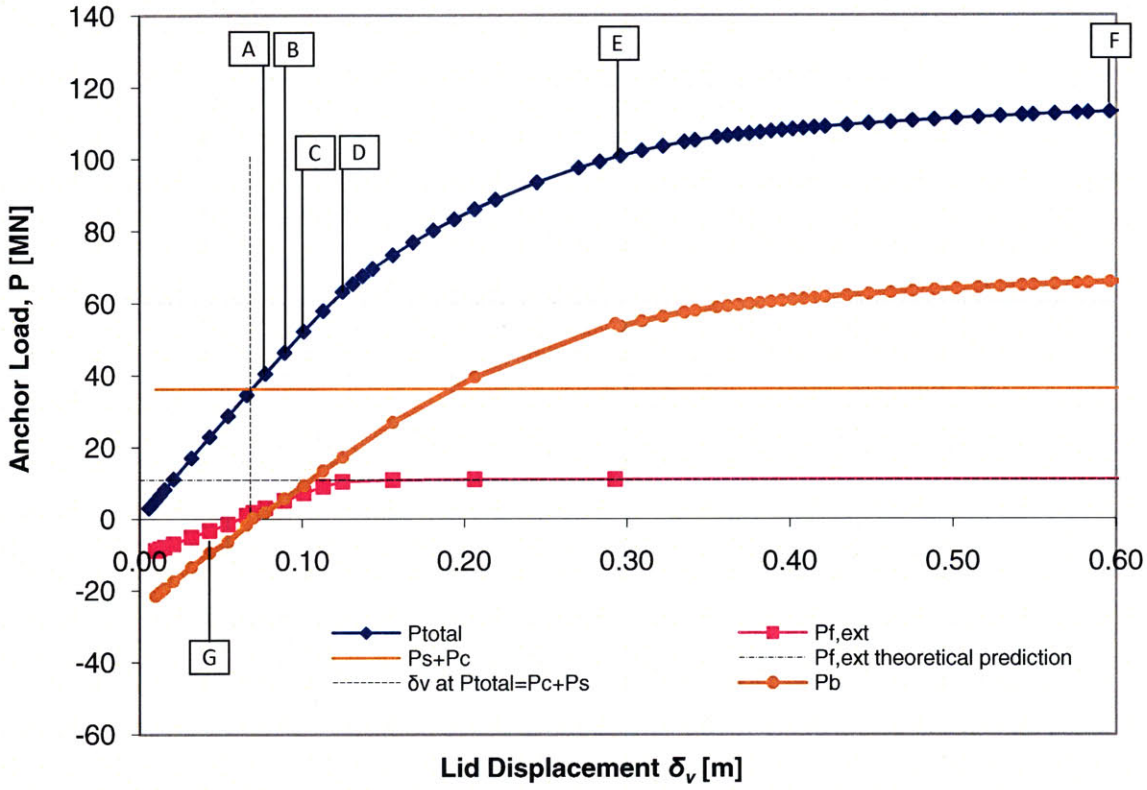

Figure 3-4 Built-up of friction and base resistance forces as applied uplift force increases

3.2.3 Failure mechanism

The initial phase of the calculations results in a net upward side friction due to the caisson self weight. The remaining part of the caisson self weight is resisted by the forces at the base of the caisson. Thus, during the first stages of the uplift loading, there is some residual upward frictional resistance as well as an upward base resistance. These are plotted on Figure 3.5. Eventually, as the applied anchor force increases, the shear stresses acting on the interface gradually reverse in direction, Figure 3.6.

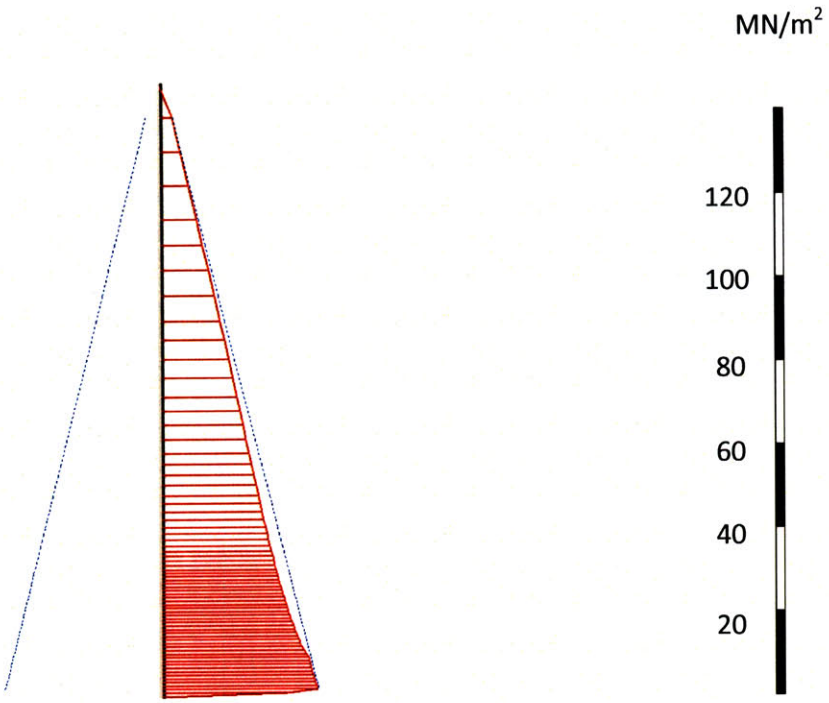

Figure 3-5 Shear stresses on external caisson wall at the beginning of uplift loading, (stage A Figure 3.4)

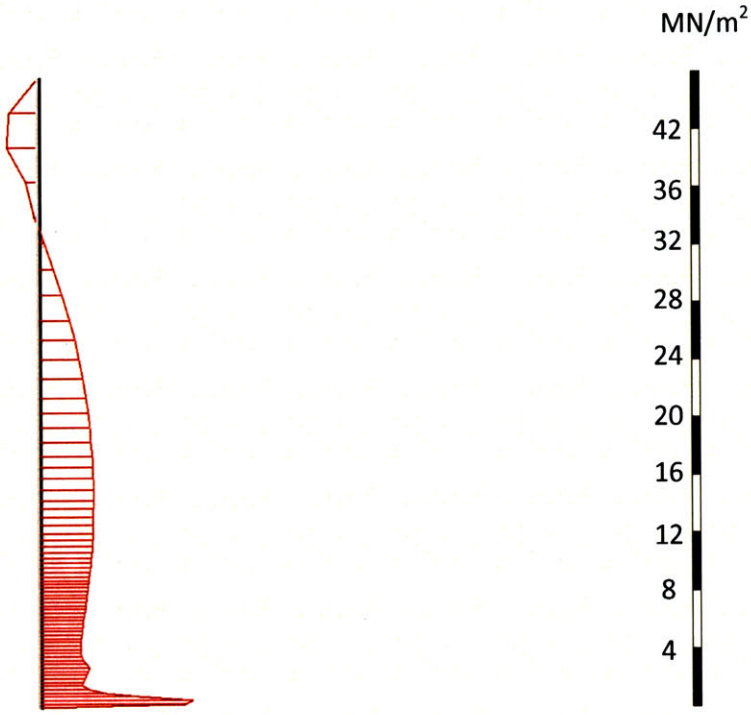

Figure 3-6 Shear stresses on external caisson wall corresponding at stage G in Figure 3.4

The vertical dotted line on Figure 3.4 indicates the point at which the applied force is exactly equal to the combined weight of the caisson and soil plug. If there were no time lag between the wished-in-place installation and the application of the uplift force, then, the friction and base resistance would be zero at this point. However, as shown in Figure 3.4 some of the friction resistance is mobilized to balance the residual base force. This effect is more pronounced in higher L/d caisson geometries which are discussed in Section 3.3.

Figure 3.7 shows the plastic points in the soil at each of the different stages in the loading process (A,B,C,D,E and F) indicated in Figure 3.4. After the residual friction force is overcome, the first plastic points appear at the top and the bottom of the external caisson-soil interface, stage A ($P/P_{ult,undrained}$ = 0.32). Plastic points keep developing on that interface until the full friction capacity in reached, stage D ($P/P_{ult,undrained}$ = 0.54). Thereafter the reverse bearing capacity mechanism starts to develop, stage E ($P/P_{ult,undrained}$ = 0.87). It can be seen that eventually the reverse bearing capacity mechanism reaches the soil surface. The base force at that point is P_b = 69.6 MN, 12% higher than estimated by limit equilibrium (Chapter 2, P_b = 62.2 MN). The caisson lid displacement at that point is δ_v = 0.6m which corresponds to 3.5% of the caisson diameter.

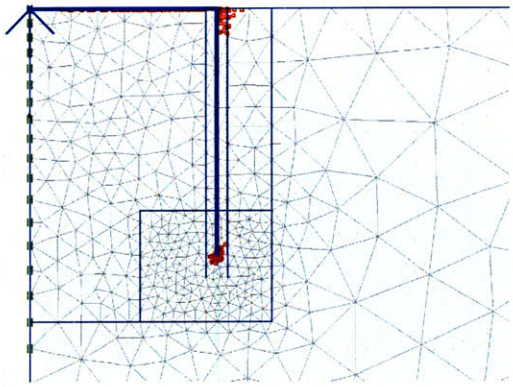

Stage A: $P / P_{ult,undrained}$ **=0.32**

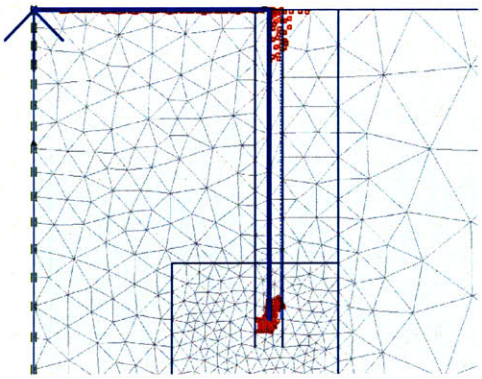

Stage B: $P / P_{ult,undrained}$ **=0.4**

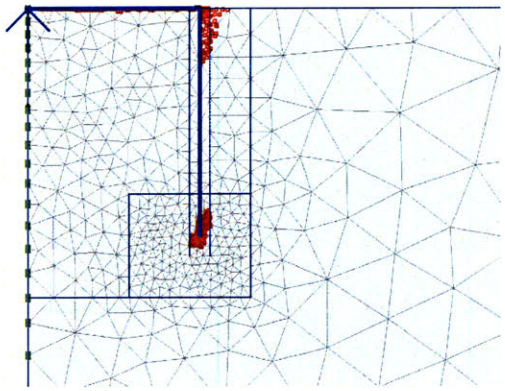

Stage C: $P / P_{ult,undrained}$ **=0.45**

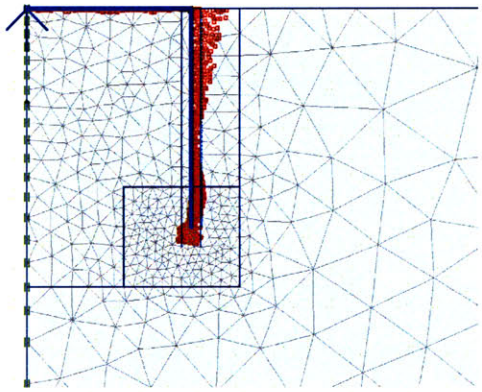

Stage D: $P / P_{ult,undrained}$ **=0.54**

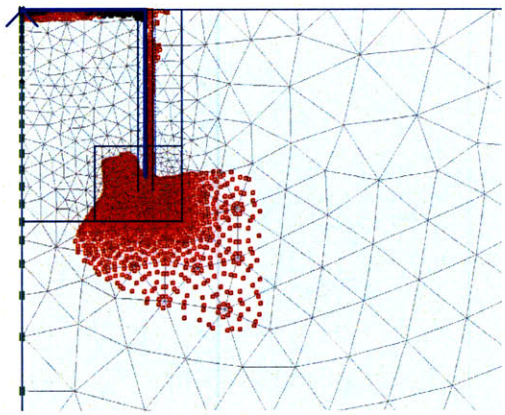

Stage E: $P / P_{ult,undrained}$ **=0.87**

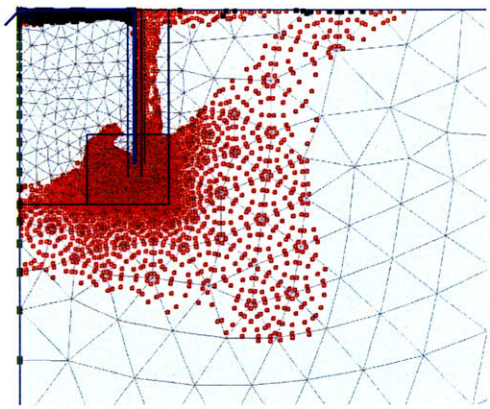

Stage F: $P / P_{ult,undrained}$ **=1**

Figure 3-7 Development of plastic points during undrained loading for base case geometry

Figure 3.8 shows the incremental displacements and the mesh deformation for the base case analysis when the caisson has reached its ultimate capacity. The caisson lid moves vertically upwards. The soil inside the caisson remains attached to the caisson lid and walls and moves upward as a plug, as assumed by mechanics of reverse bearing failure.

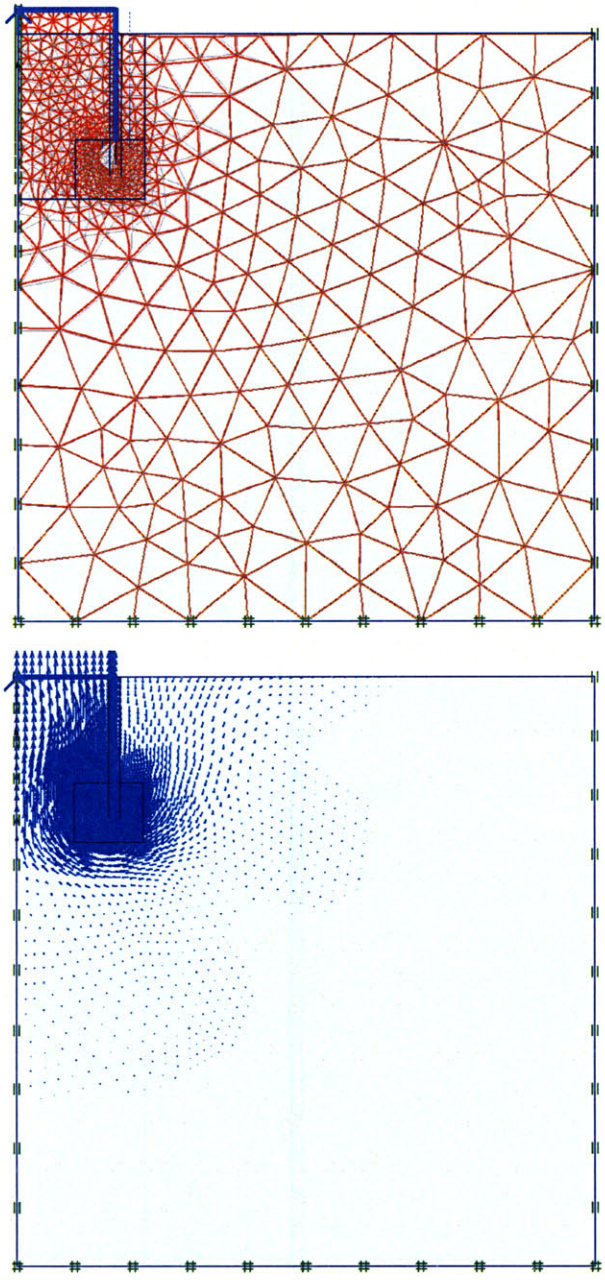

Figure 3-8 Incremental total displacements and deformed mesh at failure

3.3 Effect of caisson geometry in undrained response

The effect of caisson geometry has been established by comparing the results from analyses of caissons with different length to diameter ratios, L/d. More specifically, the diameter was held constant at d = 17m and the length was L = 8.5, 11, 17, 34, and 51m. Figure 3.9 compares the load-deformation responses of the five different geometries. From Figure 3.9 it is apparent that all of the load-displacement curves have the same characteristic form. The displacement at yield shows little variation between the different geometries and varies between δ_v = 0.13m (for L/d = 0.5) and δ_v = 0.19m (for L/d = 3).

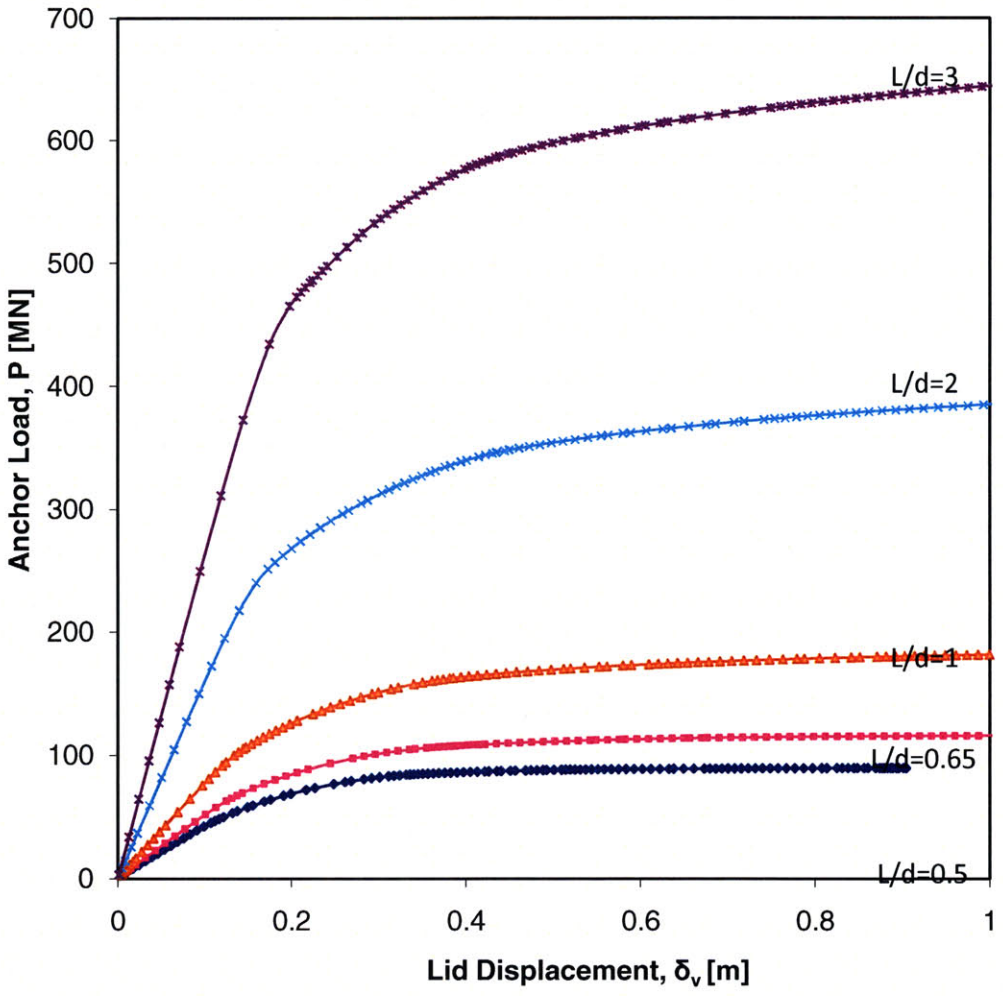

Figure 3-9 Effect of caisson geometry on undrained load-deformation response

Figure 3.10 shows the relative importance of the friction force ($P_{f,ext}$) and the base resistance (P_b) for different L/d ratios, at different loading stages. The exact values of the forces at different loading stages for each geometry are shown in Appendix B. For small L/d ratios, $P_{f,ext}$ is only 10-15% of the total caisson capacity. For the L/d = 3 geometry, side friction comprises 50% of the total load when $P / P_{ult,undrained}$ = 0.6, before falling to about 40% at failure. Figure 3.11 shows that the relative importance of the base resistance decreases with L/d. Such a variation is expected as the side friction is proportional to the square of the caisson length (L^2) whereas the base resistance is proportional to the length (L).

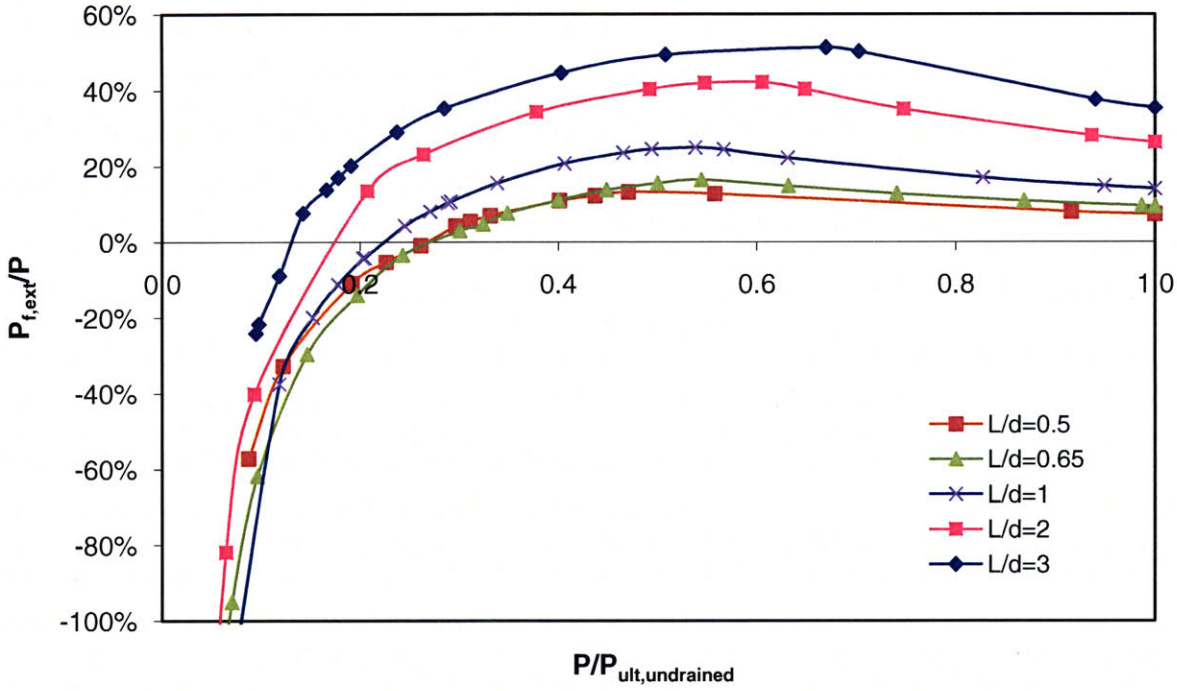

Figure 3-10 Mobilization of external side friction.

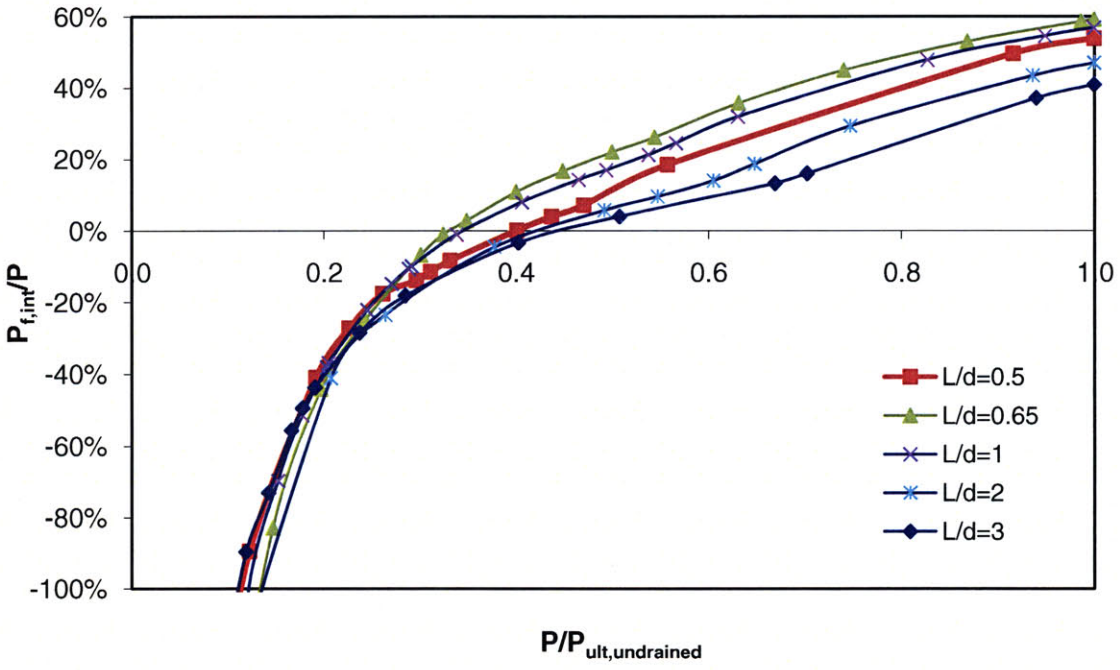

Figure 3-11 Mobilization of internal side friction

3.4 Comparison of results with existing research

Figure 3.12 summarizes the ultimate pullout capacity predictions from the current analysis with results from two recent finite element analyses discussed in Chapter 2. Zdravkovic et *al.* (2001) predict significantly lower failure loads than Deng and Carter (2002) and significantly lower than the results of this study. Differences between Zdravkovic et *al.* (2001) and Deng and Carter (2002) could be attributed to the respective use of the anisotropic MIT-E3 and isotropic Modified Cam Clay models respectively. Zdravkovic et *al.*(2001) use the same undrained strength ratio in triaxial compression as the current study ($s_u / \sigma'_{v0} = 0.33$).

The current analysis shows net capacities below the Deng and Carter prediction for L/d≤1.5. This could be attributable to the fact Deng and Carter apply a generalized empirical formula based on MCC analyses to obtain uplift capacity as a function of L/d ratio. Finite element data presented in their publication, suggest that their relationship over-predicts the capacity at L/d ratios smaller than 1. The deviation of Deng and Carter from the results of this research increases significantly for L/d ratios greater than 2. This could be attributed to the increasing importance of the friction resistance which is sensitive to the choice of soil model.

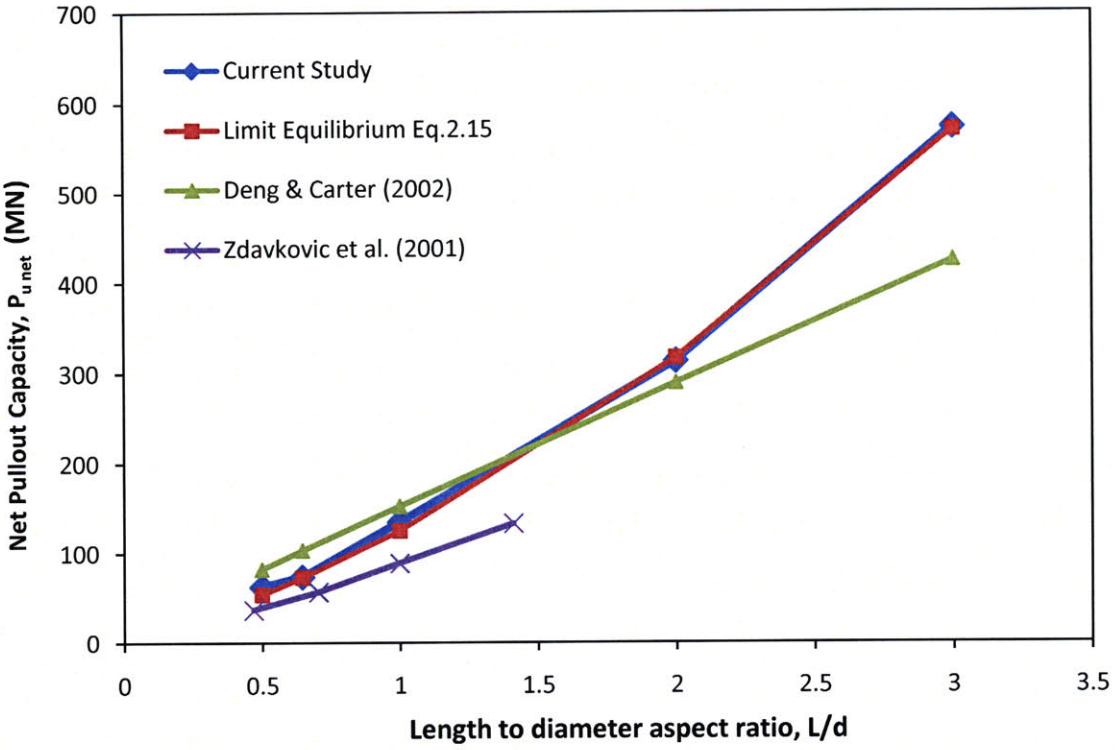

Figure 3-12 Comparison of results from current studies with existing literature for undrained loading

4. Numerical Analysis of Suction Caisson Model under Drained Conditions

This chapter describes the axial uplift load response of wished-in-place suction caissons under drained conditions, using finite element analysis.

The fully drained response of the suction caisson provides a theoretical lower limit to its uplift capacity. Drained conditions approximate the caisson behaviour when the uplift load is sustained until all the excess pore water pressures have dissipated. Given sufficient time, water flows in from the surrounding soil in order to balance the excess pore water pressures induced during the caisson installation. Eventually, as pore water pressures dissipate, the suction between the lid and the soil underneath will break down and the only resisting forces will be the side friction on the internal and external walls and the caisson self-weight. Thus, under drained conditions, there is no adhesion between the top or the tip of the caisson and the adjacent soil element.

The drained response might not accurately represent the long term capacity due to the creep effects. Experimental evidence (El-Gharbawy, 1998) has shown that prolonged application of load magnitudes greater than approximately 80% of the measured maximum pullout capacity under drained conditions resulted in progressive caisson pullout, possibly due to creep effects.

4.1 The finite element model

A number of theoretical drained case scenarios were examined using finite elements analysis based on the soil model and assumptions described in Chapter 2. The analysis was performed with caisson length to diameter aspect ratios, L/d = 0.5, 0.65, 1, 2 and 3. The finite element model assumptions are the same as those described for the undrained loading in Chapter 3.

Interfaces are used to model the interaction of the caisson walls and the soil. At the same time, interfaces make it possible to monitor the stresses on the outer and inner caisson walls throughout the loading stages. Interface elements are defined by 5 pairs of nodes as shown below.

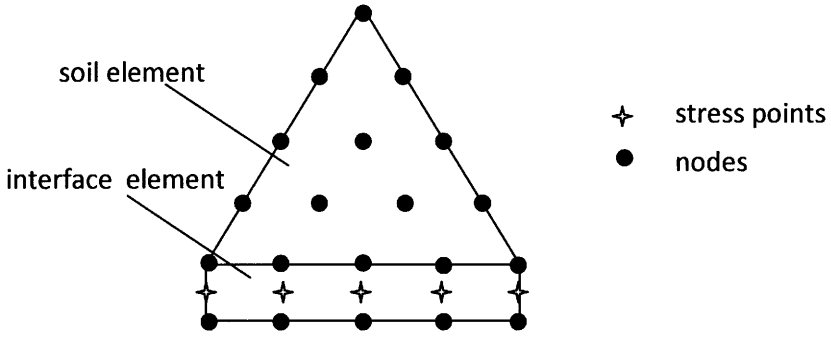

Figure 4-1 Distribution of nodes and stress points in interface elements and their connection to soil elements

The roughness of the interaction between soil and caisson is defined in Plaxis by the interface strength reduction factor ($R_{\text{int}er}$). For the purposes of this research, $R_{\text{int}er}$ = 1 so that the interface has the same properties as the adjacent soil and the full friction coefficient $\tan\phi'$ acts on the caisson walls i.e. $\tan\delta' = \tan\phi'$.

4.2 Results of Base Case geometry analysis

The base case geometry (d = 17m, L = 11m) was chosen to illustrate the full results of the numerical analysis. Appendix C shows the geometry and the mesh that was used. As in the undrained case, a single uplift point force (P) was applied on the caisson lid along the caisson centreline. The load was increased until the caisson pull-out occurred.

4.2.1 Load-deformation response

The load-displacement curve is shown in Figure 4.2. At the first stage of the calculations, the caisson was wished-in-place. The caisson self weight caused an initial displacement of δ_v = 0.15m. After the uplift force was applied, this initial displacement is reversed. This initial stage is omitted in Figure 4.3 and the load deformation curve is plotted from the point at which the initial installation displacements are reversed. Yielding occurs for loads larger than 31 MN and the lid displacement at that point is approximately δ_v = 0.1m. This corresponds to deformation to diameter ratio of δ_v /d = 0.6%. The ultimate capacity of the caisson is estimated as $P_{ult,drained}$ = 34.4MN. For the drained analysis, the net pullout capacity, $P_{ult(net),drained}$ is defined as the pullout capacity less the caisson self weight. Here $P_{ult(net),drained}$ = 16.9MN.

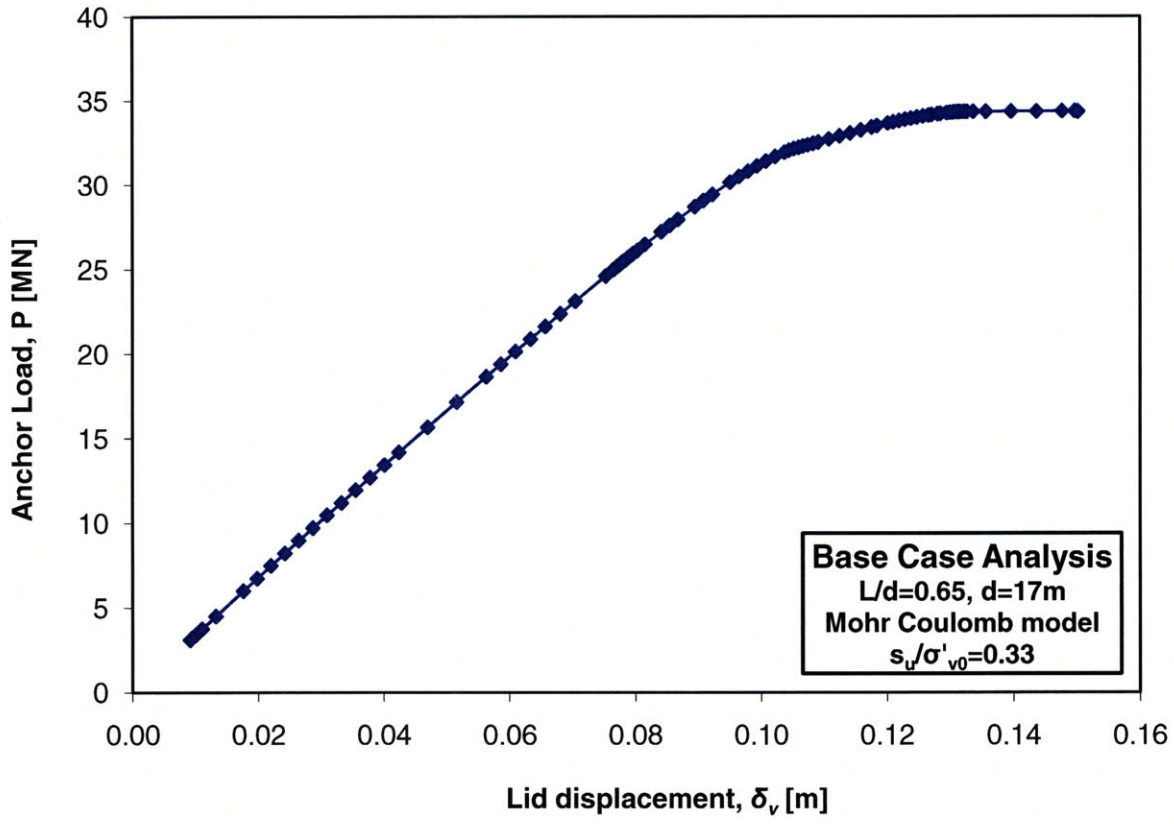

Figure 4-2 Load-deformation response for L/d=0.65

During the analysis it was observed that the use of interfaces in the finite element program affects the load deformation response and the ultimate capacity of the caisson. Figure 4.2 shows how the response varies when different interfaces are active.

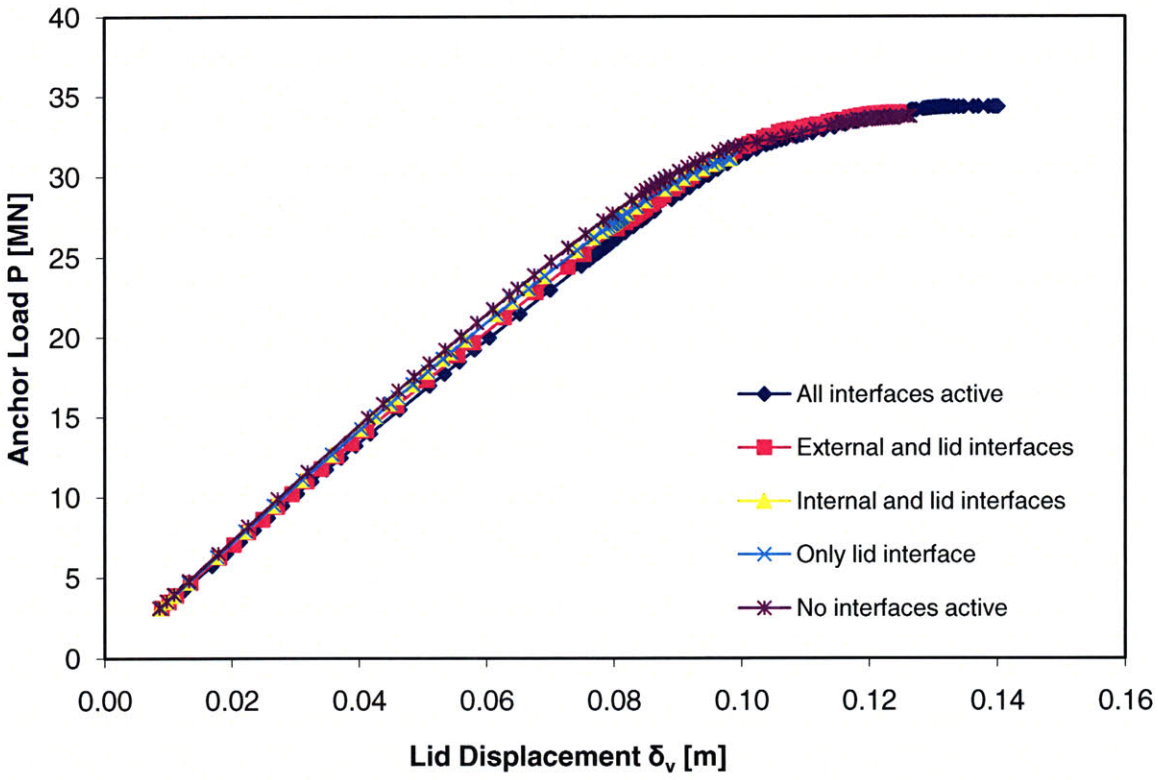

Figure 4-3 The effect of interfaces on the load-displacement response

4.2.2 Breakdown of reaction forces

As discussed in Chapter 2, we expect the following forces to be acting on the caisson at failure:

- Caisson self weight P_c = 17,511 kN
- External wall friction $P_{f,ext}$ = 8,650 kN
- Internal wall friction $P_{f,\text{int}}$ = 7,570 kN

These results assume that the horizontal stresses at the interface at failure are $\sigma'_h = \sigma'_{v0} K_0$. Figure 4.4 shows the distribution of the horizontal stress along the external caisson wall at failure, as obtained by the finite element program. Three sets of data for the horizontal stress are shown in Figure 4.4. The first set is the stress on the soil-caisson interface. The second and third set of data was obtained by drawing a cross section within the soil, 0.07 and 0.5 meters from the interface. Since in Plaxis the caisson is modelled as a dimensionless plate element of thickness 1m and radius 8.5m, the horizontal stress at x=8.57m falls within the plate element. The horizontal stress at x=8.9 should be closer to the realistic value. Nevertheless, Figure 4.4 shows that the x=8.57 set of data is in better agreement with the interface data.

The $\sigma'_{v0} K_0$ line is also plotted and it is higher than the finite element prediction. This is due to the reduction in the vertical effective stress, σ'_v which is below σ'_{v0} due to acting of stresses around the caisson. Up to a depth of approximately 6m, the horizontal and vertical stresses on the external interface at failure are related through K_0. After that, the horizontal stress increases above $\sigma'_v K_0$. At depths above approximately 8m there is a rapid increase in the horizontal stress.

We observe very large fluctuations at the tip of the caisson and this is most likely caused by the complexity of the failure mechanism in this area. These fluctuations reduce the accuracy of the friction force obtained from the analysis. The same is true for the horizontal stress on the internal wall shown in Figure 4.5.

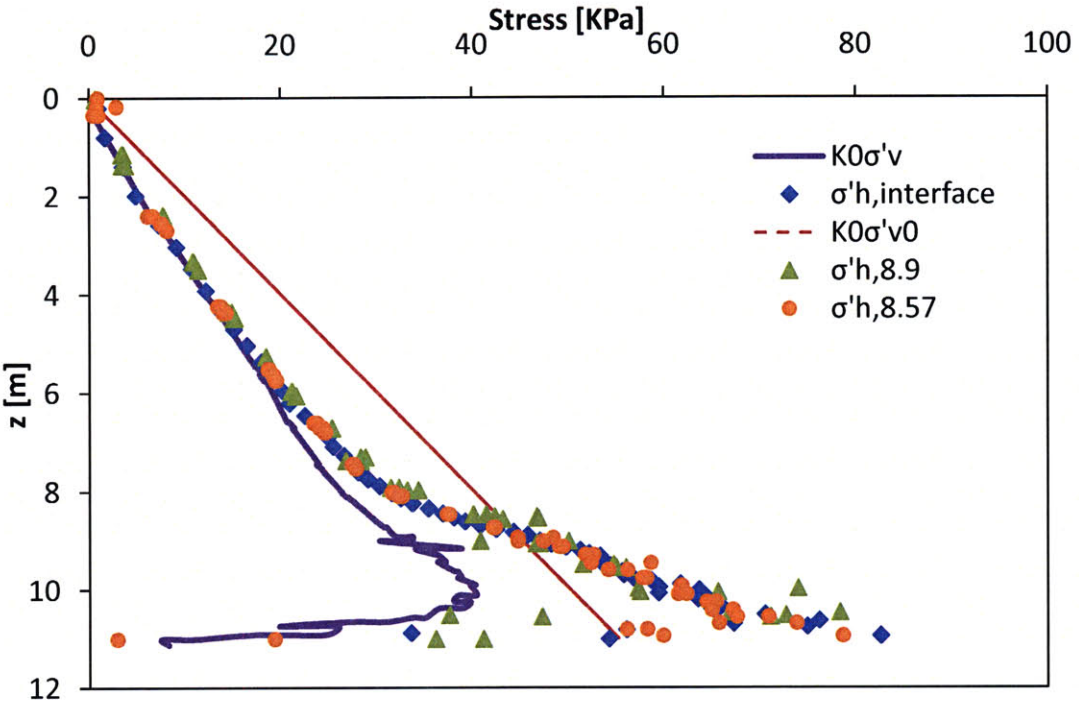

Figure 4-4 Horizontal effective stress distribution on the external caisson wall

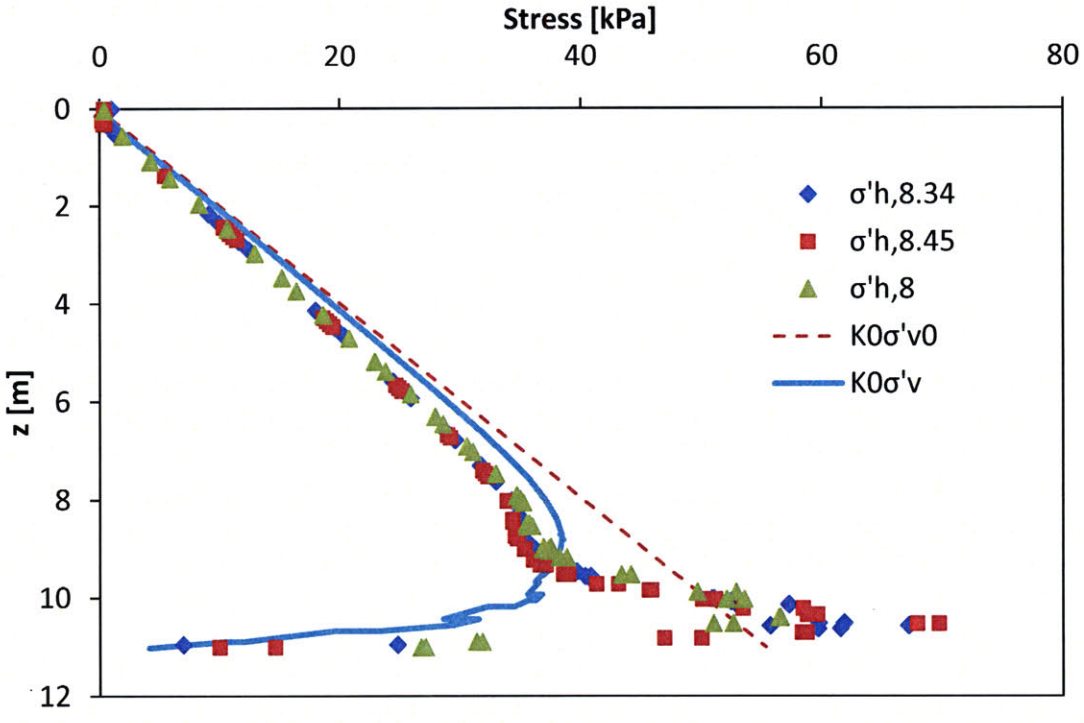

Figure 4-5 Horizontal effective stress distribution on the internal caisson wall

Figure 4.6 shows arrows of horizontal displacements. There is a pivotal point at around z=8 where the horizontal stresses on the external wall increase and reverse in direction. This helps explain the sudden increase observed on the horizontal stress in Figure 4.4.

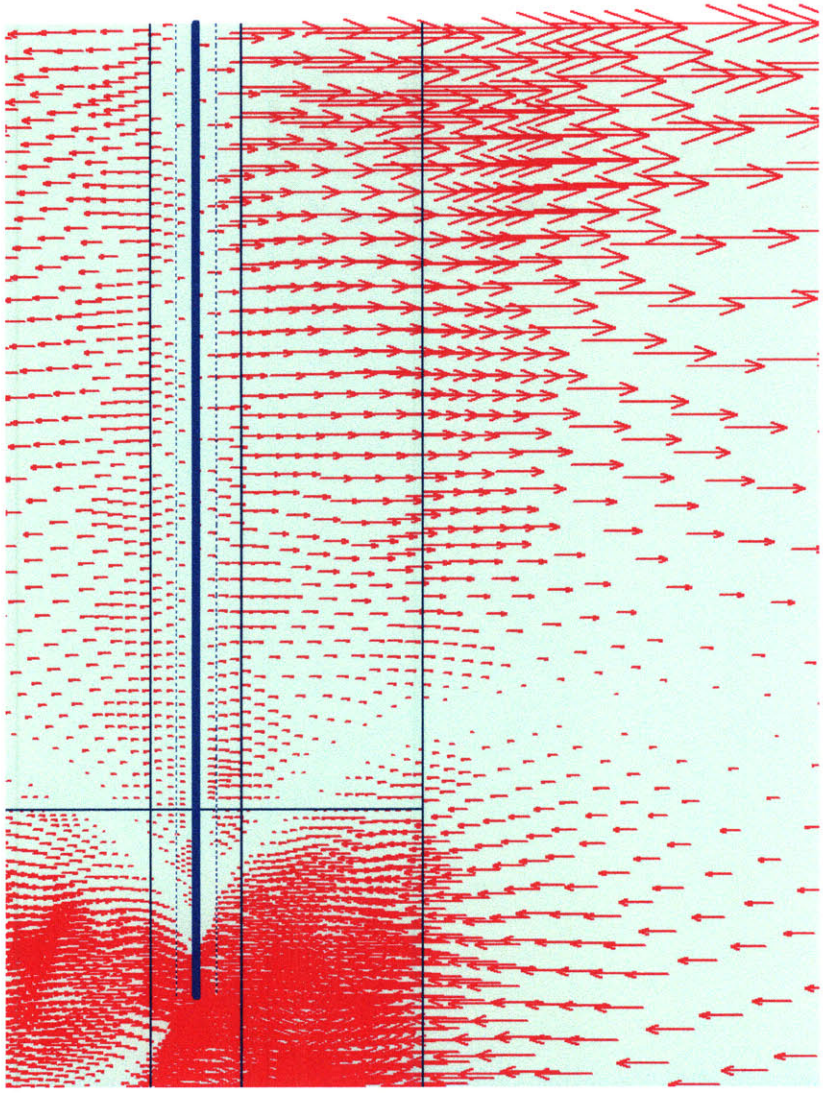

Figure 4-6 Horizontal displacements at failure

The shear stress on the external interface at failure is obtained from: $f_s = \sigma'_h \tan\delta' = \sigma'_h \tan\phi'$. Figure 4.7 shows the shear stress on the external wall as obtained from the above equation and the shear stress as obtained directly from the interface. Figure 4.8 shows the shear stress obtained directly from a cross section 0.1m from the caisson wall and the shear stress obtained by multiplying the horizontal effective stress on the interface by $\tan\phi'$.

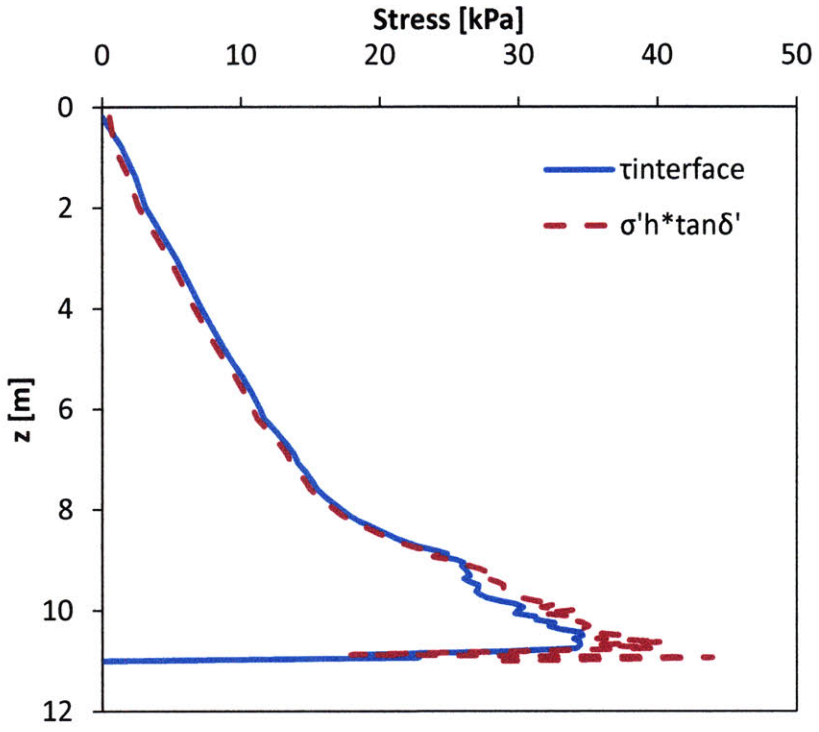

Figure 4-7 Shear stress on external caisson wall

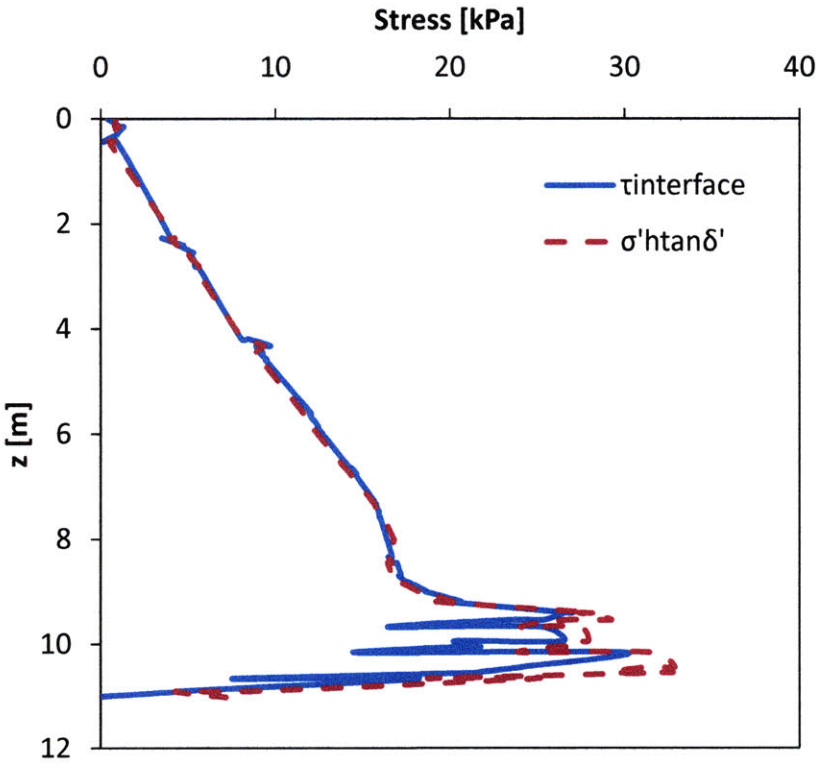

Figure 4-8 Shear stress on external caisson wall

The friction resistance on the external and internal walls can be obtained by integrating the shear stress along the interface as shown in Equation 2.3. The resulting forces are $P_{f,ext}$ = 7.5MN and $P_{f,\text{int}}$ = 7MN. The total pullout capacity of the caisson is 34.1MN and the sum of the caisson self weight and the side friction is $P_{f,ext} + P_{f,\text{int}} + P_c$ = 17.5+7.5+7= 32MN. The differences between the pullout capacity and the sum of the forces could stem from the fluctuations on the shear stress diagrams and resistance at the caisson tip.

Figure 4.9 shows the relative magnitude of each of the forces at different stages of the loading. It can be observed that the external wall reaches its frictional capacity before the internal. The tip resistance remains almost constant.

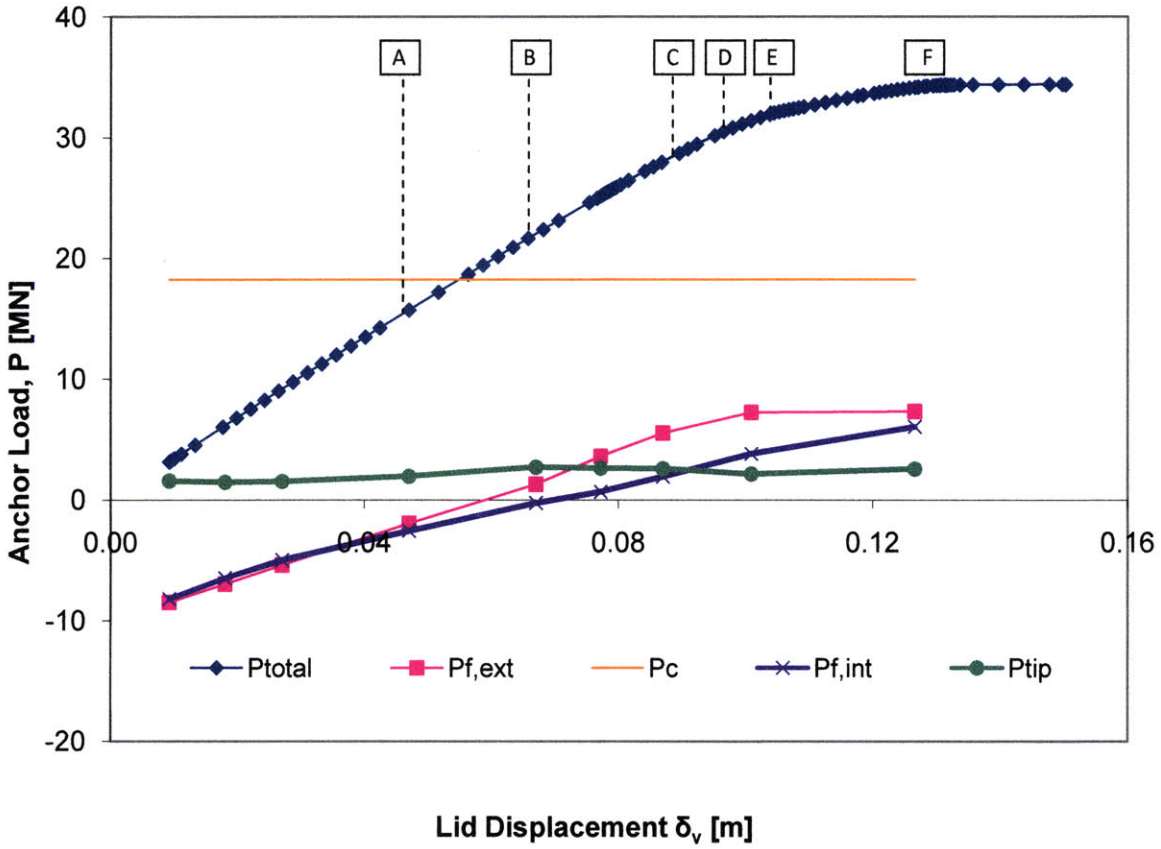

Figure 4-9 Build-up of friction resistance as applied uplift force increases

4.2.3 Failure mechanism

Similarly to the undrained case, the initial phase of the calculations results in a net upward side friction due to caisson self weight. Thus, during the first stages of the uplift loading, there is some residual upward friction resistance as shown in Figure 4.9. Eventually, as the applied anchor force increases, the shear stresses acting on the interface gradually reverse in direction.

Figure 4.10 shows the plastic points in the soil at each of the different stages in the loading process (A,B,C,D,E and F) indicated in Figure 4.10. During first loading stages, stage A (P/P_{ult} = 0.18), plastic points appear at the caisson tip and at the top of the external wall. The plastic points then extend upwards and downwards on the external wall and then less rapidly on the internal wall, stage B (P/P_{ult} = 0.83-0.87). Only after the full frictional resistance on the outside wall is mobilized, stage E (P/P_{ult} = 0.92) does the friction on the internal wall build up.

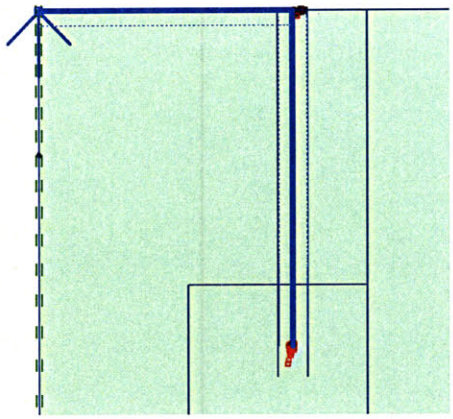

Stage A: $P / P_{ult,drained}$ **= 0.18**

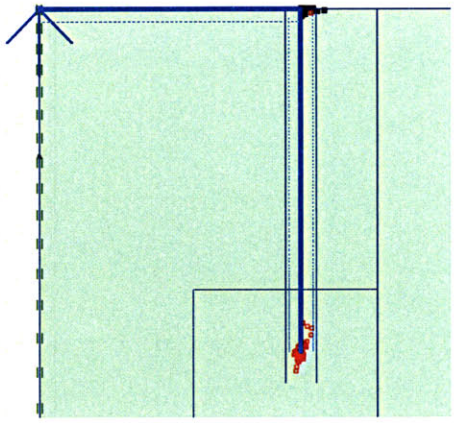

Stage B: $P / P_{ult,drained}$ **= 0.64**

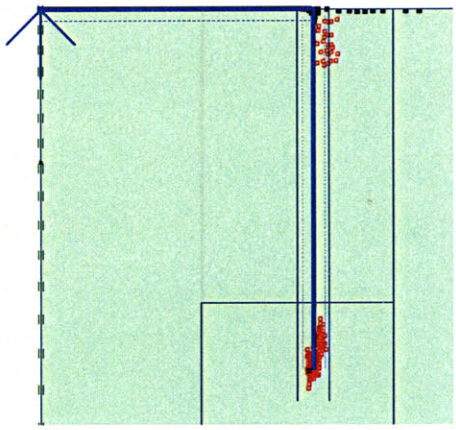

Stage C: $P / P_{ult,drained}$ **= 0.83**

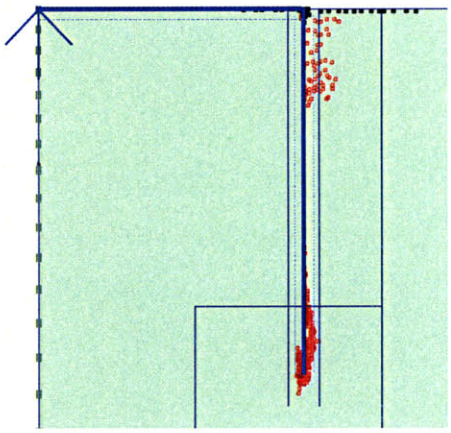

Stage D: $P / P_{ult,drained}$ **= 0.87**

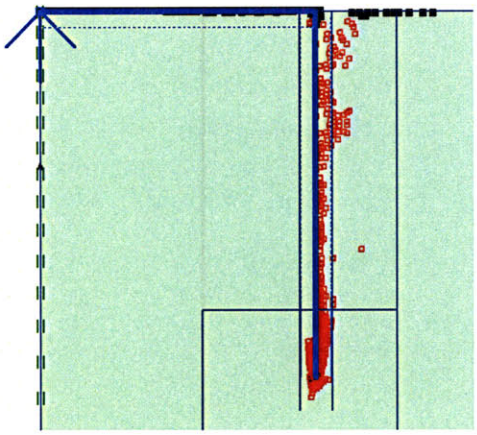

Stage E: $P / P_{ult,drained}$ **= 0.92**

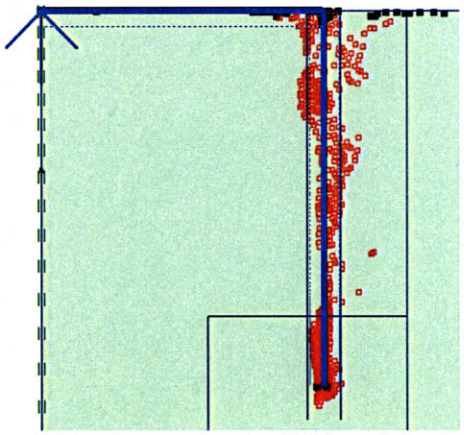

Stage F: $P / P_{ult,drained}$ **= 1**

Figure 4-10 Development of plastic points during drained loading. Red points are Mohr Coulomb plastic points and black are tension cut-off points

Figures 4.11, 4.12 and 4.13 show the mesh deformation, the vertical displacements and the vertical incremental displacements for the base cse analysis when the caisson has reached its ultimate capacity. The caisson lid slides vertically upwards and the soil below the lid is detached.

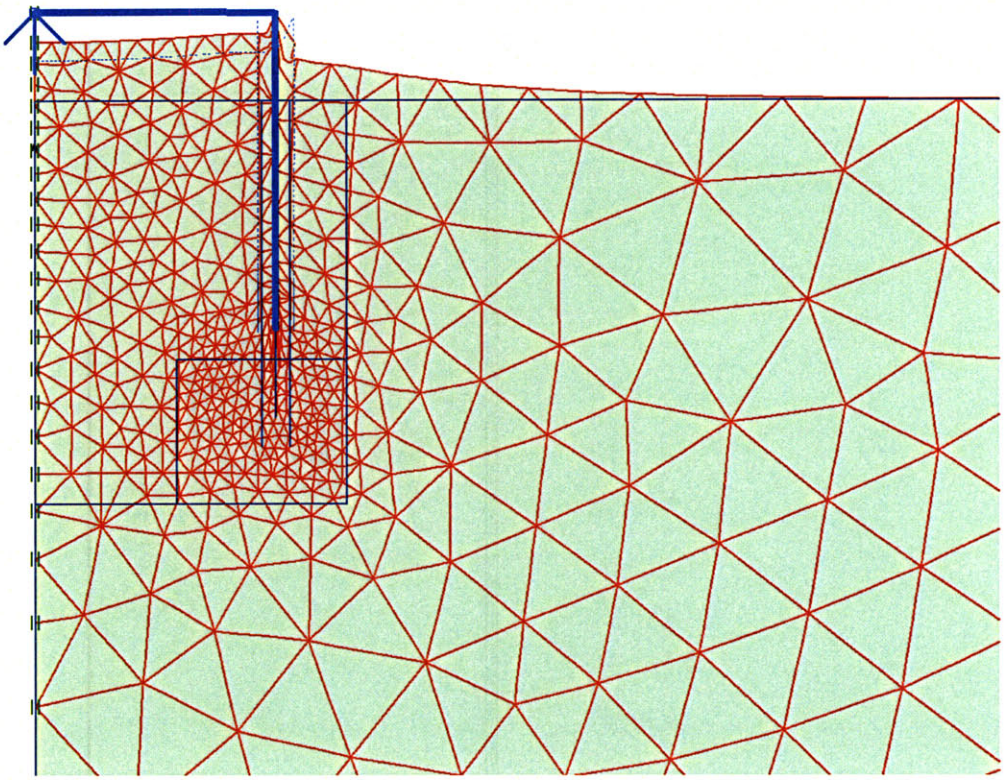

Figure 4-11 Deformed mesh at failure-drained loading case

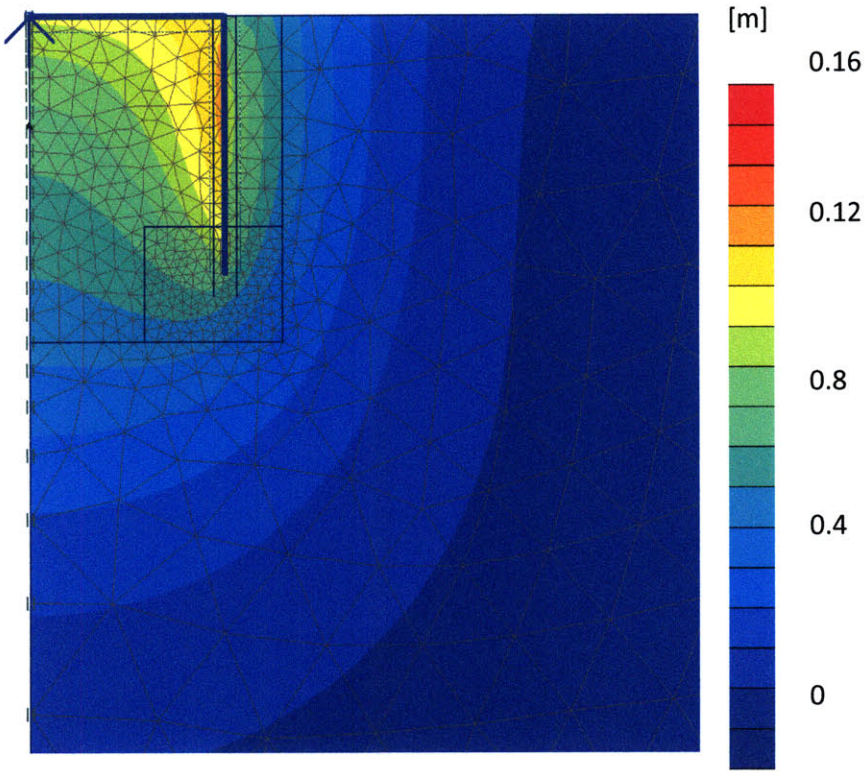

Figure 4-12 Vertical displacements at failure-drained loading case

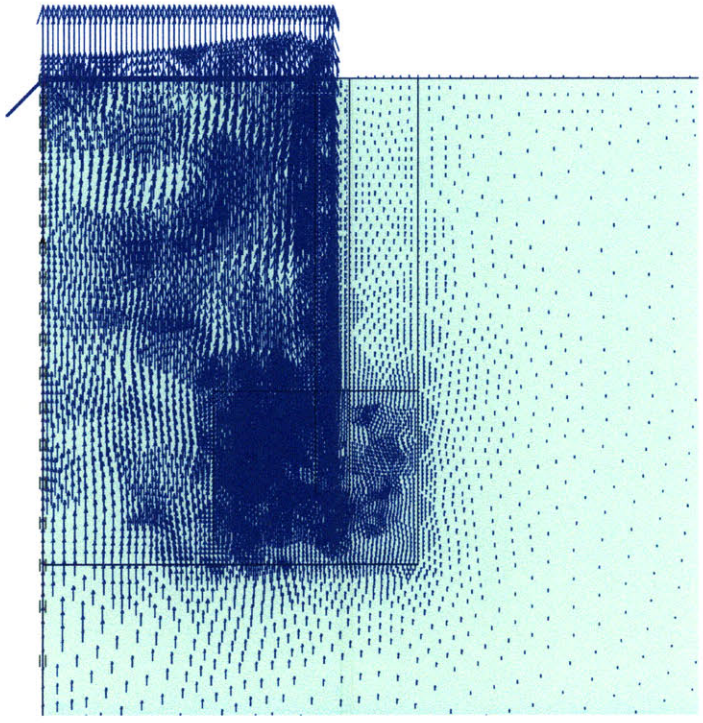

Figure 4-13 Incremental vertical displacements at failure-drained analysis for base case geometry

4.3 Effect of wall length

The effect of caisson geometry has been established by comparing results from analyses of caissons with different length to diameter ratios, L/d. Figure 4.14 compares the load-deformation responses of the five different geometries. All the load-displacement curves have similar form.

The displacement at yield shows little variation between the different geometries and varies between δ_v = 0.09m (for L/d = 0.5) and δ_v = 0.3m (for L/d = 3). Compared to the undrained loading case the response is stiffer. Also, it was not possible to get the load deformation response for large deformations because the finite element program indicated a sudden failure, unlike the undrained case where much larger pre-failure deformations were mobilized.

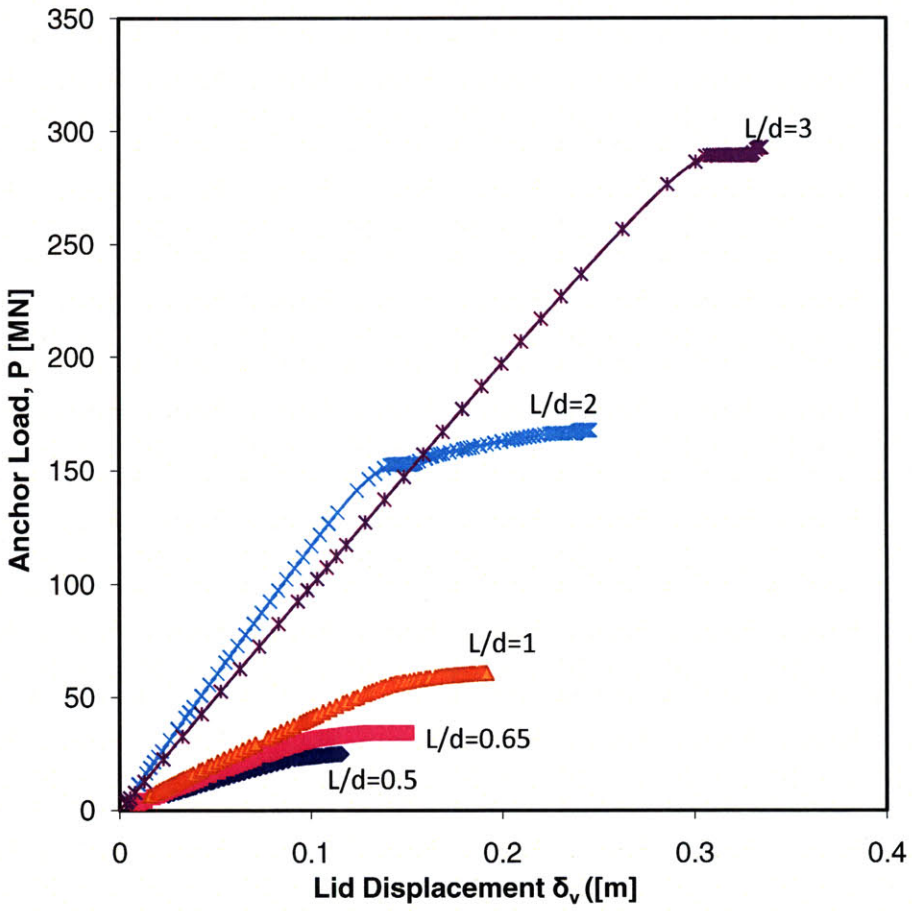

Figure 4-14 Effect of caisson geometry on drained load-deformation response

It was observed in the base case analysis that the horizontal force on the external caisson wall is very close to $\sigma'_v K_0$ up a certain depth. In addition, there is a significant fluctuation at larger depths. Figure 4.15 shows the normalized horizontal stress (σ'_h / L) for the different caisson geometries in order to investigate how these two effects vary with caisson geometry. For all caisson geometries at depths smaller than 75% of the total length, the horizontal stress at failure varies linearly with depth according to approximately $\sigma'_v K_0$. For caissons L/d = 0.5,2 and 3, fluctuations start at a depth of approximately 75% of the total caisson length. For caissons L/d = 1, 0.65, they start at a depth of 94% of the total caisson length. Therefore, the depth at which the fluctuations occur does not appear to be related to the caisson geometry.

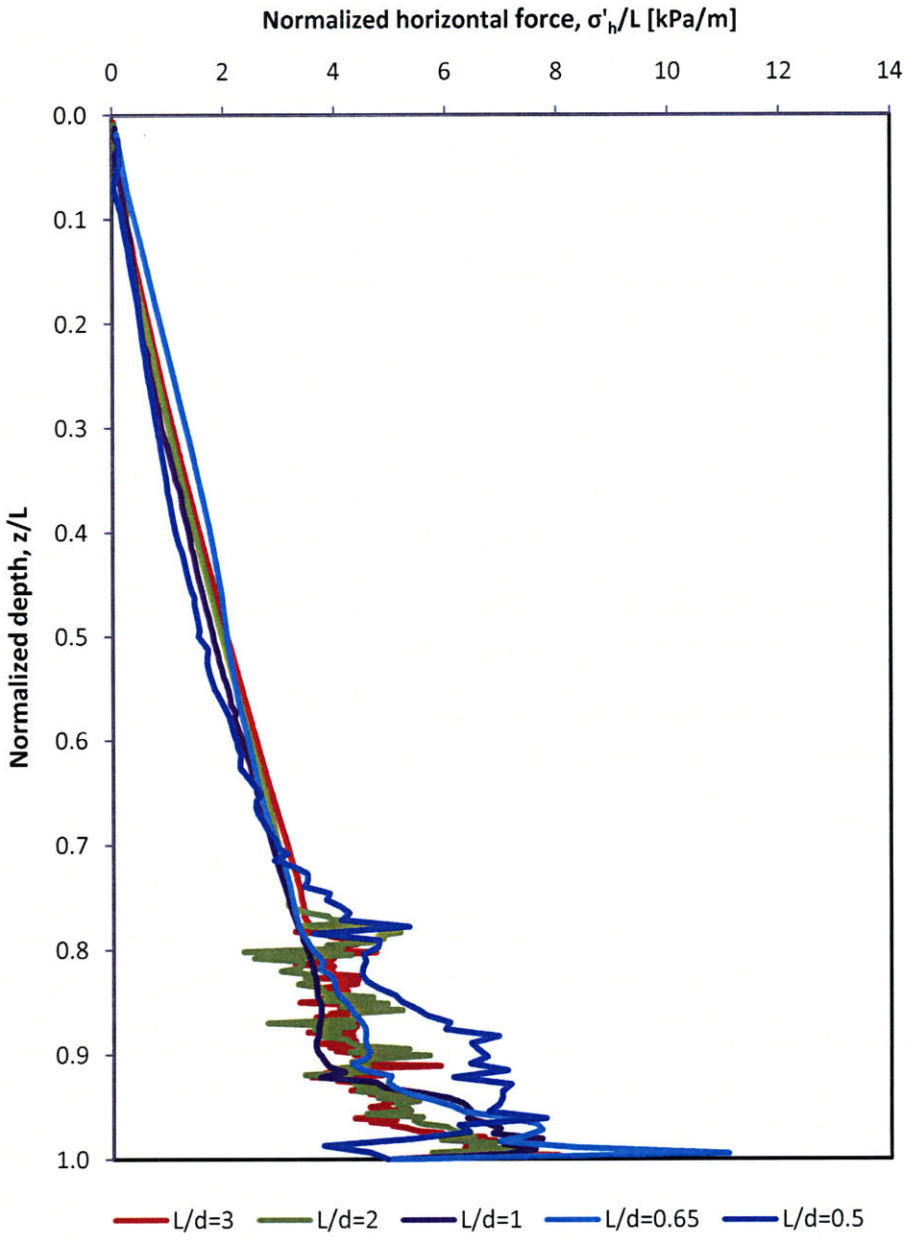

Figure 4-15 Normalized external wall horizontal stress

Figures 4.16 and 4.17 show the effect of caisson geometry on the mobilization of external and internal wall friction resistance. For all geometries, the full internal friction is mobilized only after the external friction reaches its maximum value. Eventually, the internal friction will reach the same value as the external friction. Nevertheless, this can happen at very large displacements at which point the caisson is considered to have already reached its maximum capacity. Therefore for some of the geometries the

maximum internal side friction shown is not equal to the maximum external friction shown. Caissons with larger L/d ratios have larger external and internal friction as a percentage of the total load at failure. The rate at which the internal and external friction build up is approximately the same for all geometries since the curves have similar shapes.

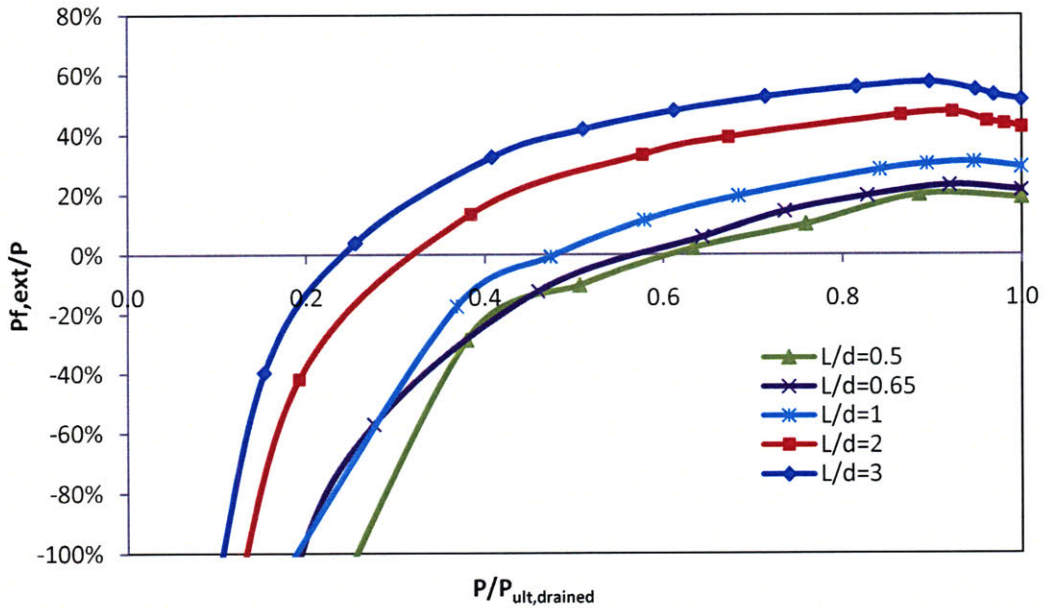

Figure 4-16 Mobilization of external side friction

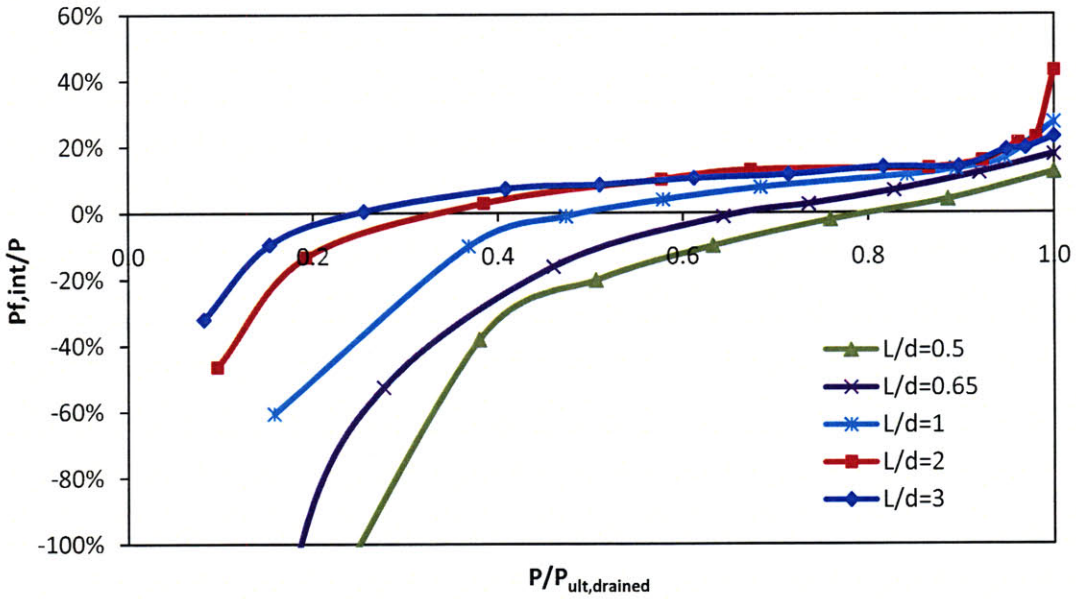

Figure 4-17 Mobilization of internal side friction

4.4 Comparisons of results with existing research

Figure 4.18 compares the results of current drained analyses with those predicted by the Deng and Carter (2002) study. The Deng and Carter predictions are obtained by applying Equation 2.16 to each of the 5 geometries considered. The net ultimate pullout capacity from these 2 studies are in very good agreement, with a maximum difference of 9% for L/d = 3. This occurs despite the fact that Deng and Carter (2002) use the Modified Cam Clay model.

The deviation from the limit calculation is due to the reduction in the vertical stress discussed in section 4.2.2. The difference between the limit calculation prediction and the results of the current study is highest for L/d = 2 and 3. This is because the reduction in the vertical stress is more significant for these geometries as shown in Figure 4.15.

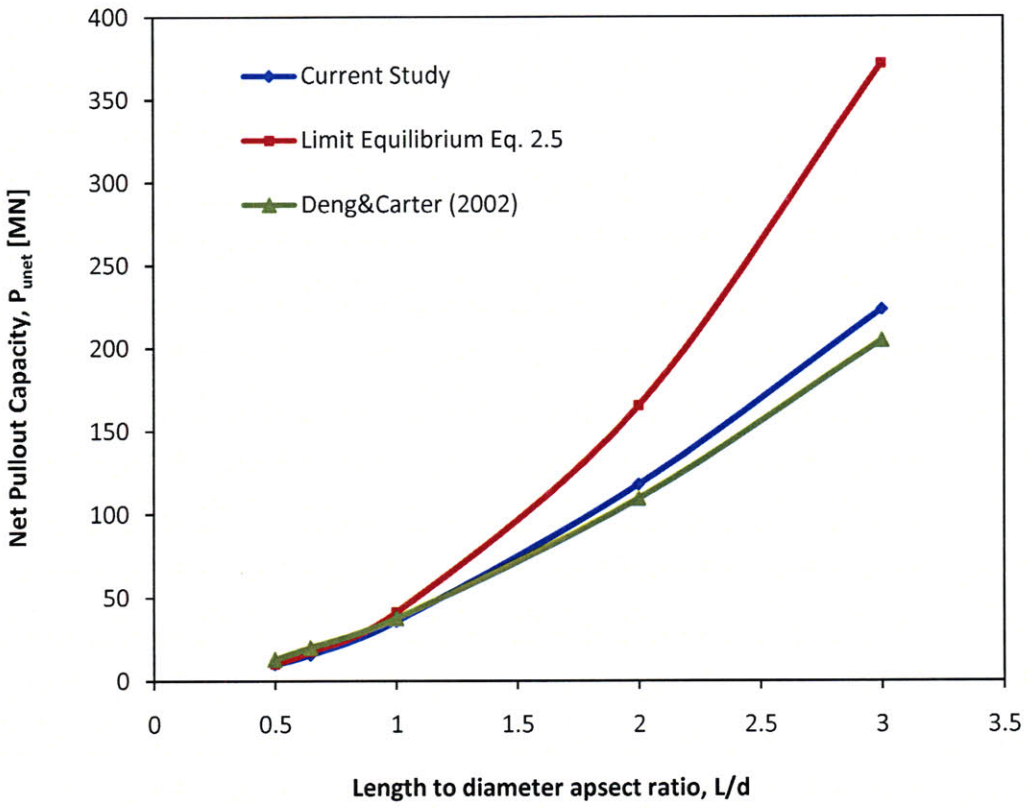

Figure 4-18 Comparison of results from current studies with existing literature for drained loading

5. Numerical Analysis of Suction Caisson under Sustained Loading

The finite element analysis in Chapters 3 and 4 established the upper and the lower limits of the caisson capacity by calculating the capacity under undrained and drained conditions. This part of the study examines the performance of suction caissons when a tensile load is sustained for a period of time while pore pressures are allowed to dissipate.

5.1 The finite element model

Finite element analyses are based on the soil model and assumptions described in Chapter 2. The analyses were performed on different caisson geometries with length to diameter aspect ratios, L/d = 0.5, 0.65, 1, 2 and 3. The finite element model assumptions are the same as those described for the undrained loading in Chapter 3. The permeability of the soil is set to $k = 8.64*10^{-5}$ m/day[2].

The first stage of the calculations is the instantaneous loading of the caisson with an uplift force equal to a percentage of the undrained capacity established in the undrained analysis. This generates an initial displacement of the caisson and the development of a field of negative excess pore pressures (Figure 5.4, t = 0). The second stage of the calculations is consolidation while the initial load is sustained. It is expected that if the load is held for a sufficient time period, the pore pressures will dissipate and hence the capacity will be below the undrained loading predictions.

5.2 Base case analysis

The same base case geometry (d = 17m, L = 11m) used in the undrained and drained analyses is used here. Four load levels are applied to the caisson equal to 57, 69, 80 and 91% of $P_{ult,undrained}$.

[2] A typical range for marine clays is 10^{-5} to 10^{-6} m/day.

5.2.1 Load deformation response

As discussed in Chapter 2, Det Norske Veritas suggest designing suction caissons by using a characteristic storm that lasts between 3 and 48 hours. Figure 5.2 shows the lid displacement after the load has been sustained for 48 hours. Even for a load level of P = 91% $P_{ult,undrained}$, the caisson displacement after 2 days is very small. Figure 5.2 also shows as a reference the displacement if the load is sustained for 20 days. At the highest load level (P = 91% $P_{ult,undrained}$) the displacement is below 2% of the caisson diameter which suggests that loads very close to the undrained capacity may be safely sustained for higher periods than those associated with storms and loop currents.

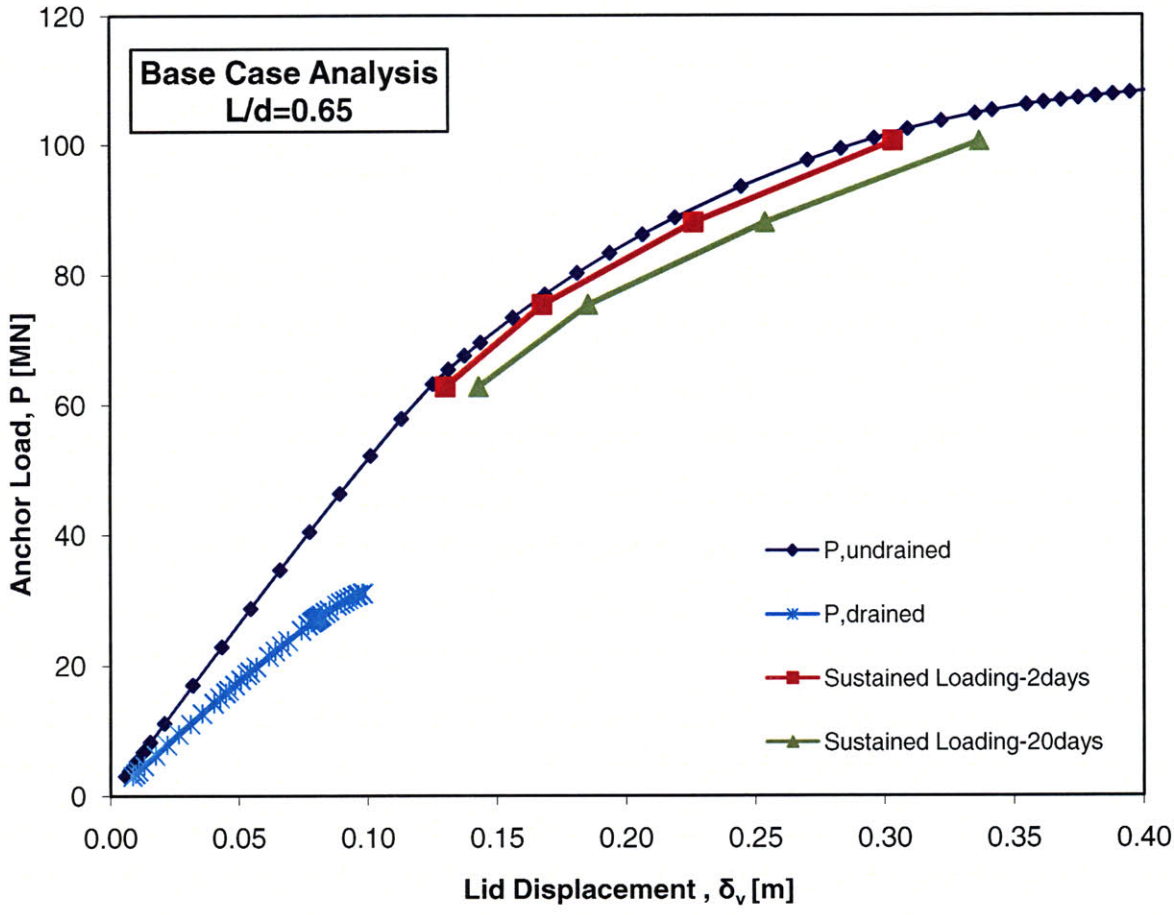

Figure 5-1 Sustained loading displacements for different load levels.

5.2.2 Capacity under sustained loading

Figure 5.2 shows the finite element prediction of the lid displacement if P = 69% $P_{ult,undrained}$ is sustained for very long periods, in order to examine the conditions under which failure will eventually occur. Figure 5.2 indicates that the caisson will continue to displace at a constant rate as the loading period increases, without pullout occurring. As the tensile load is sustained and the caisson displaces upwards, negative pore pressures increase continuously and separation between the lid and the soil underneath does not occur. The displacement of the caisson induces additional negative pore water pressures underneath the caisson lid. The constant rate at which the caisson displaces indicates that the rate at which excess pore water pressures dissipate underneath the caisson lid is smaller than the rate at which they increase as a result of the caisson upward displacement.

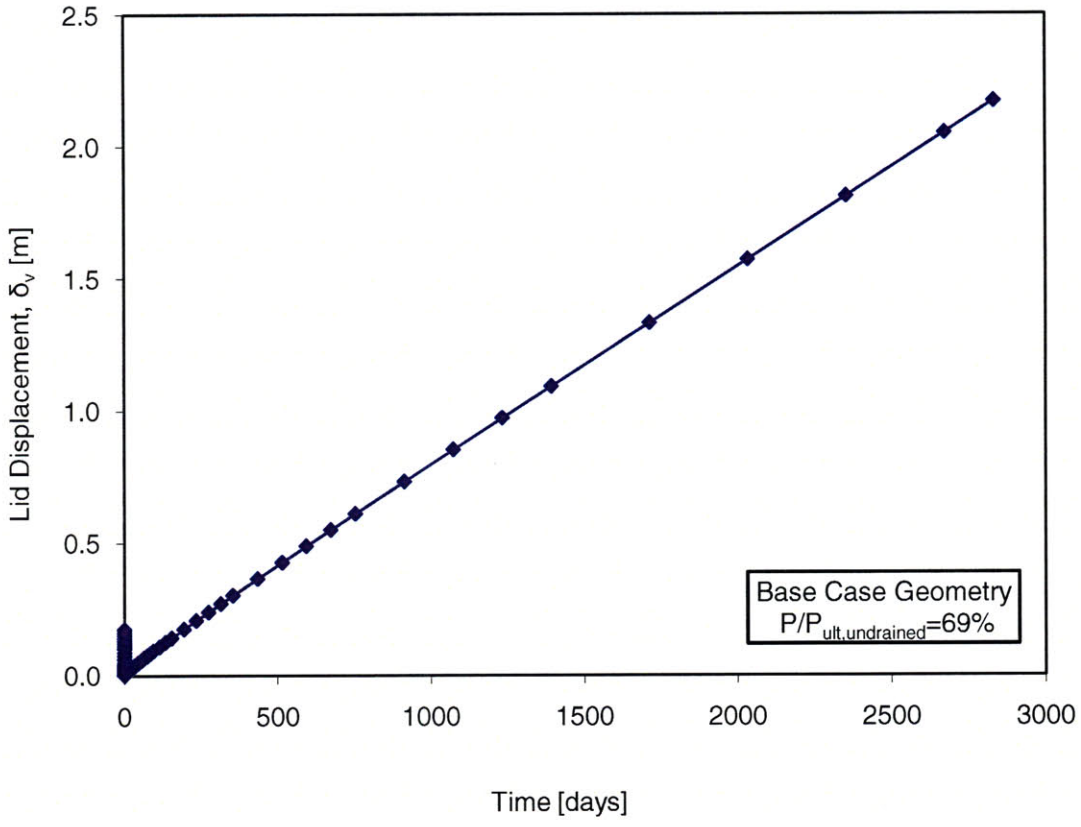

Figure 5-2 Time displacement curve for P/Pult,undrained=69%

Figure 5.3 shows the displacement of the lid and the excess pore pressures (at a reference point 1.7m below the lid at the centreline). The results in Figure 5.3 show that at each load level it is possible to identify a time after which the excess pore pressures increase (become more negative) and at the same time, the caisson starts to displace at a constant rate.

Until this occurs, we consider that the caisson is stable that the load can at least be sustained for that period of time without causing failure of the foundation. Table 5.1 shows the time at which the pore pressures begin to increase and the displacement at that point. As expected, the minimum time over which the load can be sustained decreases with increasing load levels.

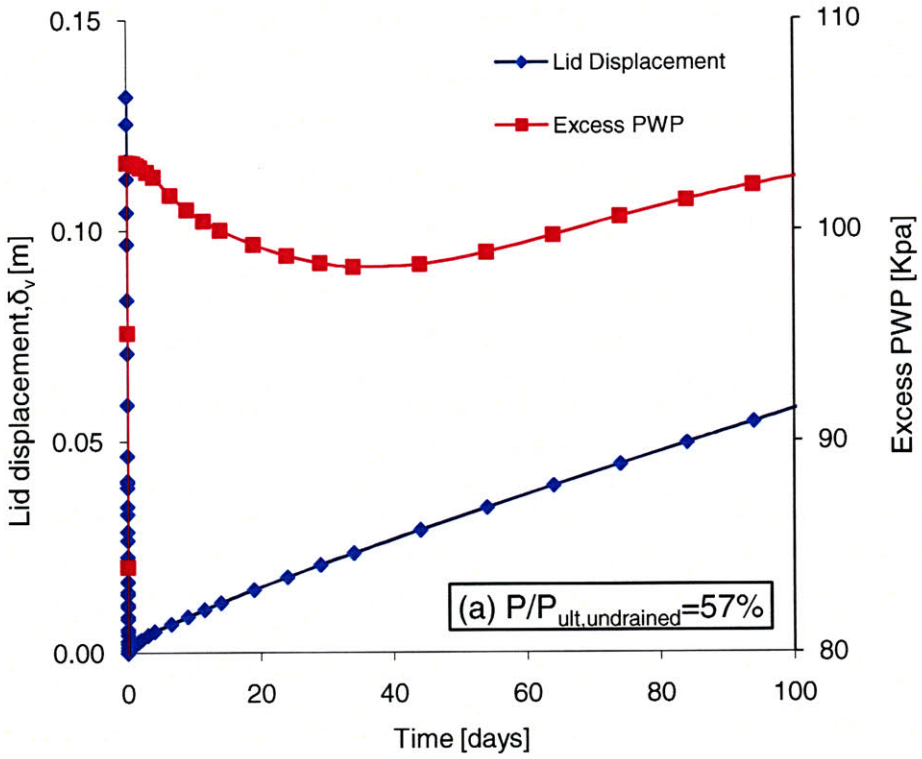
Lid Displacement
Excess PWP
(a) P/P$_{ult,undrained}$=57%
Lid displacement,δ_v [m]
Excess PWP [Kpa]
Time [days]
0.15
0.10
0.05
0.00
110
100
90
80
0
20
40
60
80
100

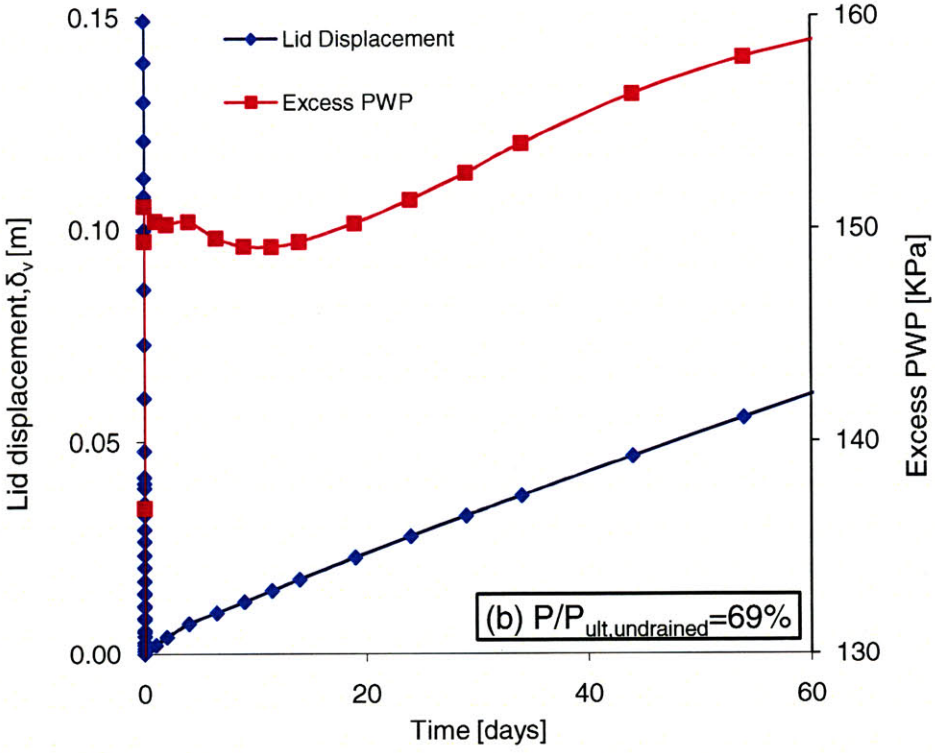
Lid Displacement
Excess PWP
(b) P/P$_{ult,undrained}$=69%
Lid displacement,δ_v [m]
Excess PWP [KPa]
Time [days]
0.15
0.10
0.05
0.00
160
150
140
130
0
20
40
60

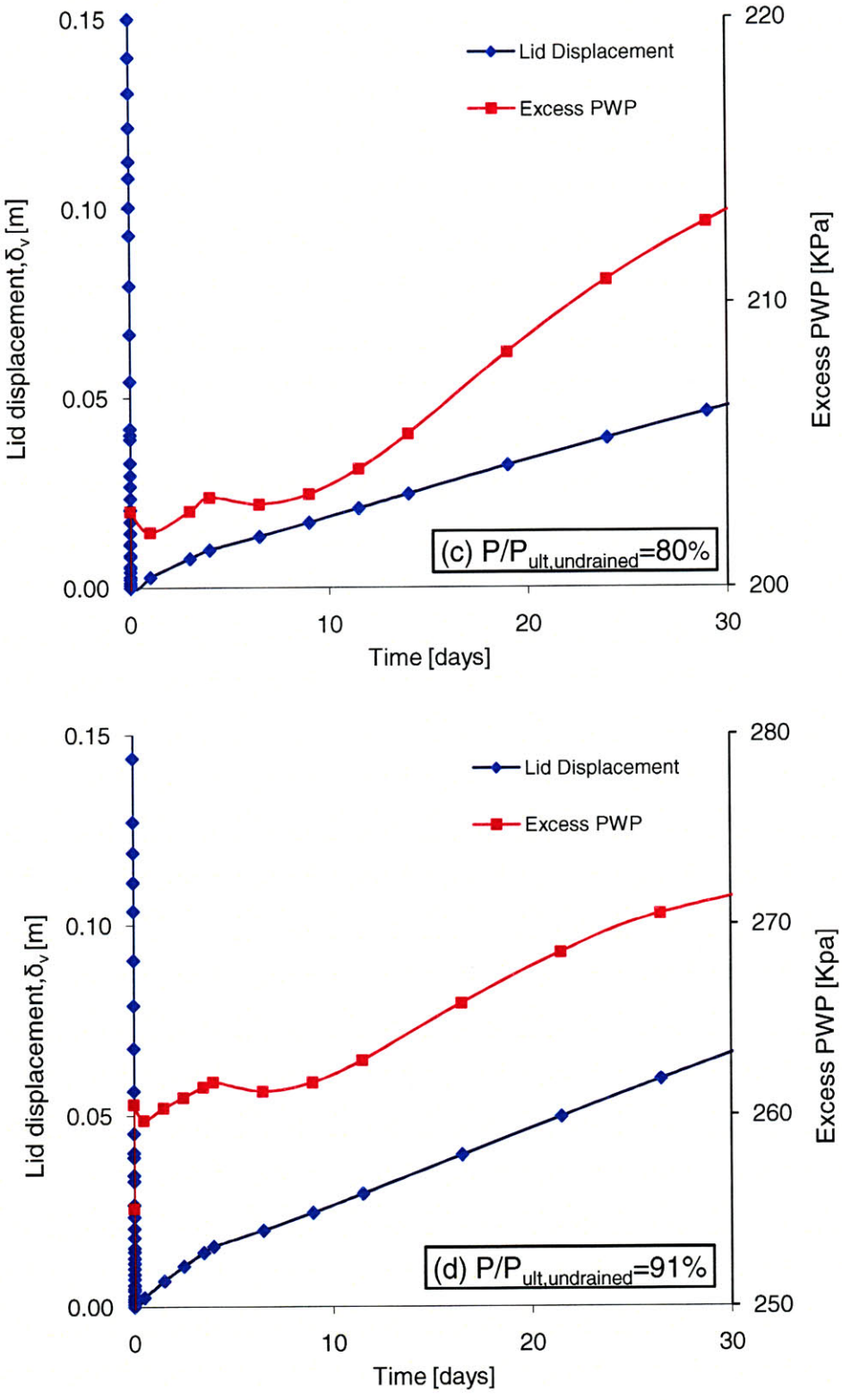

Figure 5-3 Lid displacement and excess pore water pressure with time for base case geometry. The displacements shown here for Time>0 are the incremental displacements after Time=0.

$P/P_{ult,\ undrained}$	Time (days)	δ_v (m)	δ_v/d
57%	39	0.157	0.9%
69%	13	0.184	1.1%
80%	8	0.241	1.4%
91%	7	0.326	2%

Table 5.1 Time for excess pore pressure increase, L/d=0.65

5.2.3 Failure mechanism

The process that results in the behaviour observed above is investigated with plots of the excess pore pressures and other characteristics at different locations and at different times for a specified load level P=69% $P_{ult,undrained}$.

Figure 5.4 shows the excess pore water pressures at t=0,5,15 and 45 days. The pore pressures are dissipating inside the caisson for the first 15 days. At t=45 days all the pore pressures have increased approximately by the same amount throughout the internal part of the caisson. The pullout movement of the caisson increases the excess pore water pressures at a rate larger than the rate at which they can dissipate.

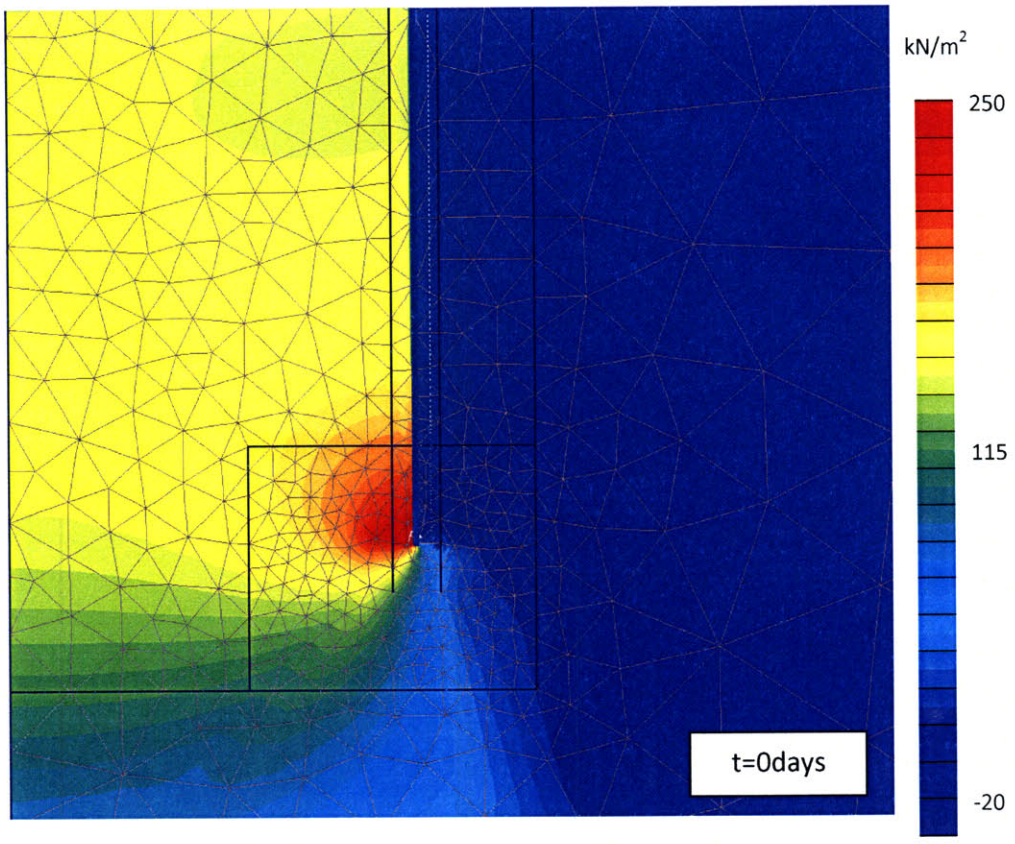
kN/m2
250
115
-20
t=0days

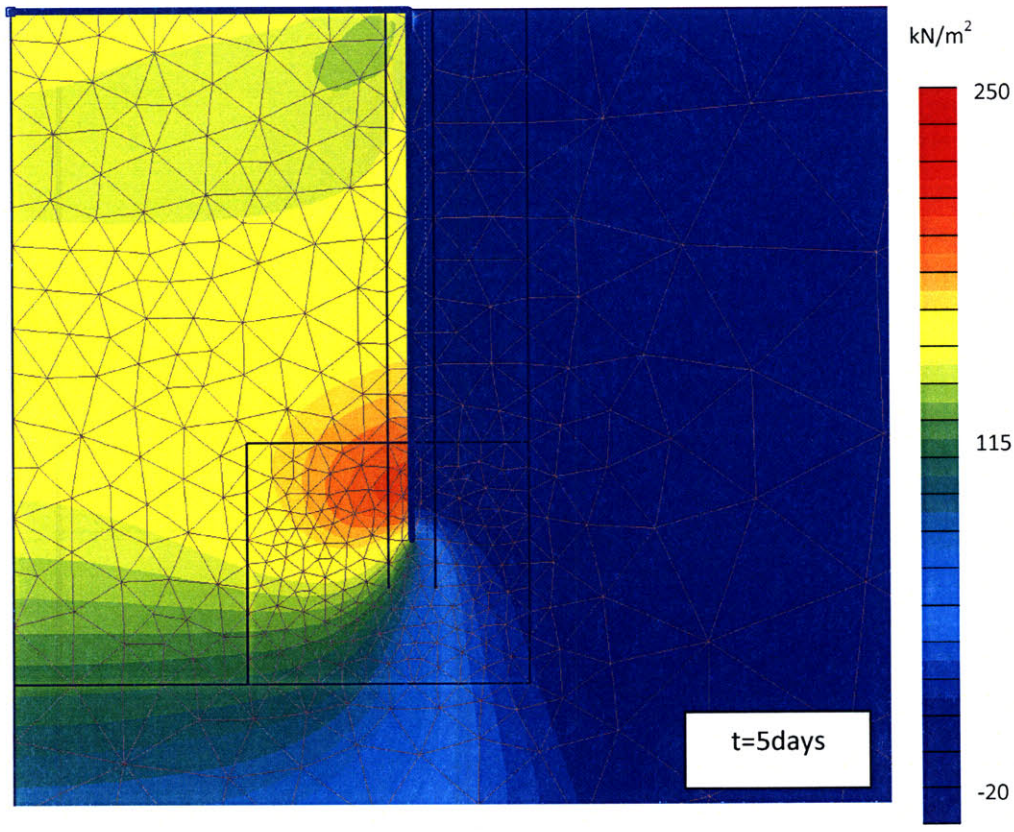
kN/m2
250
115
-20
t=5days

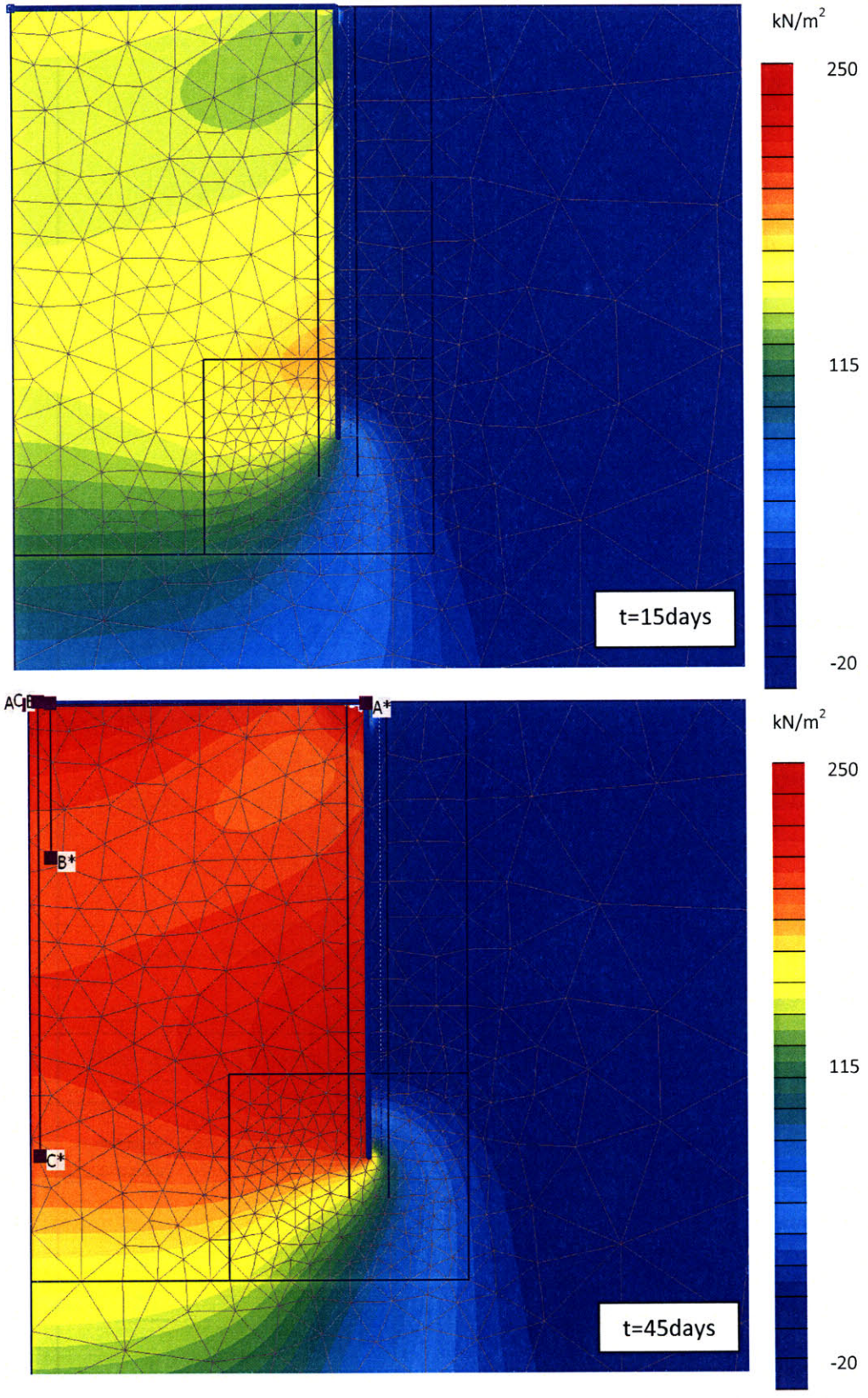

Figure 5-4 Development of excess pore pressures with time for $P/P_{ult,undrained}$=69%

Figure 5.5 shows the development of plastic point inside the soil with time. Initially, most plastic points develop on the external caisson wall and the plastic points at the tip are the beginning of the reverse bearing capacity mechanism observed in Chapter 2. With time, the shearing capacity of the internal caisson wall is reached and plastic points continue to develop inside the caisson starting from the internal wall and moving towards the centre. As the soil is allowed to consolidate, plastic points develop directly underneath the caisson lid as increasingly larger depths.

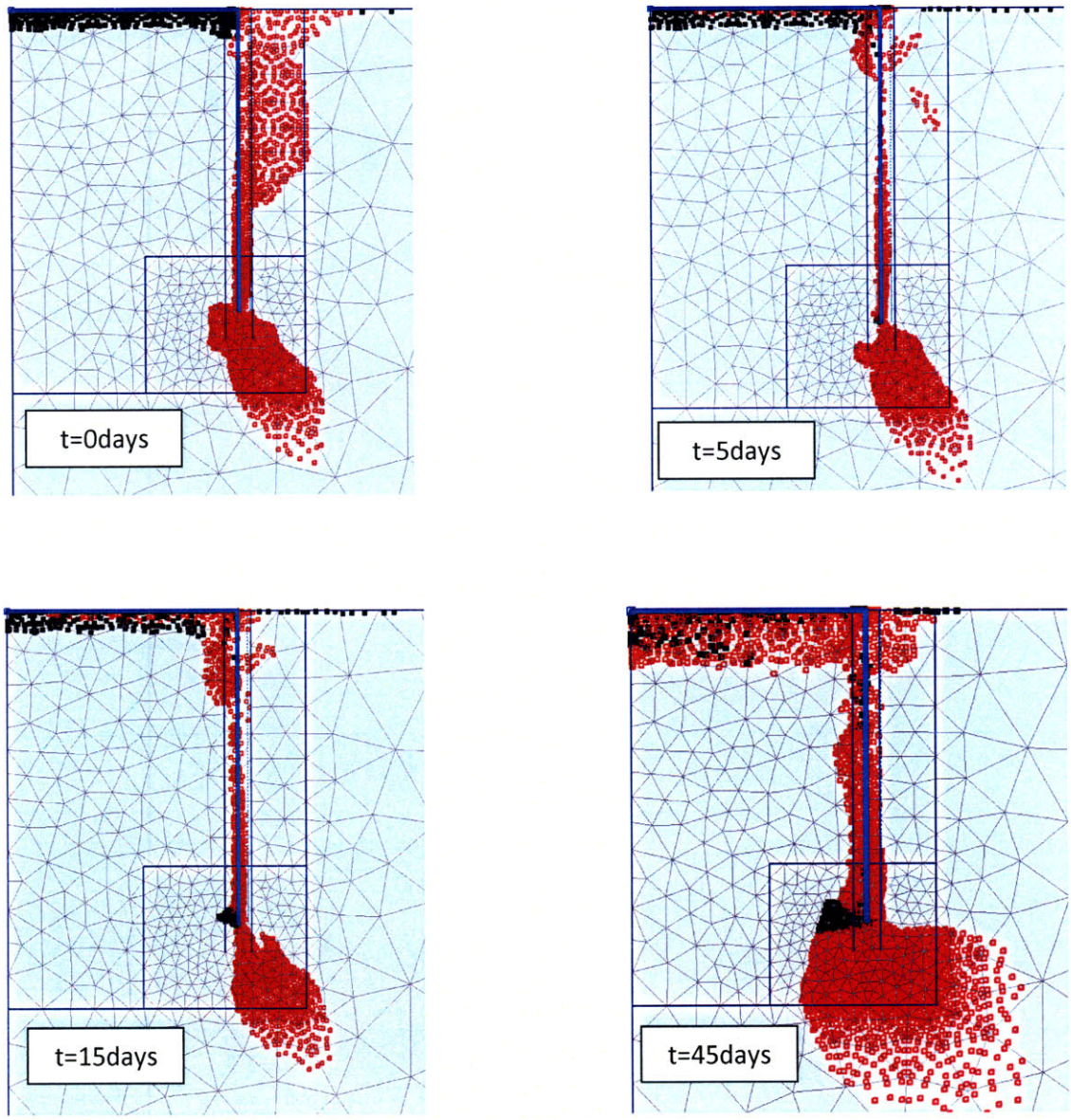

Figure 5-5 Development of plastic points with time for $P/P_{ult,undrained}$=69%

Figures 5.6 to 5.8 describe the behaviour of the caisson after pore pressures begin to increase. The plots are at time t=45days. Figure 5.8 indicates that only the upper part of the soil plug displaces and the rest of the soil plug has very little displacement. The area over which the plastic points develop (Figure 5.5, t=45days) is consistent with the area of the soil plug which undergoes large displacements. The caisson has a total vertical displacement of 0.79 m (Figure 5.7) and the caisson lid does not separate from the adjacent soil (Figure 5.6).

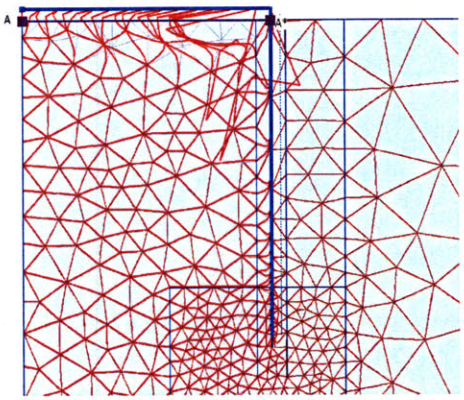

Figure 5-6 Deformed Mesh at t=45 days

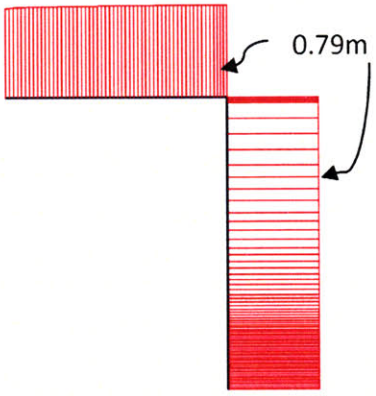

Figure 5-7 Vertical displacement of caisson at t=45 days

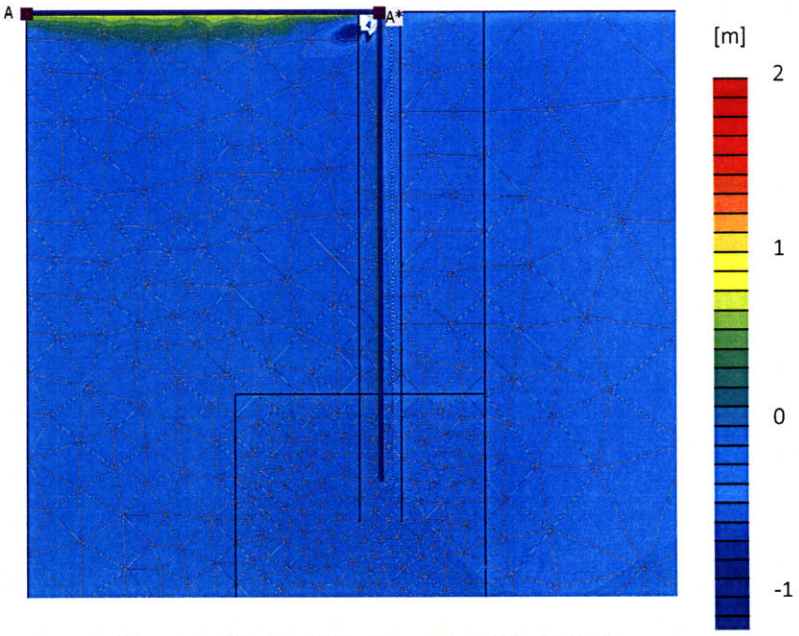

Figure 5-8 Vertical Displacement at t=45days

5.3 Sustained loading capacity for L/d ratios = 0.5,1,2 and 3

Figures 5.9 to 5.16 and Tables 5.2 to 5.5 summarize the effect of the sustained loading on each of the 4 additional geometries considered. Like in the base geometry case, the excess pore pressures at a reference point on the caisson centreline and 1.7m underneath the lid, are shown. It is assumed that the load can at least be sustained until the time when the pore pressures begin to increase. For all the geometries considered, the displacements at that point are within 7% of the caisson length. In some cases it is not possible to explain the pattern than the excess pore water pressures follow. For example, in some cases (L/d = 1 and L/d= 2) the pore pressures increase twice. Furthermore, finite element results indicate that relatively low load levels can be sustained for an infinite amount of time. For example, for load levels $P / P_{ult,undrained} \approx$ 70% and L/d = 2 or L/d = 3, the excess pore water pressures dissipate after periods in the order of 1000 days and the lid undergoes very small displacements.

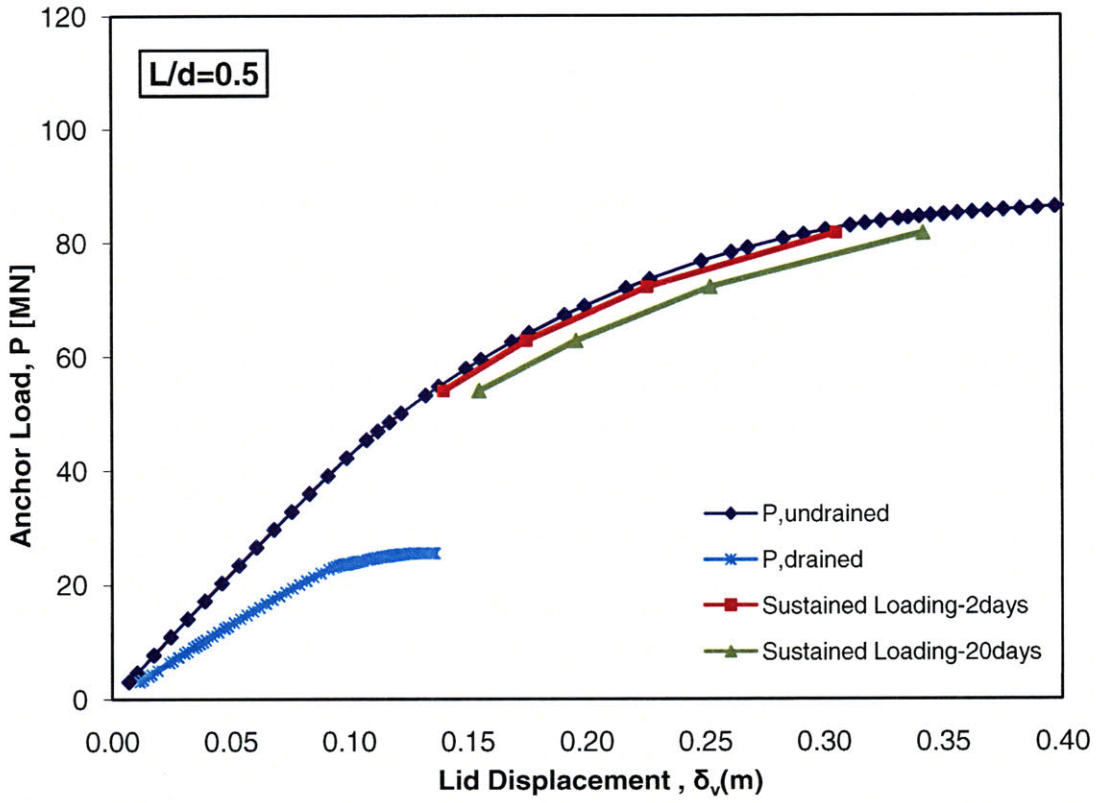

Figure 5-9 Sustained loading displacements for different load levels.

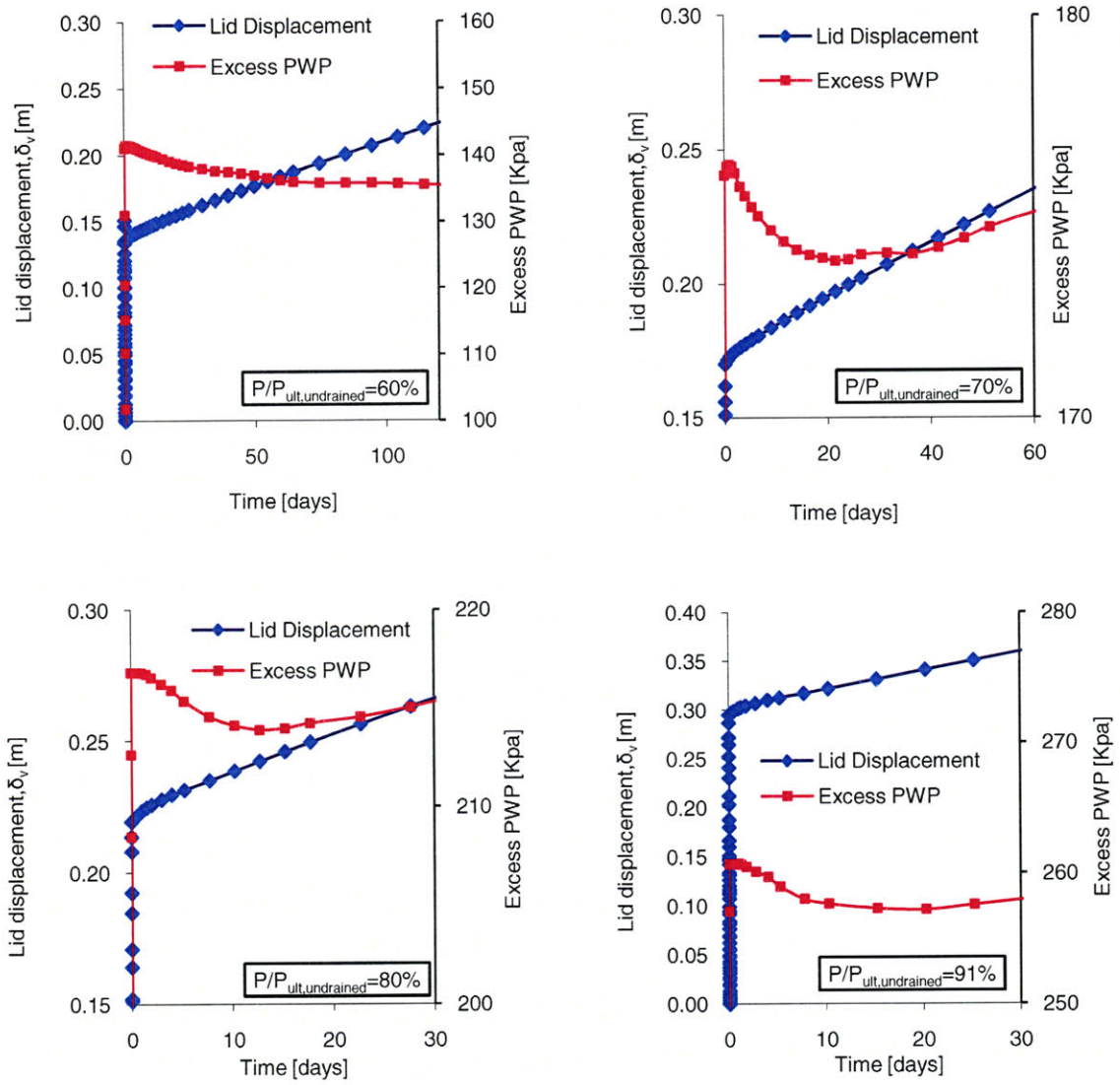

Figure 5-10 Lid displacement and Excess Pore Water Pressure with time for L/d=0.5 geometry. The displacements are absolute in this case and not incremental.

$P/P_{ult,\ undrained}$	Time (days)	δ_v (m)	δ_v /L
60%	64	0.167	2%
70%	36	0.192	2%
80%	15	0.241	3%
91%	20	0.328	4%

Table 5.2 Time for excess pore pressure increase, L/d=0.5

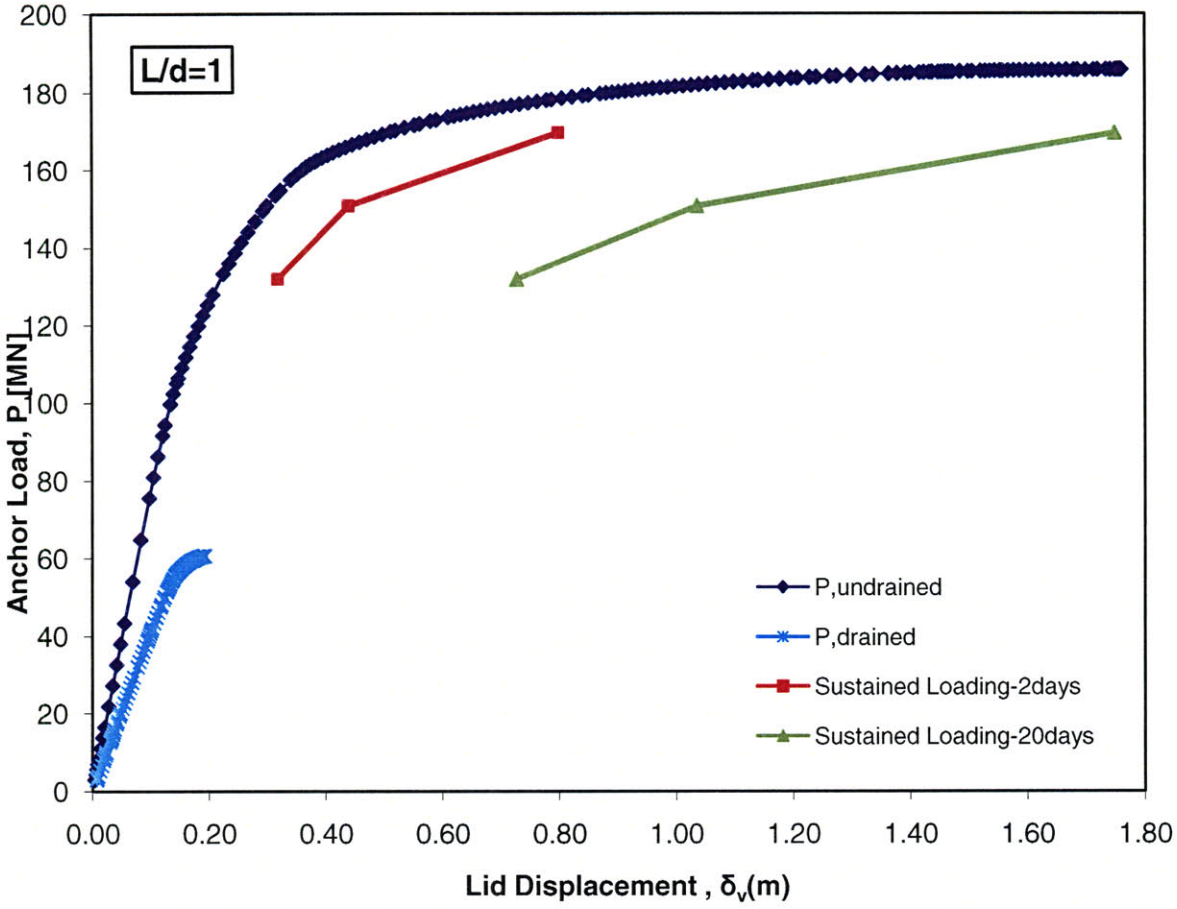

Figure 5-11 Sustained loading displacements for different load levels.

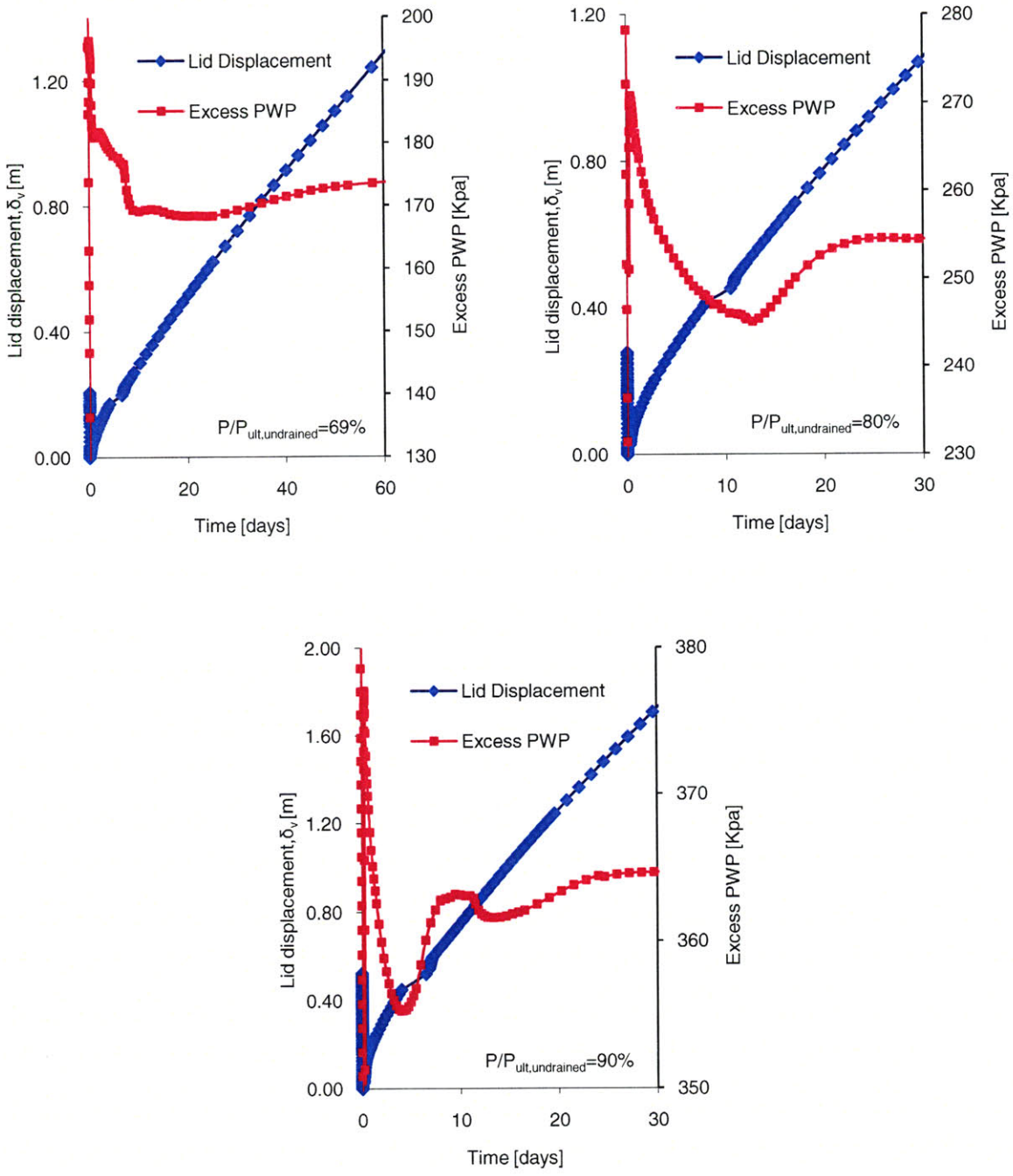

Figure 5-12 Lid displacement and Excess Pore Water Pressure with time for L/d=1 geometry.

$P/P_{ult,\ undrained}$	Time (days)	δ_v (m)	δ_v /L
68%	25	0.931	5%
78%	13	0.981	6%
91%	4	1.250	7%

Table 5.3 Time for excess pore pressure increase, L/d=1

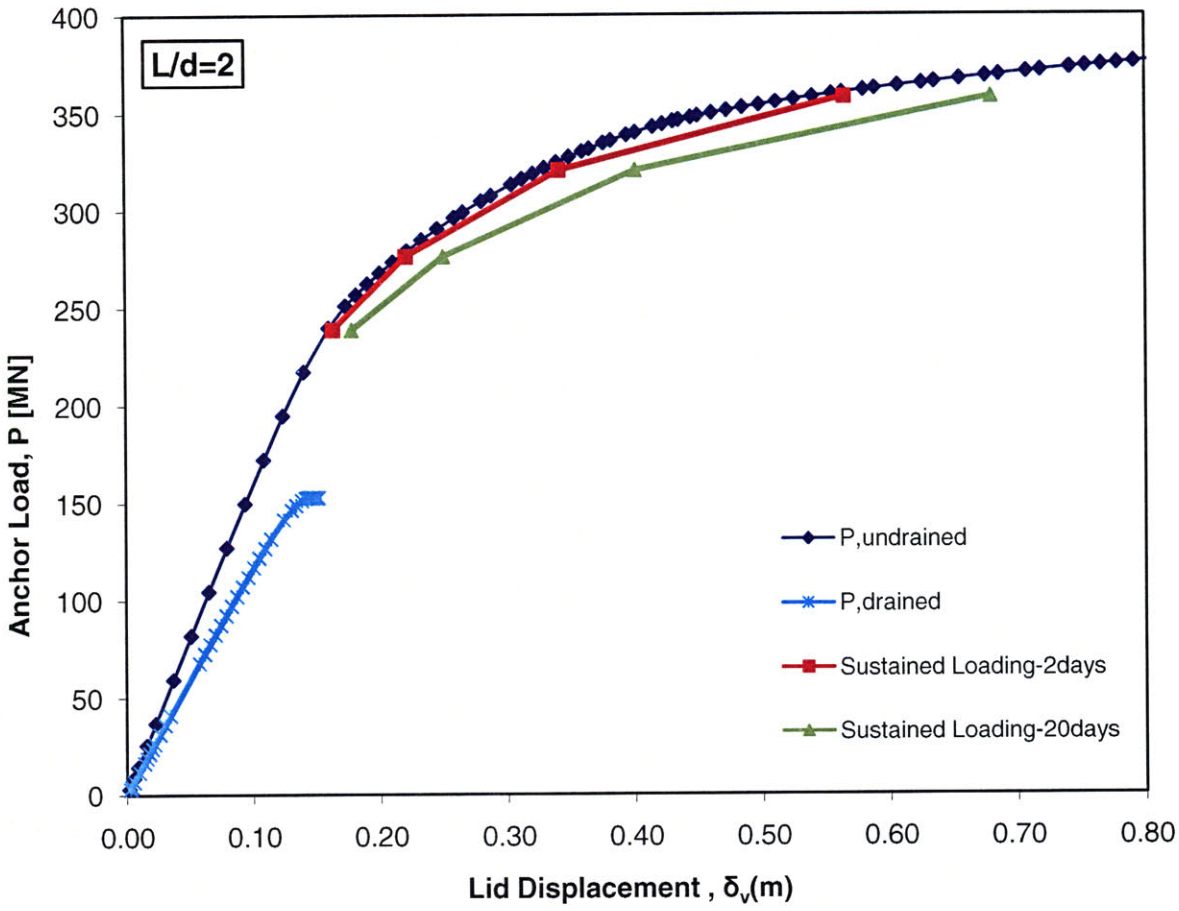

Figure 5-13 Sustained loading displacements for different load levels.

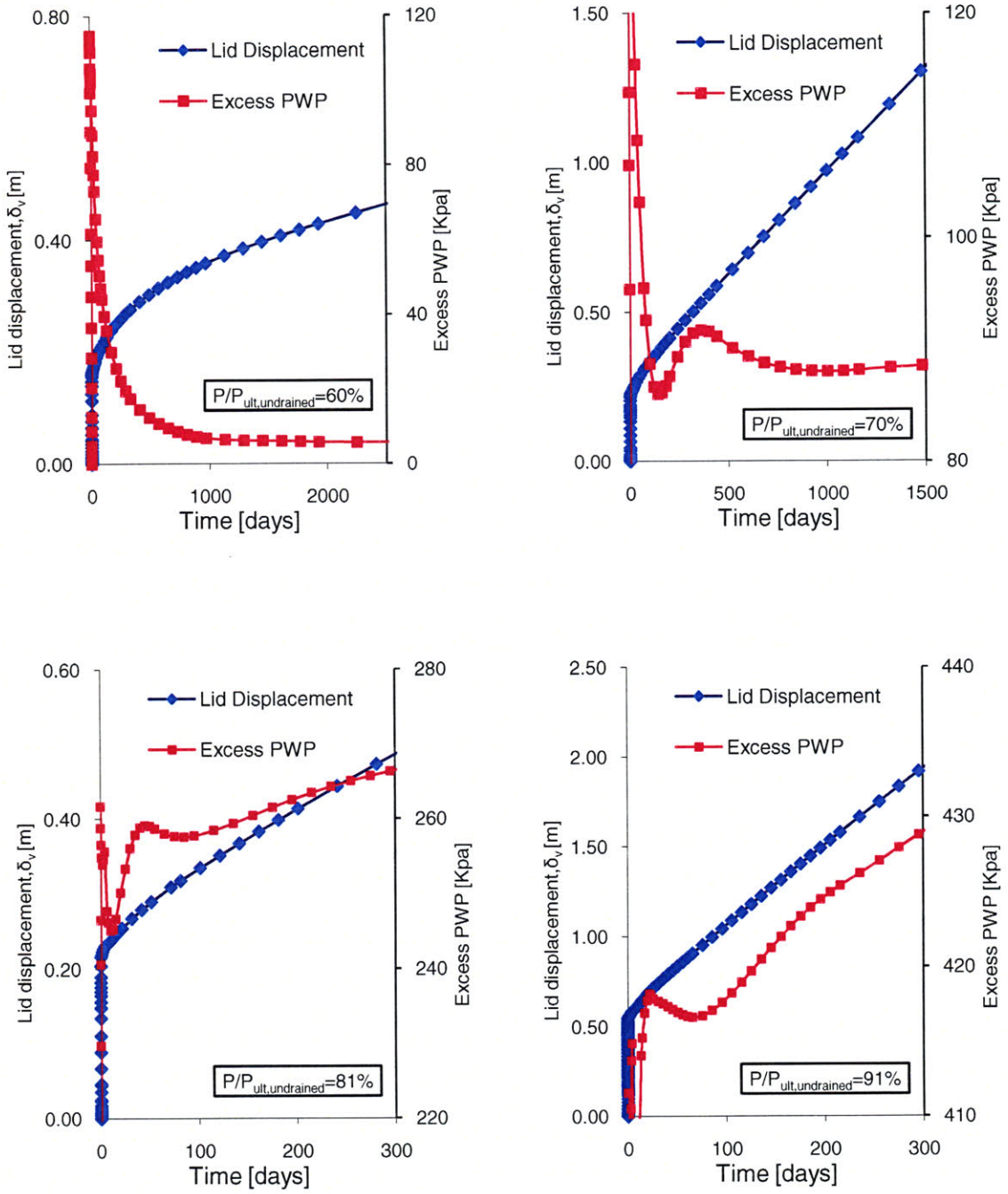

Figure 5-14 Lid displacement and Excess Pore Water Pressure with time for L/d=2 geometry. The displacements are absolute in this case and not incremental.

$P/P_{ult,\ undrained}$	Time (days)	δ_v (m)	δ_v /L
60%	inf	0.700	2%
70%	142	0.430	1%
81%	92	0.606	2%
91%	66	0.905	3%

Table 5.3 Time for excess pore pressure increase, L/d=2.

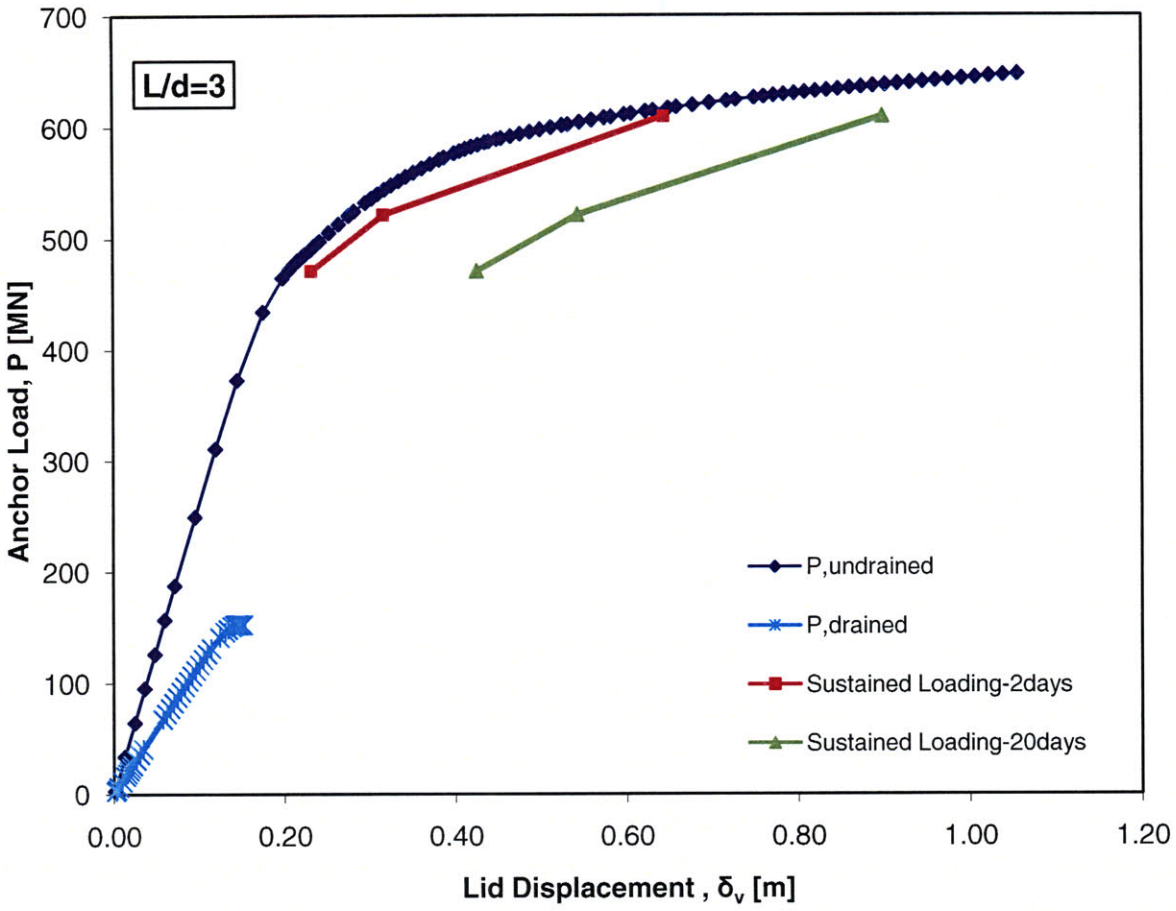

Figure 5-15 Sustained loading displacements for different load levels, L/d=3.

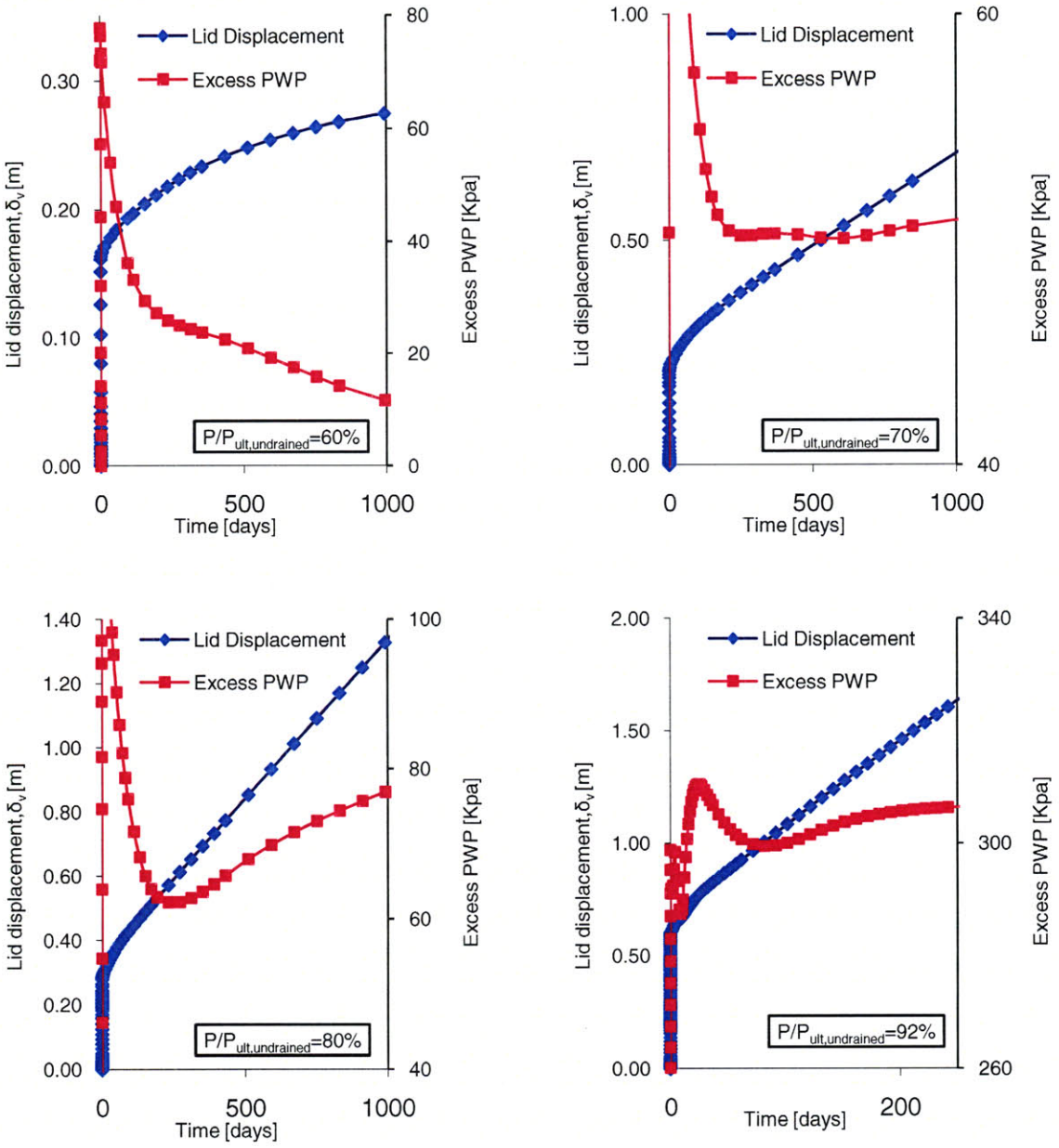

Figure 5-16 Lid displacement and Excess Pore Water Pressure with time for L/d=3 geometry. The displacements are absolute in this case and not incremental.

$P/P_{ult,\ undrained}$	Time (days)	δ_v (m)	δ_v /L
62%	infinite	0.300	1%
70%	609	0.533	1%
80%	231	0.572	1%
92%	92	1.006	2%

Table 5.5 Time for excess pore pressure increase, L/d=3.

Figure 5.17 summarizes the minimum holding periods and provides comparisons between caissons of different geometries. The general trend is for the period to increase with increasing L/d ratio. Increasing the caisson length, increases the drainage path and this makes the dissipation of excess pore water pressures increasingly harder. The rate at which drainage occurs is related to L^2 and this is why caissons with larger lengths have significantly longer minimum holding periods.

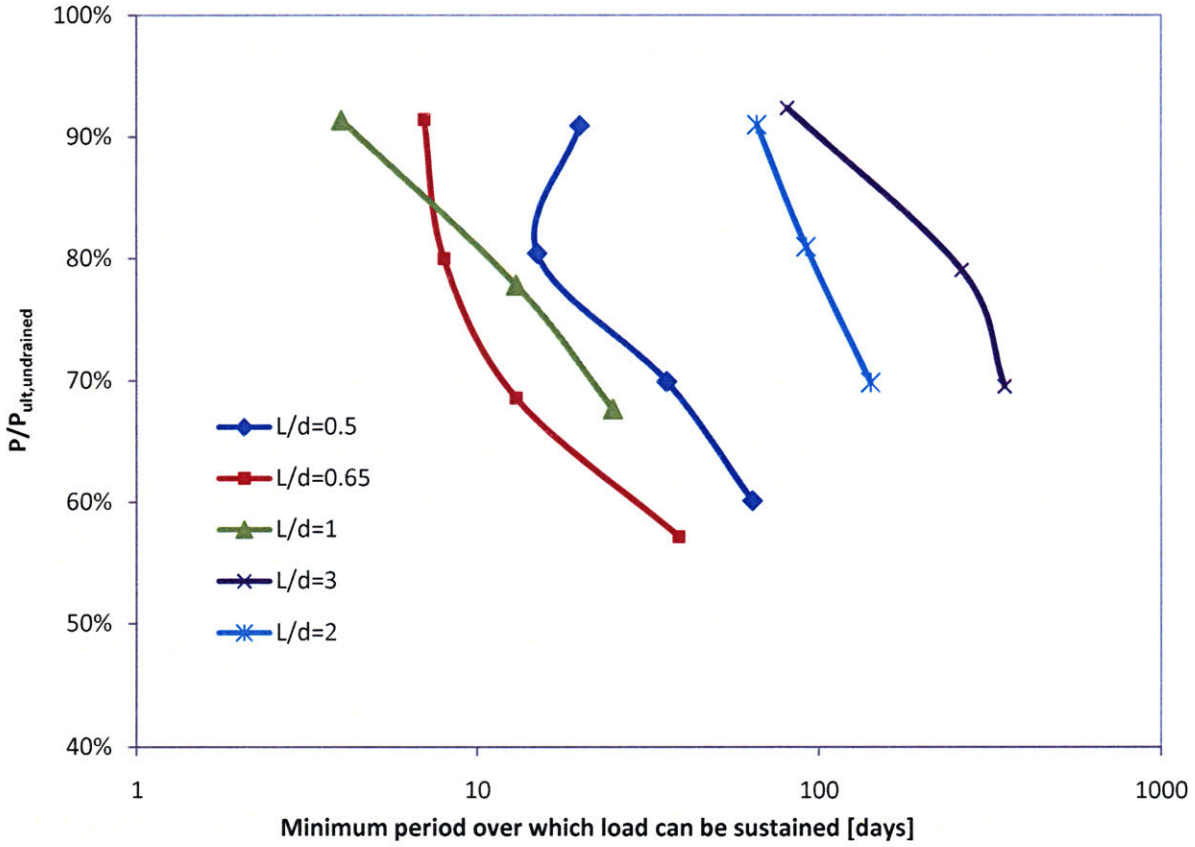

Figure 5-17 Effect of caisson geometry on minimum period over which loads can be sustained

6. Results and Recommendations

This finite element study examined the capacity of suction caissons under three loading conditions. The undrained and drained loading analyses established the upper and lower capacity limits for the 5 geometries examined. It was found that the undrained capacity can be between 3.6 and 2.3 times the drained capacity for the geometries considered and this ratio reduces as L/d decreases. This is due to the fact that a large component of the undrained capacity comes from the base resistance which varies with L^2, whereas the internal wall friction force-unique to the drained case- varies with only with L.

It was found that the predicted undrained capacity matches perfectly the limit equilibrium solutions and for L/d<1.5 is in very good agreement with the Deng and Carter (2002) results. For larger L/d ratios, the difference can increase up to 30%. This can be attributed to the fact that Deng and Carter provide an experimental formula depending only on L/d and to the fact that they use the MCC model.

The finite element prediction for the drained case is significantly lower than the capacity estimated by limit equilibrium. An important parameter neglected in the limit calculations is the reduction in vertical and horizontal effective stresses on the caisson walls that result in an equivalent reduction to the downward shear force resisting the uplift loading. Nevertheless, the predicted capacities are in very good agreement with the result of the Deng and Carter (2002) solution. One of the critical parameters in the drained analysis was the use of interfaces and their impact on caisson behaviour. An interface had to be introduced between the caisson lid and the top of the internal soil plug in order to ensure separation occurred during loading.

The final part of this study examined the behaviour of suction caissons under sustained loading by assuming one of the highest permeabilities encountered in marine clays. The rate at which negative excess pore pressures develop underneath the caisson lid was found to be smaller than the rate at which they dissipate and thus the caisson continues to displace at a constant

rate for very large time periods. By establishing the times at which the excess pore pressures start to increase, it was possible to identify minimum periods over which the load may be safely sustained by the caisson which are below the duration of storms and loop current loads.

It was found that the displacements of caissons of all geometries are under 3% the diameter for the maximum period relevant to storm loading (2 days). The only exception is the 5% the diameter displacement for the 92% $P / P_{ult,undrained}$ loading of the L/d = 3 caisson. Although it was not possible to make direct comparisons with the Clukey et *al.* (2004) results, the results of this study do not contradict the general findings such as that as L/d increases so does the period over which specific load levels can be sustained.

Further research could examine the effects of highly permeable layers within the soil as well as the effects of increasing the overall soil permeability. The presence of a drainage layer within the soil could have a critical impact on the drainage properties and hence on the capacity of the caisson under sustained loading.

References

Andersen, K.H. and Jostad, H.P. (1999). 'Foundation Design of Skirted Foundations and Anchors in Clay'. *Proc Offshore Tech Conf,* OTC 10824.

Andersen, K.H. and Jostad, H.P. (2004). 'Shear Strength Along Inside of Suction Anchor Skirt Wall in Clay'. *Proc Offshore Tech Conf,* OTC 16844.

Bye, A., Erbrich, C. Rognlien, B., Tjelta, T.I. (1995). 'Geotechnical Design of Bucket Foundations'. *Proc Offshore Tech Conf,* OTC 7793.

Byrne, B.W., and Houlsby, G.T. (2002). 'Experimental investigations of response of suction caissons to transient vertical loading'. *Journal of Geotech. and Geoenv. Engrg.*, Vol. 128, No. 11, p. 926-939.

Chen, W. and Randolph, M.F. (2007). 'External radial stress changes and axial capacity for suction caissons in soft clay'. *Geotechnique*, 57, No. 6, p.499-511.

Clukey, E. C., Morrison, M. J., Gariner, J., and Corté, J. F. (1995). 'The response of suction caissons in normally consolidated clays to cyclic TLP loading conditions'. *Proc Offshore Tech Conf*, OTC 7996.

Colliat, J-L., Boissard,P., Andersen, K.H., Schroder, K. (1995). 'Caisson foundations as alternative anchors for permanent mooring of a process barge offshore Congo'. *Proc Offshore Tech Conf*, OTC 7797, Houston, p. 919-929.

Delft University of Technology (2007). ' A course on suction caisson foundations' Available: www.offshoreengineering.org. [Accessed 20th October 2008].

Deng, W., and Carter, J.P. (2002). 'A theoretical study of the vertical uplift capacity of suction caissons'. *International Journal of Offshore and Polar Engineering*. Vol. 12, No. 2, p. 89-97.

Det Norske Veritas (2005). 'Geotechnical Design and Installation of Suction Anchors in Clay'. Recommended Practice DNV-RP-E303.

El-Gharbawy, S.L. (1998). 'The Pullout Capacity of Suction Caisson Foundations for Tension Leg Platforms', PhD Dissertation, The University of Texas, Austin.

El-Gharbawy, S., and Olson, R. (1999). 'Suction caisson foundations in the Gulf of Mexico'. Analysis, Design, Construction, and Testing of Deep Foundations, ASCE Geotechnical Sp. Pub. 88, p. 281-295.

El-Gharbawy, S.L., Olson, R.E., and Scott, S.A. (1999). 'Suction anchor installations for deep Gulf of Mexico applications'. *Proc Offshore Tech Conf*, OTC 10992, p. 747-754.

El-Gharbawy, S.L., and Olson, R.E. (2000). 'Modelling of suction caisson foundations'. *Proceedings of the International Offshore and Polar Engineering Conference*, Vol. 2, p. 670-677.

Erbrich, C.T., and Tjelta, T.I. (1999), 'Installation of bucket foundations and suction caissons in sand–Geotechnical performance'. *Proc Offshore Tech Conf*, OTC 10990, p. 725-735.

Fines, S., Stove, O., Guldberg, F. (1991) 'Snorre TLP Tethers and Foundation'. *Proc Offshore Tech Conf*, OTC 6623. p. 587-597.

Finn, W.D.L., Byrne, P.M. (1972). 'The Evaluation of the Breakout Force for a Submerged Ocean Platform', *Proc Offshore Tech Conf*, OTC 1604, Houston, p. 351-365.

Hight, D.W., Jardine, R.J., Gens, C.S. (1987). 'The behaviour of soft clays: Embankments on soft clay. Bull. Public Work Research Centre, Athens, p. 33-158.

Hogervorst, J. R. (1980), 'Field trials with large diameter suction piles'. *Proc Offshore Tech Conf*, OTC 3817, p. 217-224.

Houlsby, G. T. and Byrne, B. W. (2005). 'Calculation procedures for installation of suction caissons in sand'. *Proc. ICE Geotech. Engng,* Vol. 158, No. 3, p. 135–144.

Iskander, M., El-Gharbawy, S.L., Olson, R. (2002). 'Performance of suction caissons in sand and clay'. Canadian Geotechnical Journal, Vol. 39, p. 576-584.

Luke, A.M., Rauch, A.F., Olson, R.E., Mecham, E.C. (2005). 'Components of suction caisson capacity measured in axial pullout tests', *Ocean Engineering*, Vol. 32, p.878-891.

Maniar, D.R., Gonzalo Vásquez, L.F., Tassoulas, J.L. (2005) 'Suction Caissons: Finite Element Modelling', 5th GRACM International Congress on Computational Mechanics.

Mayne, P.W., Kulhawy, F.H. (1982). 'K_0-OCR Relationships in Soils'. *J Geotech Eng Div*, ASCE, Vol.108, GT6, p.851-873.

Newlin, J. A. (2003). 'Suction Anchor Piles for the Na Kika FDS Mooring System. Part 1: Site Characterization and Design'. *Proc. Int. Symp. on Deepwater Mooring Systems: Concepts, Design, Analysis, and Materials*, Houston, p. 55–57.

Poulos, G.H. (1988). *Marine Geotechnics*. London: Unwin Hyman. p.33-35.

Randolph, M. F., O'Neill, M. P., and Stewart, D. P. (1998). 'Performance of suction anchors in finegrained calcareous soils'. *Proc Offshore Tech Conf*, OTC 8831, p.521-529.

Rao, S. N, Ravi, R., and Ganapathy, C. (1977), "Pullout behavior of model suction anchors in soft marine clays'. *Proceedings, Seventh International Offshore and Polar Engineering Conference,* Honolulu.

Rune Dyvik, I Knut H. Andersen, Svein Borg Hansen, and Hans Peter Christophersen (1993). 'Field tests of anchors in clay. I: Description'. *J. of Geotech. Engr*, Vol. 119, No. 10.

Skempton, A.W. (1951), 'The Bearing Capacity of Clays'. *Proc. Building Research Congress*, Vol. 1, p. 180-189.

Steensen-Bach, J. O. (1992). 'Recent model tests with suction piles in clay and sand'. *Proc Offshore Tech Conf*, OTC 6844, p. 323-330.

Sukumaran, B., McCarron, W.O., Jeanjean, P., and Abouseeda, H. (1999). 'Efficient finite element techniques for limit analysis of suction caissons under lateral loads'. *Comp. and Geotech*, V. 24, p. 89-107.

Tjelta, T. I., Guttormsen, T. R., and Hermstad, J. (1986). 'Large-scale penetration test at a deepwater site'. *Proc Offshore Tech Conf*, OTC 5103, p. 201-212.

Tjelta, T.I. (1994). 'Geotechnical Aspects of Bucket Foundations Replacing Piles for the Europipe 16/11-E Jacket'. *Proc Offshore Tech Conf,* OTC 7379.

Tjelta, T.I. (1995). 'Geotechnical Experience from the Installation of the Europipe Jacket with Bucket Foundations'. *Proc Offshore Tech Conf,* OTC 7795. p. 897-908.

Vesic, A.S. (1973). 'Analysis of Ultimate Loads of Shallow Foundations'. J. Soil Mechanics & Fdn. Div., ASCE, Vol. 99, SM2, p.42-73.

Wang, M. C., Demares, K. R., and Nacci, V. A. (1977), "Application of suction anchors in the offshore technology," *Proc Offshore Tech Conf*, OTC 3203, pp. 1311-1320.

Whittle, A. J., Germaine, J. T., and Cauble, D. F. (1998). 'Behavior of miniature suction caissons in clay'. *Offshore Site Investigation and Foundation Behaviour '98*, SUT, p. 279-300.

Zdravkovic, L., Potts, D. M. & Jardine, R. J. (2001). 'A parametric study of the pull-out capacity of bucket foundations in soft clay'. *Geotechnique*, 51, No. 1, p. 55-67.

Appendix A

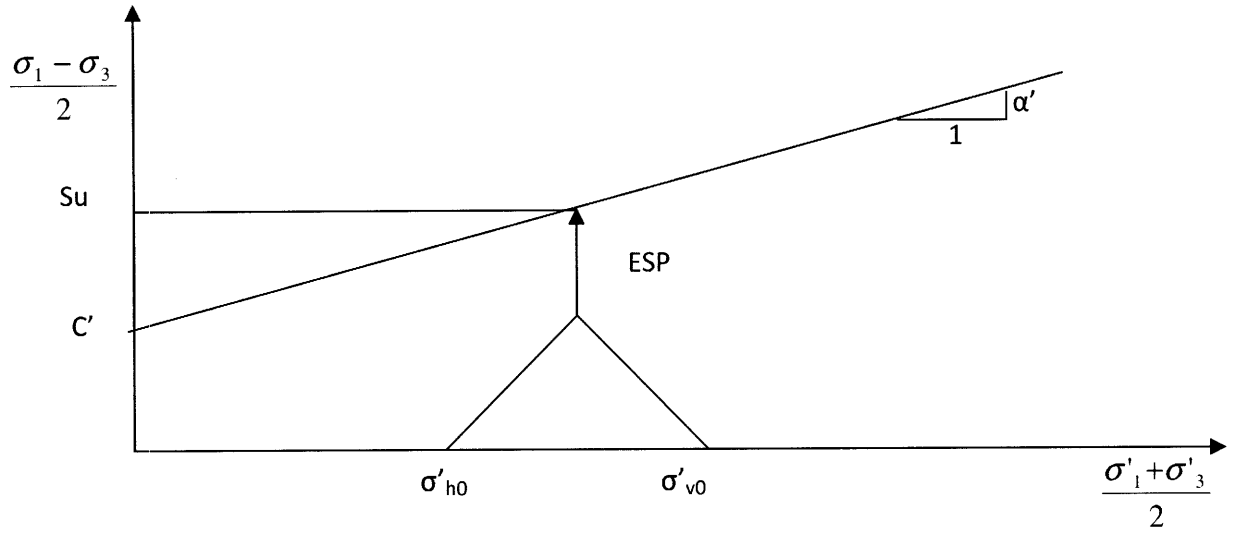

For plane stain conditions the effective stress path (ESP) is vertic*al.* In plane strain, $\varepsilon_2=0$ and $\Delta\sigma'_x+\Delta\sigma'_y=0$ and the parameter A=0.5.

Assuming such an ESP path yields the following relationship:

$$\frac{S_u}{\sigma'_{v0}} = \frac{c'\cos\phi'}{\sigma'_{v0}} + \frac{(1+K_0)\sin\phi'}{2}$$

Appendix B: Breakdown of undrained loading forces for L/d=0.5,1,2,3

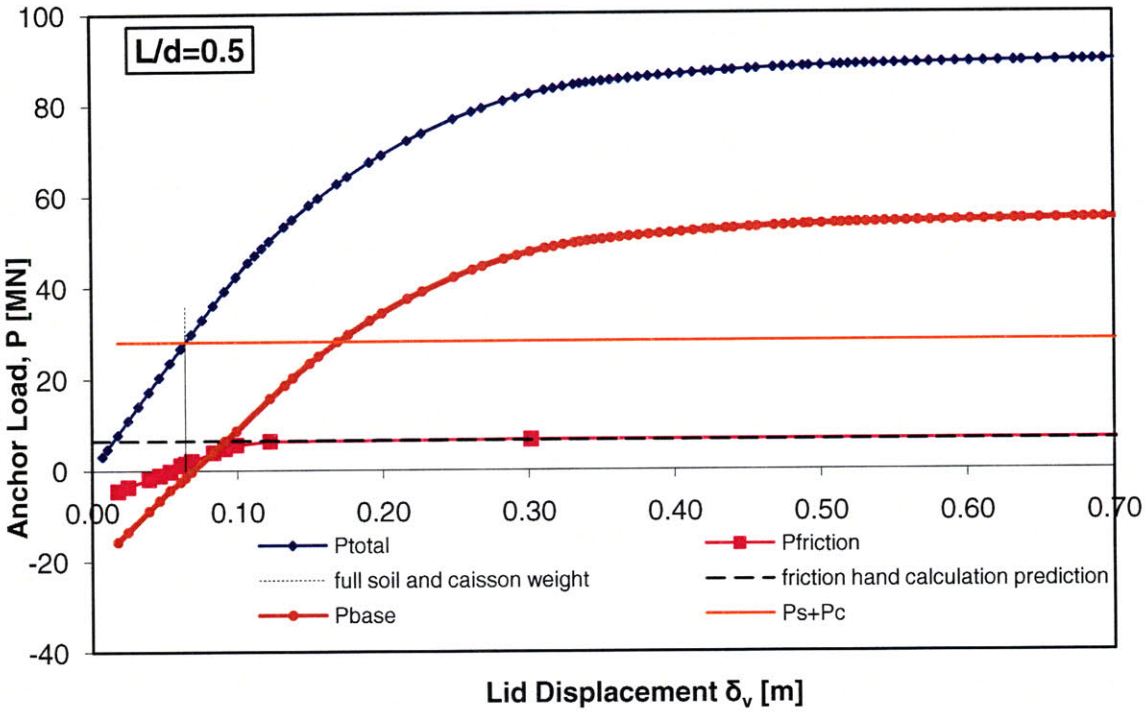

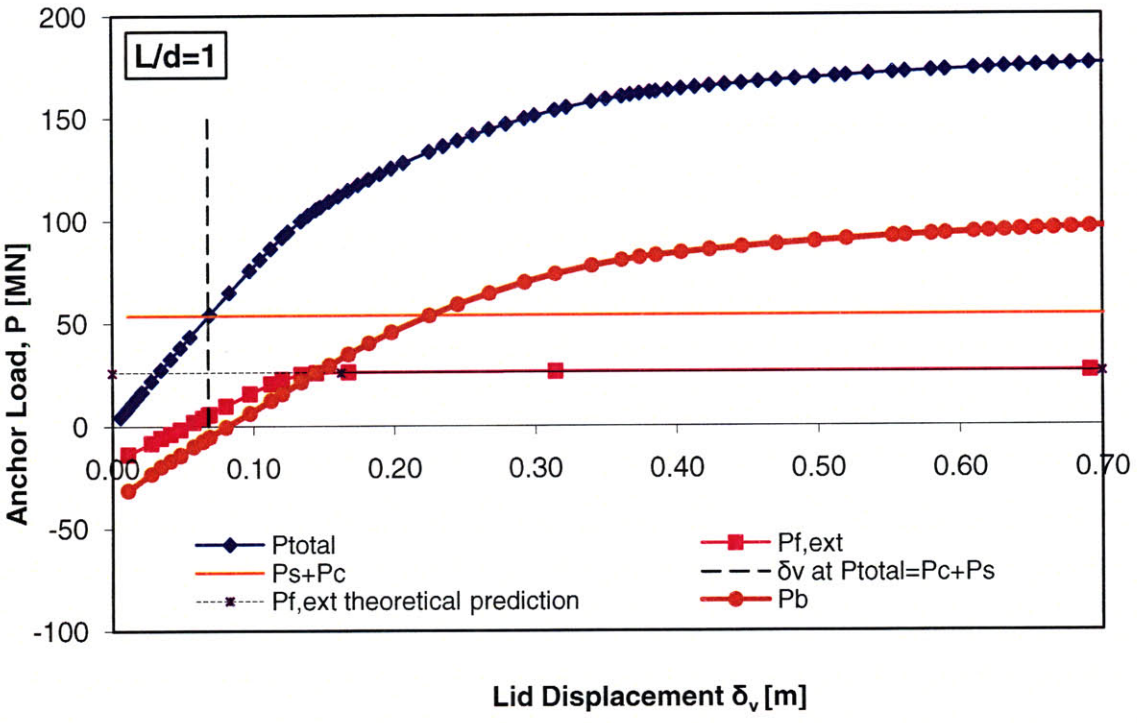

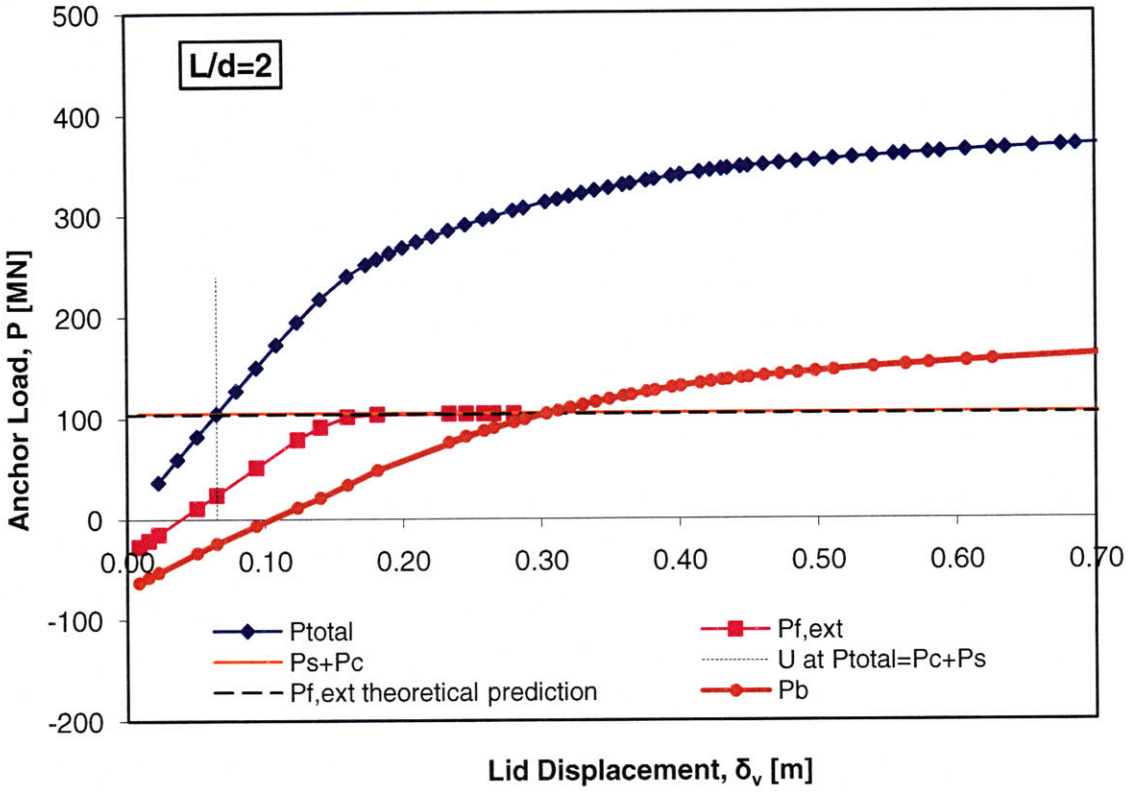
L/d=2
Anchor Load, P [MN]
500
400
300
200
100
0
-100
-200
0.00
0.10
0.20
0.30
0.40
0.50
0.60
0.70
Ptotal
Ps+Pc
Pf,ext theoretical prediction
Pf,ext
U at Ptotal=Pc+Ps
Pb
Lid Displacement, δv [m]

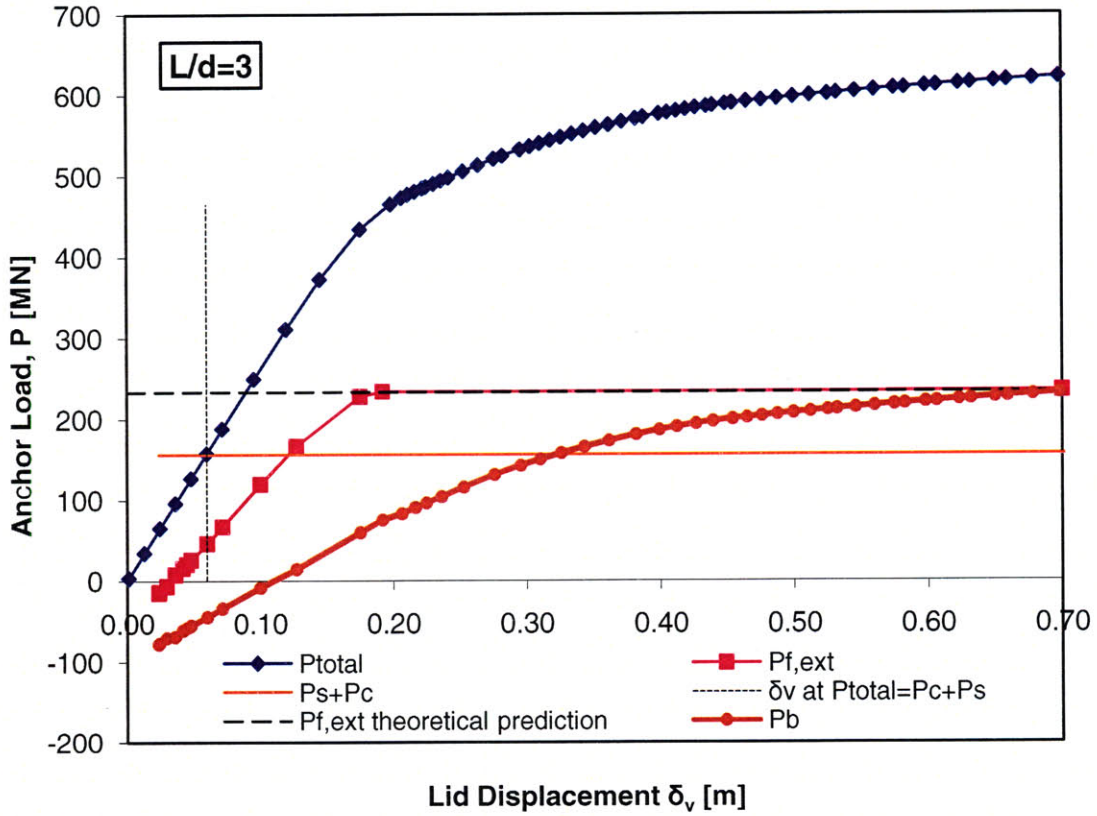
L/d=3
Anchor Load, P [MN]
700
600
500
400
300
200
100
0
-100
-200
0.00
0.10
0.20
0.30
0.40
0.50
0.60
0.70
Ptotal
Ps+Pc
Pf,ext theoretical prediction
Pf,ext
δv at Ptotal=Pc+Ps
Pb
Lid Displacement δv [m]

Appendix C: Breakdown of drained loading forces for L/d=0.5,1,2,3

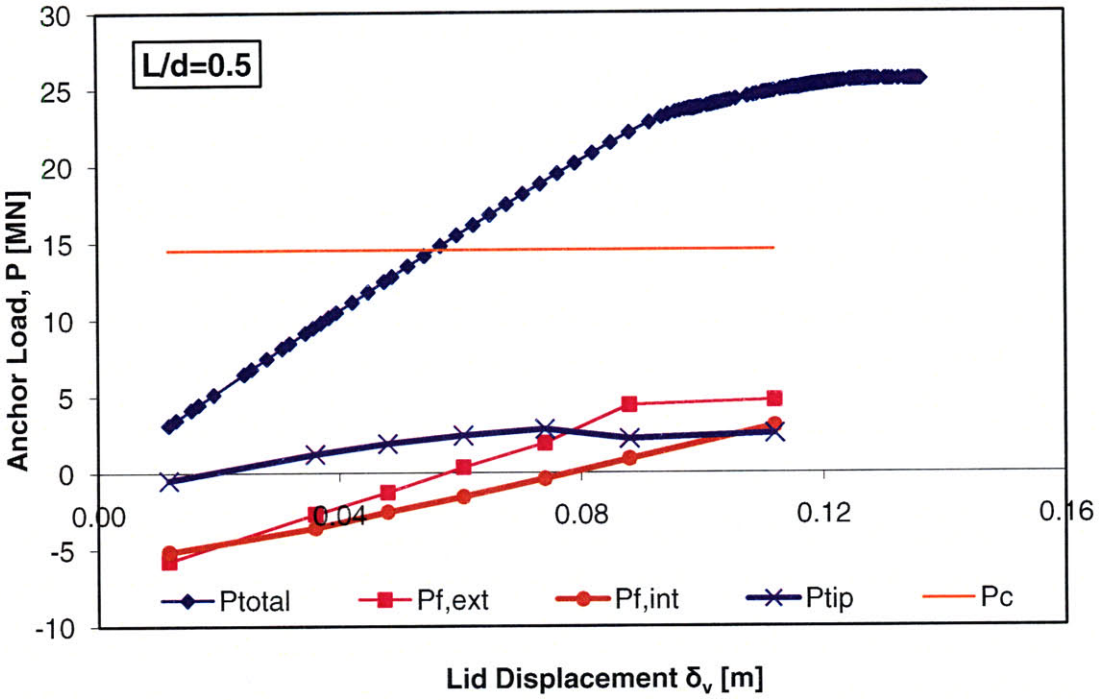

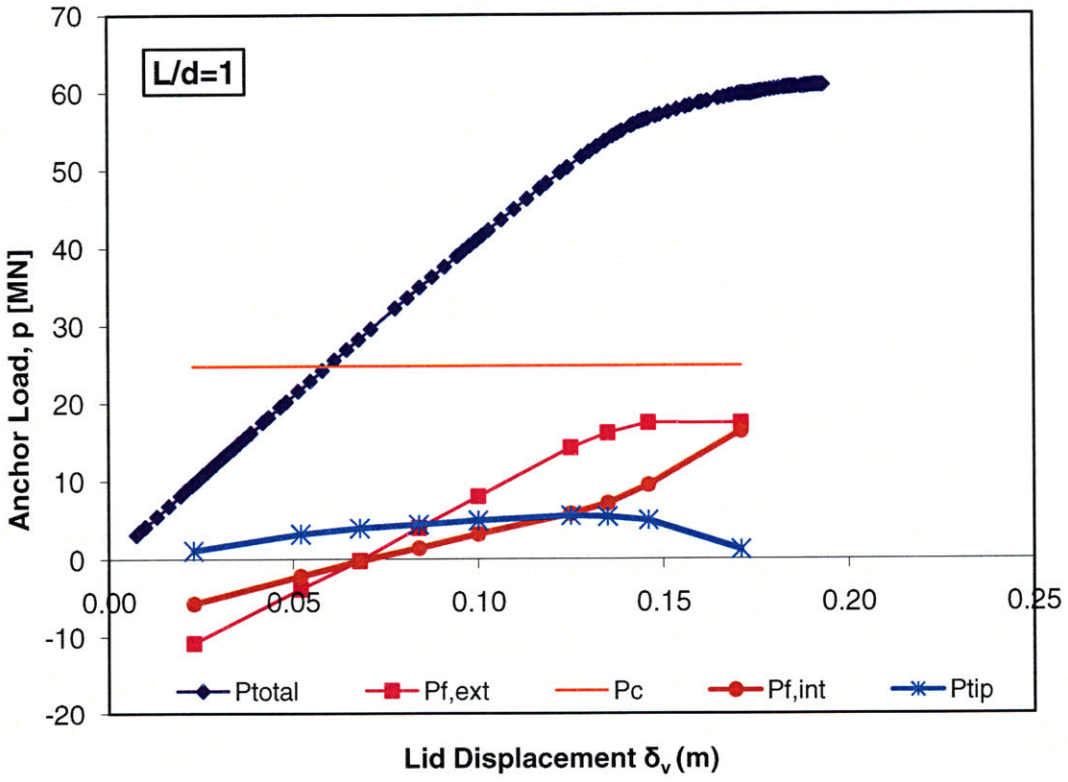

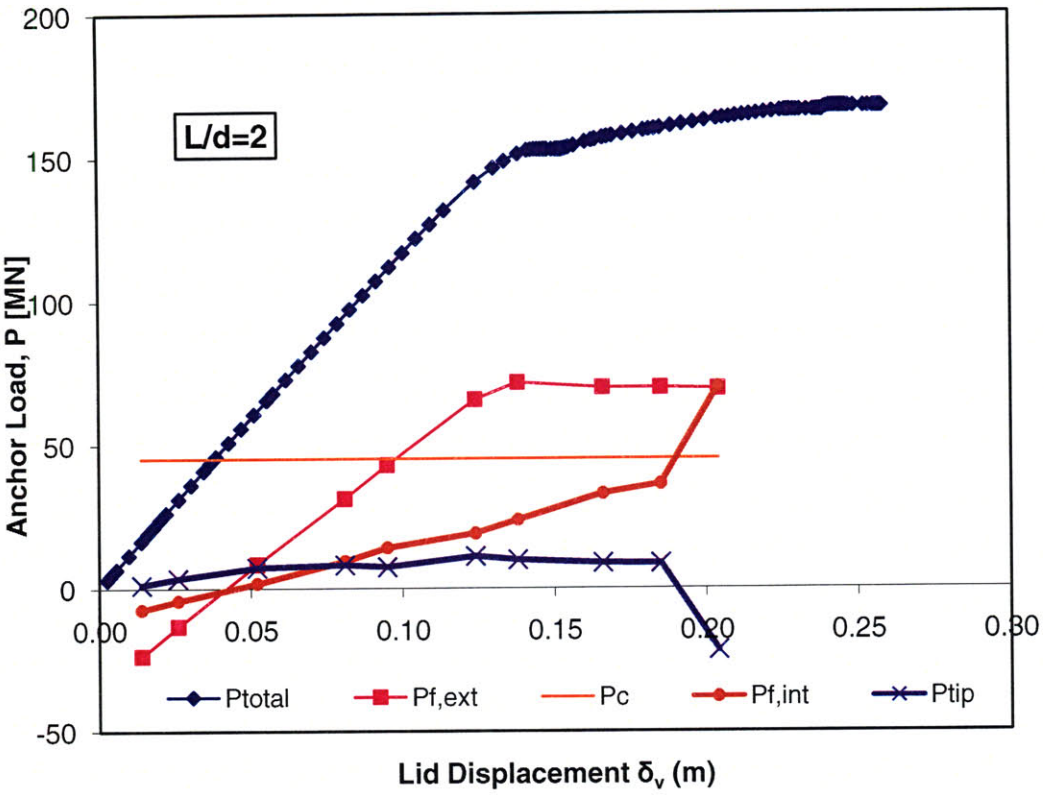
L/d=2
Anchor Load, P [MN]
200
150
100
50
0
-50
0.00
0.05
0.10
0.15
0.20
0.25
0.30
Ptotal
Pf,ext
Pc
Pf,int
Ptip
Lid Displacement δv (m)

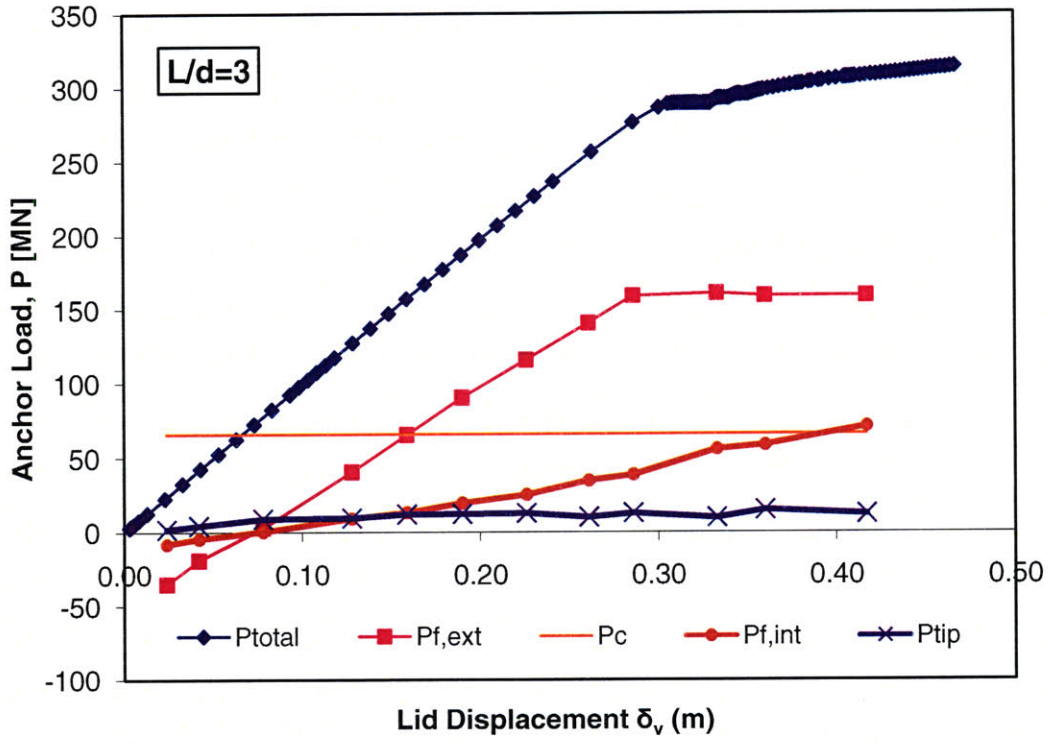
L/d=3
Anchor Load, P [MN]
350
300
250
200
150
100
50
0
-50
-100
0.00
0.10
0.20
0.30
0.40
0.50
Ptotal
Pf,ext
Pc
Pf,int
Ptip
Lid Displacement δv (m)